DEVELOPMENT AND APPLICATION OF SELF-HEALING ENGINEERED CEMENTITIOUS COMPOSITES (ECC) FOR DURABLE AND SUSTAINABLE INFRASTRUCTURE

by

Emily N. Herbert

A dissertation submitted in partial fulfillment
of the requirements for the degree of
Doctor of Philosophy
(Civil Engineering)
in The University of Michigan
2016

Doctoral Committee:

Professor Victor C. Li, Chair
Professor Gregory A. Keoleian
Professor Jerome P. Lynch
Professor Richard E. Robertson

TABLE OF CONTENTS

PART V: CONCLUSION

LIST OF TABLES

LIST OF FIGURES

ABSTRACT

While concrete is the most widely used construction material in the world, its inherent brittle behavior makes it prone to cracking, which negatively impacts the structural resiliency, durability, and sustainability of concrete infrastructure. As the demand for concrete continues to increase, the development of a concrete material that can regain any loss of performance due to cracking is highly desirable.

The development of a concrete that is capable of self-healing could solve many of the challenges associated with cracking seen in current concrete infrastructure. Although many approaches have been used to induce self-healing in concrete, the self-healing of Engineered Cementitious Composites (ECC) has proven to be one of the most promising approaches, as it has shown the ability to achieve recovery of transport and mechanical properties.

This research focused on the further characterization of the self-healing phenomena in ECC and developing a scientific understanding of the observed behavior. In addition to characterizing the self-healing behavior of ECC under the random and sometimes extreme conditions of the natural environment, the effects of age and exposure temperature on the self-healing phenomena were also determined. The experimental observations indicated a strong correlation between the recovery of mechanical properties and cracking characteristics of ECC, and this led to the development of an analytical scale-linking model to predict the level of material stiffness recovery due to self-healing as a function of imposed tensile strain.

Lastly, this work investigated the potential application of self-healing ECC in the railroad industry. There are many technical challenges associated with the prestressed concrete railroad ties in use today, and the development of an ECC railroad tie could mitigate many of these challenges. While the self-healing functionality of ECC would allow ECC ties to regain transport and mechanical properties should damage occur, the ductile nature of ECC could eliminate the need for prestressing steel. These benefits of ECC could increase the durability and sustainability

of railroad infrastructure by increasing the service life of ties, decreasing the need for track maintenance, simplifying the tie manufacturing process, and reducing the use of raw materials in comparison to current prestressed concrete ties.

PART I: INTRODUCTION

CHAPTER 1: INTRODUCTION

1.1 Motivation

The demand for infrastructure is expected to increase exponentially in the 21st century. Both developed and developing countries are making huge investments in their infrastructure systems to increase quality of life and economic growth. Developing countries are making investments in the design and construction of new infrastructure to support their rapid economic growth and increasing populations. It is estimated that developing countries in Asia require investments of $776 billion per year between 2010 and 2020 to meet the growing infrastructure demand.[1] Developed countries are focusing their investments in the maintenance and repair of existing infrastructure. The current state of existing infrastructure in the United States was recently given a grade of D+ by the American Society of Civil Engineers in their 2013 Report Card for America's Infrastructure. It is estimated that an investment of $3.6 trillion is needed by 2020 to ensure America's infrastructure is in a state of good repair.[2] Increasing both the quantity and quality of infrastructure worldwide to satisfy the growing demand for infrastructure development and maintenance will be a major challenge for engineers in the 21st century.

Concrete is the most widely used construction material in the world, with annual global consumption amounting to 12 billion metric tons.[3] It uses widely available and relatively inexpensive raw materials, which makes it appropriate for use in both developed and developing countries. Concrete is also a versatile building material since it is moldable and its mechanical properties can be utilized in numerous structural applications. Due to the extensive use of concrete in construction, the material properties and performance of concrete greatly impact the overall health of infrastructure worldwide.

Unfortunately, while concrete is the most widely used construction material, it is also one of the most brittle. The brittle nature of concrete makes it prone to cracking and this reduces the durability and sustainability of concrete infrastructure. Concrete structures are susceptible to cracking from factors such as excessive loading, restrained shrinkage, and harsh environmental conditions. Cracking weakens a structure by negatively impacting the mechanical properties, and it lowers the durability by creating pathways for harmful agents to penetrate the structure and attack the reinforcing steel or surrounding concrete. These and other problems associated with cracking increase the maintenance and repair costs of concrete structures and decrease the service life, making concrete infrastructure unsustainable. Therefore, the development of a concrete that can regain any loss of performance due to cracking is highly desirable.

In order to make infrastructure more durable and sustainable, it is necessary to develop a concrete material that is capable of self-healing. Self-healing concrete would be able to repair itself when damaged and cracked, without the need for human intervention. Healing products would fill cracks if damage occurred, reducing permeability and preventing corrosion, which would increase the durability of a structure. In some cases, mechanical properties may be recovered as well, further increasing durability and the ability of the structure to withstand further damage. Self-healing would also enhance sustainable development by increasing infrastructure service life and decreasing the amount of resources and energy needed for repairs.

Studies have shown that cracked concrete has the ability to heal itself over time when exposed to water. It has been found that there is a gradual reduction in permeability of damaged concrete as water is allowed to flow through the cracks, and this decrease in permeability is due to diminishing crack widths as healing occurs.[4-6] Healing has been shown to be a complex process involving several chemical and physical mechanisms, including hydration of unreacted cement, swelling of C-S-H, precipitation of calcium carbonate crystals, closing of cracks by impurities within the water, and the closing of cracks by concrete particles spalling from the crack faces.[4]

The extent of self-healing in cracked concrete was found to be highly dependent on the crack width, with smaller cracks healing more completely and at a faster rate than larger cracks. In some cases with small crack widths, cracks may heal completely, thus increasing the durability and sustainability of the damaged material.[4,7] However, this is rare since concrete is brittle and incapable of achieving crack widths small enough to undergo complete self-healing.

A number of approaches to induce self-healing in concrete have been attempted. Of these approaches, the most common are: chemical encapsulation[8,9], bacterial encapsulation[10-12], mineral admixtures[13-17], chemicals in glass tubing[18-21], and intrinsic healing with self-controlled tight crack widths.[22-26] Chemical encapsulation utilizes self-healing chemical agents contained in microcapsules, which are dispersed uniformly within the concrete matrix and fracture to release a healing agent when cracking occurs. The bacterial encapsulation technique is similar, but bacteria that induce precipitation of calcium carbonate are used as the self-healing agent. The mineral admixture approach utilizes expansive agents and geo-materials dispersed within the concrete matrix, which expand to fill cracks when damage occurs. Glass tubing is considered an alternative approach to chemical encapsulation since a self-healing chemical agent is used, but it is stored within the concrete matrix in glass tubes instead of microcapsules. Intrinsic healing with self-controlled tight crack width utilizes continued hydration of unreacted cement, pozzolanic reactions, and carbonation to produce C-S-H and calcium carbonate within microcracks. The majority of these self-healing approaches focus on the closing of cracks and permeability reduction. However, the intrinsic healing with self-controlled tight crack width approach is one that has demonstrated the potential to achieve both water permeability reduction and recovery of mechanical properties.[22-26]

The present doctoral research aims to the further the understanding and development of a self-healing concrete that achieves both reduction of transport properties and recovery of mechanical properties for the construction for more durable and sustainable infrastructure.

1.2 Research Objectives

The problems associated with cracking in concrete may be solved with the further development of a self-healing engineered cementitious composite (ECC).[27-29] ECC is a fiber reinforced cementitious composite that has been systematically tailored through the use of micromechanics to achieve high tensile ductility and tight crack widths. These tight crack widths are an intrinsic material property of ECC and promote robust self-healing behavior that is not easily attainable in brittle concrete with uncontrolled crack widths.

Self-healing has been shown to be extensive and reliable in ECC when specimens are healed under controlled laboratory conditions. Specimens have regained both permeability and

mechanical properties under a variety of healing regimens and harsh conditions, including chloride and highly alkaline envionments.[22-26] However, much is still unknown about the fundamental behavior of the self-healing phenomena in ECC. This doctoral research addresses many of these unknowns by further characterizing the self-healing phenomena and developing a scientific understanding of the observed behavior.

In addition, this doctoral research also determines the feasibility of developing a railroad tie manufactured with self-healing ECC. Railroad ties are an integral part of any railroad track infrastructure, and while ties have historically been manufactured with timber, prestressed concrete ties were first constructed and installed in North America in the early 1960s. However, unexpected and excessive cracking of the concrete has led to the premature failure of many prestressed concrete ties since their inception. Harsh environmental conditions, such as freeze-thaw cycles, and chemical attack, including alkali silica reactions and delayed ettringite formation, cause internal pressures that are large enough to induce cracking within the brittle concrete matrix. In addition, overloading and increasing speeds on railroad tracks cause flexural cracking and rail seat deterioration, which leads to abrasion and cracking of concrete ties under the surface of the rail.[30-37] The stiffness of prestressed concrete ties is also a cause of concern in the rail industry, as the excessive tie stiffness caused by the use of high strength concrete and prestressing leads to large track vibrations which increase the occurrence and magnitude of impact loads, causing damage to track infrastructure. The development of a self-healing ECC railroad tie could mitigate many of these problems associated with traditional concrete ties, and lead to more durable and sustainable railroad infrastructure.

1.3 Research Approach

The approach utilized in this doctoral research was based on two frameworks. The first framework focused on tailoring materials for robust self-healing performance, while the second framework focused on the tailoring of materials for specific mechanical properties.

Tailoring materials for robust self-healing performance can be accomplished using the framework outlined in Figure 1.1. This framework utilizes the knowledge of the fundamental behavior of the self-healing phenomena of a material to design that material for robust self-healing functionality. Once material design and development have occurred, the self-healing

performance of the material can be evaluated. If the material does not demonstrate robust self-healing behavior, the reason for this can be determined through knowledge of the fundamental science behind self-healing of the material and a new iteration of the material can be designed accordingly. This doctoral research aimed at evaluating and developing a scientific understanding of the self-healing behavior in ECC. With this knowledge, recommendations can be made for the development of future ECC materials with robust self-healing functionality.

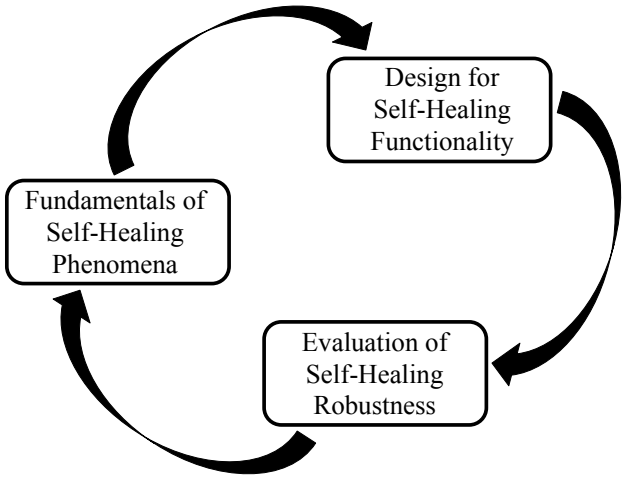

Figure 1.1: Framework for design of robust self-healing functionality.

Mechanical properties of materials can be tailored using the integrated structures and materials design (ISMD) framework shown in Figure 1.2.[38] As depicted in the upper triangle in Figure 1.2, structural engineers design member shapes and sizes based on given material properties and these members are then assembled into structural systems to meet required performance targets. The majority of material properties are considered fixed and are not altered based on the structural application. In materials engineering, depicted in the lower triangle in Figure 1.2, knowledge of micromechanics and processing techniques allow engineers to systematically develop materials to achieve specified properties. However, this development is done without consideration for structural performance and field conditions. This separation between structural and materials engineering leads to inefficient infrastructure design, which can cause problems with performance throughout the service life of a structure.

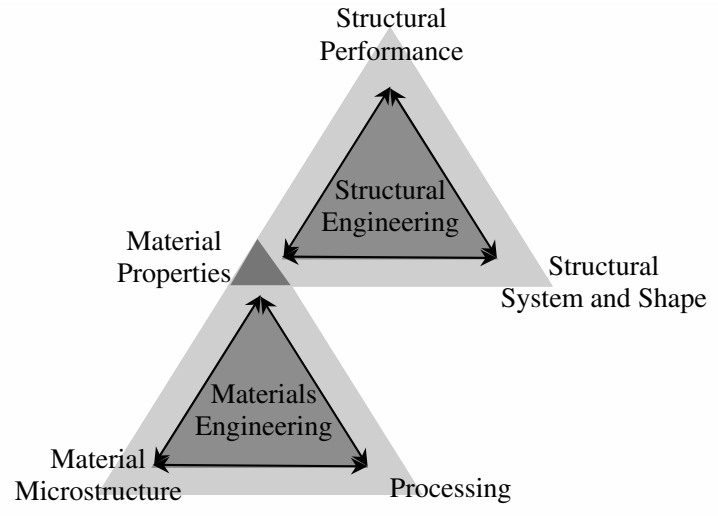

Figure 1.2: The Integrated Structures and Materials Design (ISMD) framework links material microstructure to desired structural performance.[38]

ISMD aims to connect structural and materials design through the common link of material properties. Structural design will include the selection of material properties that efficiently meet the structural performance targets, while materials engineering will provide the knowledge necessary for tailoring material ingredients to meet these composite property requirements. This approach ensures structural performance requirements are met by controlling material development at the microstructure level.

The use of micromechanics in the development of ECC makes the ISMD framework ideal for tailoring ECC for use in various field applications. In this doctoral research, mechanical properties required by the railroad industry will be used to determine the feasibility of developing an ECC railroad tie, and direct future development of an ECC material that can be used to manufacture a tie that will meet all rail industry performance targets.

1.4 Dissertation Organization

This dissertation is organized into five parts containing a total of ten chapters. Part I contains only the introductory chapter, where the background and motivation behind this doctoral research are presented. In addition, research objectives and underlying approaches are also included in this chapter.

Part II contains four chapters, all focusing on characterizing the self-healing phenomena in ECC. Chapter 2 outlines previous self-healing research, including work on traditional brittle concrete and ECC, which was performed under controlled laboratory environments. Chapters 3 and 4 build on previous research by characterizing the self-healing behavior of ECC in the natural environment, under random and sometimes extreme environmental conditions. An attempt to improve the self-healing functionality of ECC through the use of bacteria is described in Chapter 5, characterizing the self-healing behavior and determining the benefits and drawbacks of this approach.

Part III contains two chapters, aimed at developing a scientific understanding of the self-healing behavior observed and described in Part II. Chapter 6 examines the robustness of the self-healing functionality in ECC and determines how and why the self-healing behavior changes as ECC ages and is exposed to various temperature environments. Chapter 7 determines the correlation between self-healing behavior and crack characteristics, describing the correlation between ECC crack width and observed healing products, as well as stiffness recovery.

Part IV contains two chapters, describing the potential application of self-healing ECC in the railroad industry. Chapter 8 presents the background and motivation behind this specific application, describing the technical challenges associated with current railroad ties and the potential benefits of the manufacture and use of an ECC rail tie. Chapter 9 then describes the feasibility of developing an ECC railroad tie, combining past ECC research with experimental tests conducted as part of this dissertation work.

Part V contains the concluding chapter, summarizing the major findings and impacts of this doctoral research. In addition, recommendations for future research are also included in this chapter.

References

[1] Bhattacharyay, B. (2010). *Estimating Demand for Infrastructure in Energy, Transport, Telecommunications, Water and Sanitation in Asia and the Pacific: 2010-2020 - ADBI Working Paper 248.* Tokyo, Japan: Asian Development Bank Institute.

[2] ASCE. (2013). 2013 Report Card for America's Infrastructure. Washington DC: American Society of Civil Engineers.

[3] Ashby, M. F. (2009). *Materials and the Environment: Eco-Informed Material Choice.* Burlington, MA: Butterworth-Heinemann.

[4] Edvardsen, C. (1999). Water Permeability and Autogenous Healing of Cracks in Concrete. *ACI Materials Journal, 96*, 448–455.

[5] Granger, S., Loukili, A., Pijaudier-Cabot, G., & Chanvillard, G. (2007). Experimental Characterization of the Self-Healing of Cracks in an Ultra High Performance Cementitious Material: Mechanical Tests and Acoustic Emission Analysis. *Cement and Concrete Research, 37*, 519–527.

[6] Wang, K., Jansen, D., Shah, S., & Karr, A. (1997). Permeability Study of Cracked Concrete. *Cement and Concrete Research, 27*, 381–393.

[7] Reinhardt, H.W. & Jooss, M. (2003). Permeability and self-healing of cracked concrete as a function of temperature and crack width. *Cement and Concrete Research, 33*, 981-985.

[8] Huang, H. & Ye, G. (2011). Application of sodium silicate solution as self-healing agent in cementitious materials. In Christopher, L. & Wan, K.T. (Eds.), *International RILEM Conference on Advances in Construction Materials through Science and Engineering* (pp. 530–536). Hong Kong, China: RILEM Publications SARL.

[9] Yang, Z., Hollar, J., He, X., & Shi, X., (2011). A self-healing cementitious composite using oil core/silica gel shell microcapsules. *Cement and Concrete Composites, 33,* 506-512.

[10] Jonkers, H.M. (2011). Bacteria-based self-healing concrete. *Heron, 56*, 1-12.

[11] Wiktor, V. & Jonkers, H.M. (2011). Quantification of crack-healing in novel bacteria-based self-healing concrete. *Cement and Concrete Composites, 33*, 763-770.

[12] Wang, J., van Tittelboom, K., de Belie, N., & Verstraete, W. (2012). Use of silica gel or polyurethane immobilized bacteria for self-healing concrete. *Construction and Building Materials, 26*, 532-540.

[13] Kishi, T., Ahn, T., Hosoda, A., Suzuki, S., & Takaoka, H. (2007). Self-healing behavior by cementitious recrystallization of cracked concrete incorporating expansive agent. In *Proceedings of the 1st International Conference on Self-Healing Materials*. Noordwijkaan Zee, The Netherlands.

[14] Ahn, T.H. & Kishi, T. (2010). Crack self-healing behavior of cementitious composites incorporating various mineral admixtures. *Journal of Advanced Concrete Technology, 8*, 171-186.

[15] Hosoda, A., Kishi, T., Arita, H., & Takakuwa, Y. (2007). Self healing of crack and water permeability of expansive concrete. In *Proceedings of the 1st International Conference on Self-Healing Materials*. Noordwijkaan Zee, The Netherlands.

[16] Sisomphon, K. & Copuroglu, O. (2011). Self healing mortars by using different cementitious materials. In Christopher, L. & Wan, K.T. (Eds.), *International RILEM Conference on Advances in Construction Materials through Science and Engineering* (pp. 545–552). Hong Kong, China: RILEM Publications SARL.

[17] Sisomphon, K., Copuroglu, O., & Koenders, E.A.B. (2011). Surface crack self-healing behavior of mortars with expansive additives. In *Proceedings of the 3rd International Conference on Self-Healing Materials*. Bath, UK.

[18] Li, V.C., Lim, Y.M., & Chan, Y. (1998). Feasibility study of passive smart self-healing cementitious composite. *Composites Part B: Engineering, 29*, 819-827.

[19] Dry, C. & McMillan, W. (1996). Three-part methylmethacrylate adhesive system as an internal delivery system for smart responsive concrete. *Smart Materials and Structures, 5*, 297-300.

[20] Joseph, C., Jefferson, A.D., Isaacs, B., Lark, R., & Gardner, D. (2010). Experimental investigation of adhesive-based self-healing of cementitious materials. *Magazine of Concrete Research, 62*, 831-843.

[21] Van Tittelboom, K., de Belie, N., van Loo, D., & Jacobs, P. (2011). Self-healing efficiency of cementitious materials containing tubular capsules filled with healing agent. *Cement and Concrete Composites, 31*, 497-505.

[22] Sahmaran, M. & Li, V.C. (2008). Durability of mechanically loaded engineered cementitious composites under highly alkaline environments. *Cement and Concrete Composites, 30*, 72-81.

[23] Yang, Y., Lepech, M.D., Yang, E., & Li, V.C. (2009). Autogenous healing of engineered cementitious composites under wet-dry cycles. *Cement and Concrete Research, 39*, 382-390.

[24] Yamamoto, A., Watanabe, K., Li, V.C., & Niwa, J. (2010). Effect of wet-dry condition on self-healing property of early-age ECC. *Japan Concrete Institute, 32*, 251-256.

[25] Li, M. & Li, V.C. (2011). Cracking and Healing of Engineered Cementitious Composites under Chloride Environment. *ACI Materials Journal, 108*, 333-340.

[26] Yang, Y., Yang, E.H., & Li, V.C. (2011). Autogenous healing of engineered cementitious composites at early age. *Cement and Concrete Research, 41*, 176-183.

[27] Li, V.C., Wang, S., & Wu, C. (2001). Tensile Strain-Hardening Behavior of PVA-ECC. *ACI Materials Journal, 98*, 483-492.

[28] Li, V.C. (2003). On Engineered Cementitious Composites (ECC): A Review of the Material and Its Applications. *Journal of Advanced Concrete Technology, 1*, 215-230.

[29] Li, V.C. (1993). From Micromechanics to Structural Engineering – The Design of Cementitious Composites for Civil Engineering Applications. *JSCE Journal of Structural Mechanics and Earthquake Engineering, 10*, 37-48.

[30] Zehman, J.C., Edwards, J.R., Barkan, C.P.L., & Lange, D.A. (2009). Failure Mode and Effect Analysis of Concrete Ties in North America. In *Proceedings of the 9th International Heavy Haul Conference* (pp. 270-278). Shanghai, China.

[31] Zehman, J.C., Kernes, R.G., Edwards, J.R., Lange, D.A., & Barkan, C.P.L. (2011). Moisture-Driven Deterioration and Abrasion of Concrete Sleeper Rail Seats. In *Proceedings of the 9th World Congress on Railway Research*.

[32] Kernes, R.G., Edwards, J.R., Dersch, M.S., Lange, D.A., & Barkan, C.P.L. (2011). Investigation of the Impact of Abrasion as a Concrete Crosstie Rail Seat Deterioration (RSD) Mechanism. In *AREMA 2011 Annual Conference in Conjunction with Railway Interchange 2011*.

[33] Kernes, R.G., Edwards, J.R., Dersch, M.S., Lange, D.A., & Barkan, C.P.L. (2011). Investigation of the Dynamic Frictional Properties of a Concrete Crosstie Rail Seat and Pad and its Effect on Rail Seat Deterioration (RSD). In *Transportation Research Board 91st Annual Meeting*.

[34] Shurpali, A.A., Kernes, R.G., Edwards, J.R., Dersch, M.S., Lange, D.A., & Barkan, C.P.L. (2013). Investigation of the Mechanics of Rail Seat Deterioration (RSD) and Methods to Improve the Abrasion Resistance of Concrete Sleeper Rail Seats. In *Proceedings of the 10th International Heavy Haul Association Conference*. New Delhi, India.

[35] Mielenz, R.C., Marusin, S.L., Hime, W.G., & Jugovic, Z.T. (1995). Investigation of prestressed concrete railway tie distress. *Concrete International, 17*, 62-68.

[36] Collepardi, M. (2003). A state-of-the-art review on delayed ettringite attack on concrete. *Cement and Concrete Composites, 25*, 401-407.

[37] Kaewunruen, S. & Remennikov, A.M. (2010). Dynamic Crack Propagations in Prestressed Concrete Sleepers in Railway Track Systems Subjected to Severe Impact Loads. *ASCE Journal of Structural Engineering, 136*, 749-754.

[38] Li, V. C. (2007). Integrated structures and materials design. *RILEM Journal of Materials and Structures, 40*(4), 387-396.

PART II: CHARACTERIZATION OF THE SELF-HEALING PHENOMENA IN ECC

CHAPTER 2: SELF-HEALING CHARACTERIZATION UNDER CONTROLLED LABORATORY ENVIRONMENTS

2.1 Introduction

Studies have shown that cracked concrete has the ability to heal itself over time when exposed to water under controlled laboratory conditions. It has been found that there is a gradual reduction in permeability of damaged concrete as water is allowed to flow through the cracks, and this decrease in permeability is due to diminishing crack widths as healing occurs.[1-3] Several chemical and physical mechanisms have been found to contribute to self-healing, and the extent of healing has been found to be highly dependent on the crack widths developed within the concrete, with smaller cracks healing more completely than larger cracks.[1,4] Since concrete is brittle and often incapable of achieving crack widths small enough to undergo complete self-healing, a number of approaches to induce self-healing have been attempted.[5-20] All of these approaches aim to recover transport (permeability) properties of the damaged concrete material, while some also aim to recover mechanical (strength and stiffness) properties as well.

This chapter will review the chemical and physical mechanisms that contribute to self-healing, as well as the most common approaches currently used to induce self-healing in the laboratory. The final sections of this chapter will focus on the design philosophy and previous research associated with self-healing in ECC, demonstrating that self-healing in ECC achieves recovery of both transport and mechanical properties under controlled laboratory environments.

2.2 Self-Healing Mechanisms

Self-healing has been shown to be a complex process involving several chemical and physical mechanisms. The following mechanisms have been cited by previous research: hydration of unreacted cement and pozzolans, swelling of C-S-H, precipitation of calcium carbonate crystals, closing of cracks by impurities within the water, and the closing of cracks by concrete particles from spalling on the crack faces. Although all of these mechanisms contribute to healing, it has been shown that the precipitation of calcium carbonate is the main mechanism for the self-healing of cracks in concrete.[1]

The reaction of calcium ions (Ca^{2+}) with bicarbonates and carbonates (HCO_3^- and CO_3^{2-}) present in the crack water triggers the precipitation of calcium carbonate ($CaCO_3$) as shown in Equations 2.1 and 2.2. Ca^{2+} is present in the crack water due to the high calcium content of concrete and the dissolution of calcium hydroxide ($Ca(OH)_2$), which is a product of the hydration reaction. Due to the high alkalinity of the crack water, carbon dioxide from the atmosphere dissolves in the water to create a combination of HCO_3^- and CO_3^{2-}, providing the final reactants needed to form $CaCO_3$.[1]

$$Ca^{2+} + CO_3^{2-} \rightarrow CaCO_3 \ (pH_{water} > 8) \tag{2.1}$$

$$Ca^{2+} + HCO_3^- \rightarrow CaCO_3 + H^+ \ (7.5 < pH_{water} < 8) \tag{2.2}$$

Initially, the formation of $CaCO_3$ is rapid and surface controlled since there is an abundance of Ca^{2+} located on the crack faces. However, as healing progresses, the process slows and the formation of $CaCO_3$ becomes diffusion controlled. The shift from surface to diffusion controlled healing occurs when the readily available Ca^{2+} on the crack faces is consumed and Ca^{2+} diffusion occurs due to the concentration gradient between the matrix and crack water. This slows the healing process since the calcium ions must diffuse through both the concrete matrix and newly formed healing products on the surface of the crack.[1] Therefore, it is important to keep crack widths to a minimum, thus reducing the thickness of the healing product layer in order to minimize the amount of diffusion controlled healing that needs to occur.

For this reason, self-healing has been shown to be highly dependent on crack width, with smaller cracks healing more completely and at a faster rate than larger cracks. In some cases with small crack widths, cracks may heal completely, thus decreasing the permeability and potentially recovering the mechanical properties of the damaged material.[1,4] However, this is rare since most concrete materials are brittle and incapable of achieving crack widths small enough to undergo complete self-healing, even with the use of reinforcing steel.

2.3 Self-Healing Approaches

Since most cracks in concrete are too large to undergo complete self-healing, a number of approaches to induce and improve self-healing in concrete have been attempted. Of these approaches, the most common are: chemical encapsulation, bacterial encapsulation, mineral admixtures, chemicals in glass tubing, and intrinsic healing with self-controlled tight crack widths.[5]

Chemical encapsulation utilizes self-healing chemical agents contained in microcapsules, which are dispersed uniformly within the concrete matrix. The healing agents remain in the microcapsules until a concrete crack propagates and breaks the capsules open. The self-healing agent then leaks out of the microcapsules, sealing the crack and binding the crack faces. This approach is versatile since the capsules can incorporate a variety of healing agents and be manufactured in any size. For example, the use of 5 mm wax capsules containing a sodium silicate solution proved to be effective in regaining mechanical properties, specifically stiffness and flexural strength when measured with three point bending tests.[6] In addition, another study, which utilized 4.15 μm capsules filled with methylmethacrylate and triethylborane, demonstrated the ability of this approach to improve cracking resistance and toughness of damaged concrete under fatigue loading.[7] However, one major drawback of this approach is that it is not repeatable. Once a capsule breaks, all of the healing agent is released. This means that if damage occurred again in the same location, there would be no chemical agent left to repeat the healing process.

The bacterial encapsulation technique is similar to chemical encapsulation, but bacteria that induce precipitation of calcium carbonate are used as the self-healing agent. Bacteria are encapsulated with an organic growth substrate and the metabolic conversion of this substrate leads to the precipitation of healing products. The bacteria chosen for use with this approach

must be able to withstand the highly alkaline environment of the concrete matrix as well as the large compressive force generated within the matrix due to continued hydration. Spores of *Bacillus pseudofirmus* and *Bacillus cohnii*, along with calcium lactate, have been encapsulated within 4 mm expanded clay particles. When a crack propagates and the bacterial spores within the clay particles are exposed to water, they germinate into vegetative cells and begin consuming calcium lactate. This metabolic conversion of calcium lactate produces both $CaCO_3$ and CO_2. CO_2 then reacts with available calcium ions to further increase the production of $CaCO_3$.[8,9] Although this technique is promising, it has not been proven to regain mechanical properties and it is unclear if the bacterial spores could remain viable throughout the entire service life of a structure due to the harsh conditions within the concrete matrix. Also, this approach must be used in structures that are continuously exposed to water since bacterial spores lose viability under drying conditions.

The mineral admixture approach utilizes expansive agents and geo-materials dispersed within the concrete matrix, which expand to fill cracks when exposed to water. Cracks up to 0.22 mm have been completely sealed using a mixture of expansive agents, swelling geo-materials, and carbonates as partial cement replacement (up to 10% by weight). The swelling of geo-materials upon hydration, the increase in volume of expansive agents, and the precipitation of carbonates were found to be the primary sealing mechanisms.[10,11] Although this approach has been demonstrated to be effective for sealing cracks and reducing permeability, the recovery of mechanical properties has not been verified.

Glass tubing is considered an alternative approach to chemical encapsulation since a self-healing chemical agent is used, but in this approach it is stored within the concrete matrix in glass tubes instead of microcapsules. When a crack in the concrete passes through the glass tubing, the tubing fractures and releases a low viscosity chemical healing agent that leaks into the crack. Numerous chemicals including methyl methacrylate[12], ethyl cyanoacrylate[13, 14], and polyurethane[15] have proven to be successful in recovering both permeability and mechanical properties. However, one major drawback of this approach is that it is not pervasive unless an extensive network of tubing is used throughout the structure. Also, similar to the chemical encapsulation approach, this technique is not repeatable since all of the healing agent would be released during the first damage event.

Intrinsic healing with self-controlled tight crack width utilizes continued hydration of unreacted cement, pozzolanic reactions, and carbonation to produce C-S-H and calcium carbonate. These reactions occur naturally when a crack is exposed to water, so no special additives are needed to induce healing. However, complete healing with this technique is only possible when crack widths are below 100 μm. ECC, which has self-controlled crack widths less than 100 μm, has demonstrated the ability to undergo complete self-healing from these intrinsic reactions. Both permeability and mechanical properties have been recovered under a variety of healing environments and harsh conditions, including chloride and highly alkaline environments.[16-20]

Although all of these techniques are promising, the intrinsic healing with self-controlled tight crack width approach is one that has clearly demonstrated the ability to achieve both water permeability reduction and recovery of mechanical properties.

2.4 Self-Healing in ECC

As described in Section 2.3, self-healing in ECC utilizes the intrinsic healing with self-controlled tight crack width approach. The unique design philosophy behind ECC allows it to achieve tight crack widths capable of undergoing complete self-healing, as described in the following sections.

2.4.1 Mechanical Properties and Design Philosophy

ECC is a high performance fiber reinforced cementitious composite (HPFRCC) that has been optimized through the use of micromechanics to achieve high tensile ductility and tight crack widths. As seen in Figure 2.1, ECC has the ability to reach tensile strain capacities of 3-5% under loading while maintaining tight crack widths of less than 60 μm.[21-23] These tight crack widths are an intrinsic material property of ECC and do not depend on the amount of steel reinforcement or the size of a structure.

Unlike the trial and error methodology used in traditional concrete design, ECC is systematically designed based on micromechanics.[21-2223] Knowledge of material microstructure and mechanics of deformation are used as the basis of design to tailor the material behavior at nano- and micro-length scales. Scale-linking is then used to predict the macroscopic composite material behavior, which can then be optimized based on the desired structural application. This systematic

micromechanics-based engineering approach creates an efficient material design framework and reduces the need for intensive experimental effort.

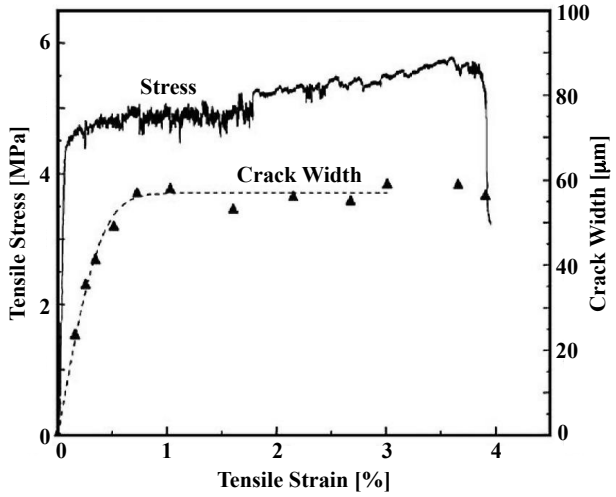

Figure 2.1: Representative tensile stress-strain curve and crack width development of ECC.[21] The self-controlled tight crack widths of ECC promote robust self-healing behavior.

The strain-hardening behavior of ECC under tensile loading is achieved by the formation of multiple microcracks. In order to achieve the multiple microcracking behavior, ECC must be designed to satisfy the following strength and energy criteria (Equations 2.3 and 2.4, Figure 2.2):

$$\text{Strength: } \sigma_0 > \sigma_{cs} \tag{2.3}$$

$$\text{Energy: } J_{tip} \le \sigma_0 \delta_0 - \int_0^{\delta_0} \sigma(\delta) d\delta \equiv J'_b \tag{2.4}$$

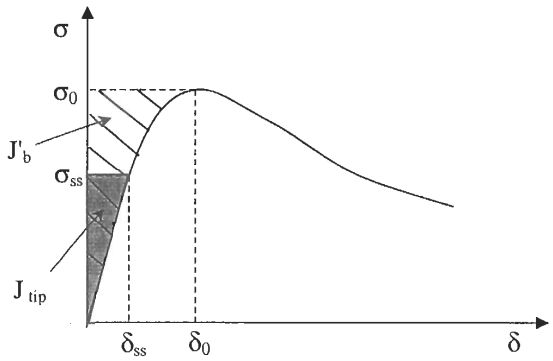

Figure 2.2: Illustration of the strain-hardening energy criterion.[21]

The strength criterion requires that the maximum fiber bridging stress (σ_0) be greater than the matrix first cracking strength (σ_{cs}), which is a function of the maximum preexisting matrix flaw size and the matrix fracture toughness (K_m). The energy criterion requires that the crack tip toughness ($J_{tip} = K_m^2/E_m$) be less than the complimentary energy (J'_b), which is calculated from the bridging stress versus crack opening curve (Equation 2.4 and Figure 2.2), where E_m is the matrix elastic modulus and σ_0 is the maximum bridging stress corresponding to the crack opening δ_0. The composite material should be tailored to maximize the difference between J_{tip} and J'_b in order to ensure saturated multiple cracking behavior. If either of these criteria is not satisfied, strain-hardening behavior will be terminated and a single localized fracture will occur, resulting in tension-softening.

Many components of the ECC material microstructure can be altered to optimize the macroscopic material properties and ensure multiple cracking behavior. Some of these components include the matrix flaw size and distribution, matrix toughness, fiber geometric and mechanical properties, fiber content, and fiber-matrix interfacial chemical and frictional bond. ECC often needs to be tailored for specific applications, and the tailoring of these components using the micromechanics-based design approach allows for efficient material design.

2.4.2 Previous Research

Self-healing has been shown to be extensive and reliable in ECC when specimens are healed under controlled laboratory conditions due to the tight cracks widths of the material. Samples are typically damaged under uniaxial tensile loading, while resonant frequency (RF), permeability, and uniaxial tension reloading tests are used to assess the rate of self-healing and the level of transport and mechanical property recovery. Previous studies have shown that self-healing in ECC leads to the recovery of both permeability and mechanical properties, and the healing products have begun to be characterized to further understand the mechanisms behind the self-healing phenomena.

It has been shown that both 3 day and 6 month old ECC samples can be healed under cyclic wetting and drying in the laboratory.[17,18,20] Samples were preloaded to specified tensile strain values to induce damage and then allowed to heal under various exposure environments. The most common exposure environment consisted of cyclic wetting and drying, which included

submerging the samples in water for 24 hours followed by 24 hours of drying in laboratory air. It was found that only 4 to 5 of these healing cycles were needed to attain the full benefit of self-healing. Permeability tests showed that after healing, specimens with crack widths less than 50 μm had nearly identical permeability values to those of undamaged samples, indicating a full recovery of transport properties. It was also found that specimens preloaded to lower tensile strain values experienced higher RF and stiffness recoveries than those loaded to larger values. For example, 6 month old specimens preloaded to 0.3% tensile strain were able to recover 100% of their initial RF values while those preloaded to 3.0% recovered 76%. In addition, stiffness recovery was found to be greater in the 6 month old samples. This was attributed to the fact that the 6 month old samples were able to maintain tighter crack widths than samples preloaded at 3 days.

Self-healing in ECC can also occur in adverse exposure conditions, including chloride and highly alkaline environments. Samples preloaded to 1.5% tensile strain and immersed in a 3% sodium chloride solution for 30 days were able to recover nearly all of their material stiffness when reloaded using uniaxial tension tests.[19] In addition, samples with 50 μm cracks exposed to a highly alkaline environment for one month were also able to recover nearly all of their original stiffness values.[16] These studies show that self-healing in ECC is quite versatile, and can be reliable under a variety of different exposure conditions.

Lastly, the self-healing products formed in ECC have begun to be characterized by the complimentary use of energy dispersive spectroscopy (EDS), transmission electron microscopy (TEM), Fourier transform infrared spectroscopy (FTIR), and X-ray diffraction (XRD).[24] The healing products were identified as a combination of C-S-H and $CaCO_3$, and the formation of these products was found to vary by crack width. C-S-H was found to be the main healing product in cracks less than 15 μm, while both C-S-H and $CaCO_3$ were found to be present in larger cracks. However, further studies described in Chapter 7 show that the chemical species formed during self-healing are less dependent on crack width than this original study suggests.

2.5 Conclusions

Background information regarding the mechanisms that contribute to self-healing and a review of previous research encompassing the most common approaches used to induce self-healing in

the laboratory were presented in this chapter. Based on this information, the following conclusions can be drawn:

- Self-healing has been studied extensively in concrete materials under controlled laboratory conditions.
- The chemical and physical mechanisms contributing to self-healing have been identified, and numerous approaches to induce and improve self-healing have been developed.
- The intrinsic healing with self-controlled tight crack width approach utilized in ECC has proven to be one of the most promising approaches, with ECC recovering both transport and mechanical properties when exposed to cyclic wetting and drying in the laboratory.
- However, in order to determine the feasibility of using self-healing ECC in full-scale applications, the self-healing behavior must be studied in the natural environment as well. Studies characterizing the self-healing behavior of ECC in the natural environment are described in Chapters 3 and 4.

References

[1] Edvardsen, C. (1999). Water Permeability and Autogenous Healing of Cracks in Concrete. *ACI Materials Journal, 96*, 448–455.

[2] Granger, S., Loukili, A., Pijaudier-Cabot, G., & Chanvillard, G. (2007). Experimental Characterization of the Self-Healing of Cracks in an Ultra High Performance Cementitious Material: Mechanical Tests and Acoustic Emission Analysis. *Cement and Concrete Research, 37*, 519–527.

[3] Wang, K., Jansen, D., Shah, S., & Karr, A. (1997). Permeability Study of Cracked Concrete. *Cement and Concrete Research, 27*, 381–393.

[4] Reinhardt, H.W. & Jooss, M. (2003). Permeability and self-healing of cracked concrete as a function of temperature and crack width. *Cement and Concrete Research, 33*, 981-985.

[5] Li, V.C. & Herbert, E.N. (2012). Robust Self-Healing Concrete for Sustainable Infrastructure. *Journal of Advanced Concrete Technology*, *10*, 207-218.

[6] Huang, H. & Ye, G. (2011). Application of sodium silicate solution as self-healing agent in cementitious materials. In Christopher, L. & Wan, K.T. (Eds.), *International RILEM Conference on Advances in Construction Materials through Science and Engineering* (pp. 530–536). Hong Kong, China: RILEM Publications SARL.

[7] Yang, Z., Hollar, J., He, X., & Shi, X., (2011). A self-healing cementitious composite using oil core/silica gel shell microcapsules. *Cement and Concrete Composites, 33,* 506-512.

[8] Jonkers, H.M. (2011). Bacteria-based self-healing concrete. *Heron, 56*, 1-12.

[9] Wiktor, V. & Jonkers, H.M. (2011). Quantification of crack-healing in novel bacteria-based self-healing concrete. *Cement and Concrete Composites, 33*, 763-770.

[10] Kishi, T., Ahn, T., Hosoda, A., Suzuki, S., & Takaoka, H. (2007). Self-healing behavior by cementitious recrystallization of cracked concrete incorporating expansive agent. In *Proceedings of the 1st International Conference on Self-Healing Materials*. Noordwijkaan Zee, The Netherlands.

[11] Ahn, T.H. & Kishi, T. (2010). Crack self-healing behavior of cementitious composites incorporating various mineral admixtures. *Journal of Advanced Concrete Technology, 8*, 171-186.

[12] Dry, C. & McMillan, W. (1996). Three-part methylmethacrylate adhesive system as an internal delivery system for smart responsive concrete. *Smart Materials and Structures, 5*, 297-300.

[13] Li, V.C., Lim, Y.M., & Chan, Y. (1998). Feasibility study of passive smart self-healing cementitious composite. *Composites Part B: Engineering, 29*, 819-827.

[14] Joseph, C., Jefferson, A.D., Isaacs, B., Lark, R., & Gardner, D. (2010). Experimental investigation of adhesive-based self-healing of cementitious materials. *Magazine of Concrete Research, 62*, 831-843

[15] Van Tittelboom, K., de Belie, N., van Loo, D., & Jacobs, P. (2011). Self-healing efficiency of cementitious materials containing tubular capsules filled with healing agent. *Cement and Concrete Composites, 31*, 497-505.

[16] Sahmaran, M. & Li, V.C. (2008). Durability of mechanically loaded engineered cementitious composites under highly alkaline environments. *Cement and Concrete Composites, 30*, 72-81.

[17] Yang, Y., Lepech, M.D., Yang, E., & Li, V.C. (2009). Autogenous healing of engineered cementitious composites under wet-dry cycles. *Cement and Concrete Research, 39*, 382-390.

[18] Yamamoto, A., Watanabe, K., Li, V.C., & Niwa, J. (2010). Effect of wet-dry condition on self-healing property of early-age ECC. *Japan Concrete Institute, 32*, 251-256.

[19] Li, M. & Li, V.C. (2011). Cracking and Healing of Engineered Cementitious Composites under Chloride Environment. *ACI Materials Journal, 108*, 333-340.

[20] Yang, Y., Yang, E.H., & Li, V.C. (2011). Autogenous healing of engineered cementitious composites at early age. *Cement and Concrete Research, 41*, 176-183.

[21] Li, V.C., Wang, S., & Wu, C. (2001). Tensile Strain-Hardening Behavior of PVA-ECC. *ACI Materials Journal, 98*, 483-492.

[22] Li, V.C. (2003). On Engineered Cementitious Composites (ECC): A Review of the Material and Its Applications. *Journal of Advanced Concrete Technology, 1*, 215-230.

[23] Li, V.C. (1993). From Micromechanics to Structural Engineering – The Design of Cementitious Composites for Civil Engineering Applications. *JSCE Journal of Structural Mechanics and Earthquake Engineering, 10*, 37-48.

[24] Kan, L.L., Shi, H.S., Sakulich, A.R., & Li, V.C. (2010). Self-Healing Characterization of Engineered Cementitious Composite Materials. *ACI Materials Journal, 107*, 617-624.

CHAPTER 3: FEASIBILITY OF SELF-HEALING IN THE NATURAL ENVIRONMENT

3.1 Introduction

While extensive research has been done on the self-healing of ECC under controlled laboratory conditions, no research has been completed on the self-healing of ECC in the natural environment. Therefore, the work detailed in this chapter expands on previous research by allowing ECC to heal outdoors, in the natural environment, under random and sometimes extreme environmental conditions to determine the feasibility of using self-healing ECC in field applications. Once feasibility was established, a more extensive study, detailed in Chapter 4, was performed to fully characterize the self-healing behavior of ECC in the natural environment.

3.2 Experimental Investigation

3.2.1 Mix Proportion and Raw Materials

The ECC mix proportion used in this feasibility study is given in Table 3.1. Type I ordinary Portland cement, Class F fly ash, silica sand with an average particle size of 110 μm, a polycarboxylate-based high range water reducing admixture (HRWRA), and polyvinyl alcohol (PVA) fibers were used to prepare the ECC specimens. The PVA fibers accounted for 2% of the total mix volume and were 12 mm in length with an average diameter of 39 μm. The fibers had a tensile strength of 1600 MPa, a density of 1300 kg/m^3, an elastic modulus of 42.8 GPa, and a maximum elongation of 6%. In addition, the surfaces of the fibers were coated with an oiling agent (1.2% by weight) to reduce the interfacial chemical bond between the fiber and matrix caused by the strong hydrophilic nature of the PVA fibers.[1,2]

Table 3.1: ECC mix proportion.

Component	Cement	Fly Ash	Sand	Water	HRWRA	Fiber
Weight %	27	33	22	16	0.4	1.3

3.2.2 Specimen Preparation and Preloading

The raw materials were mixed in a 20 L force-based Hobart mixer according to the proportions shown in Table 3.1. After mixing, the fresh ECC was cast into molds measuring 300 mm x 76 mm x 12.5 mm and covered in plastic sheeting. After 24 hours, the specimens were removed from the molds and cut to 200 mm in length to minimize edge effects and bending stresses caused during uniaxial tensile loading. Specimens were then air cured at room temperature until testing. The day prior to testing, aluminum plates were glued to both ends of the specimens to facilitate gripping within the load frame.

All specimens were preloaded to 0.5% tensile strain at an age of 3 days. Uniaxial tensile loading was applied using a 25 kN capacity load frame (MTS Model 810) under displacement control and a loading rate of 0.5 mm/min. Two Linear Variable Displacement Transducers (LVDTs) were attached to the specimens during loading to measure tensile elongation. When the tensile strain reached 0.5%, the tensile load was released and the samples were unloaded and removed from the load frame.

3.2.3 Natural Environment Exposure

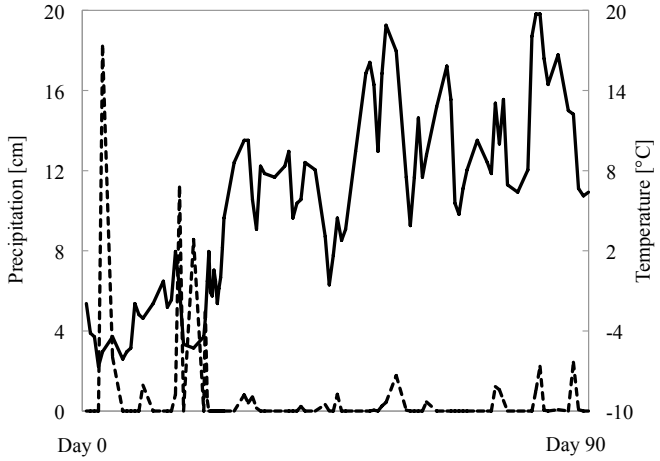

Figure 3.1: Precipitation and average daily temperature during 90 day period of natural environment study.

After preloading, specimens were placed outdoors in a location where they would be fully exposed to all environmental conditions. This experiment took place in Ann Arbor, Michigan,

between February and May, so the samples were exposed to rain, snow, and average daily temperatures ranging from -7 to 20°C (Figure 3.1).

3.2.4 Evaluation Methods

In order to determine the feasibility of self-healing in the natural environment, self-healing progress was examined using three evaluation methods: photo documentation, resonant frequency (RF) recovery, and stiffness recovery.

To obtain visual evidence of self-healing, images of cracks in the preloaded specimens were taken once a week while they were exposed to the natural environment. Specimens were chosen for photo documentation based on crack width data in order to determine the largest crack width capable of self-healing under these conditions.

RF measurements based on ASTM C215 for the longitudinal mode were used to monitor the rate of self-healing in the preloaded specimens. RF measurements were taken before and after preloading the specimens to quantify the amount of damage, and then twice a week throughout the duration of natural environment exposure to evaluate the rate of self-healing. The RF value of a specimen was calculated as the average of three consecutive RF measurements.

To assess the regain of mechanical properties due to self-healing, the secant stiffness between 0.5 and 2.0 MPa was measured under uniaxial tensile loading during preloading and after the specimens were allowed to heal in the natural environment (reloading). The preloading and reloading stiffness values were then compared to determine the level of recovery. Two sets of specimens were used for reloading: one set was reloaded after one month of natural environment exposure, and the other was reloaded after three months of exposure. These reloading tests were conducted using the same method described in Section 3.2.2 for preloading, but the specimens were reloaded until failure.

3.3 Experimental Results and Discussion

3.3.1 Photo Documentation

Figure 3.2 shows a 10 μm crack before and after self-healing was allowed to occur. This crack healed gradually over time as various precipitation events occurred and, after one month of

natural environment exposure, the crack appeared to be completely healed. This gradually type of healing was found to be typical of cracks that were 10 μm or less in width.

(a) 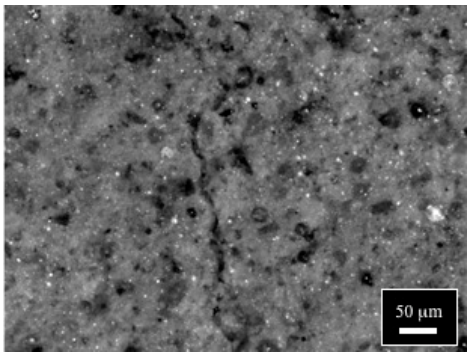

(b) 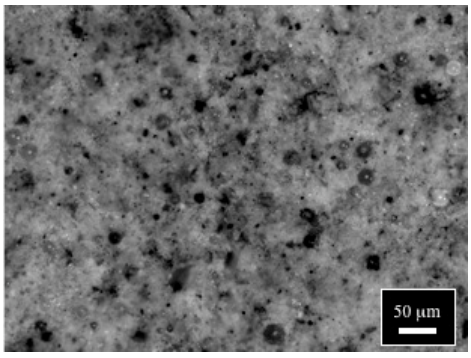

Figure 3.2: 10 μm crack (a) after preloading to 0.5% and
(b) after 1 month of natural environment exposure (48.3 cm of precipitation).

Figure 3.3 shows another 10 μm crack that experienced a slightly different form of healing than the crack in Figure 3.2. Figure 3.3 (a) and (b) show the crack before environmental exposure and after the crack appears to be completely healed. However, in Figure 3.3 (c), the crack becomes much more visible and, after two more weeks of environmental exposure, appears to be completed healed again in (d). Based on these images, it seems as though healing products are being dissolved during heavy rainfalls. Although other studies have found that healing products in ECC are a combination of calcium carbonate ($CaCO_3$) and C-S-H, these would not easily dissolve during large precipitation events.[3,4] Therefore, it is believed that the healing product being dissolved is calcium hydroxide ($Ca(OH)_2$), which is formed during cement hydration. Typically the large fraction of fly ash in the ECC mix would consume $Ca(OH)_2$ during the pozzolanic reaction, but the kinetics of this reaction are slow and may not be occurring fast enough during each precipitation event to transform $Ca(OH)_2$ into the more stable C-S-H gel.

Although most self-healing was visible in cracks that were 10 μm or less in width, healing products were seen in cracks as large as 20 μm. It has been found in previous research that cracks must be below 100 μm for self-healing to occur under controlled laboratory conditions[3],

however, no significant amount of healing products were observed in cracks larger than 20 μm under the natural environment in this experiment.

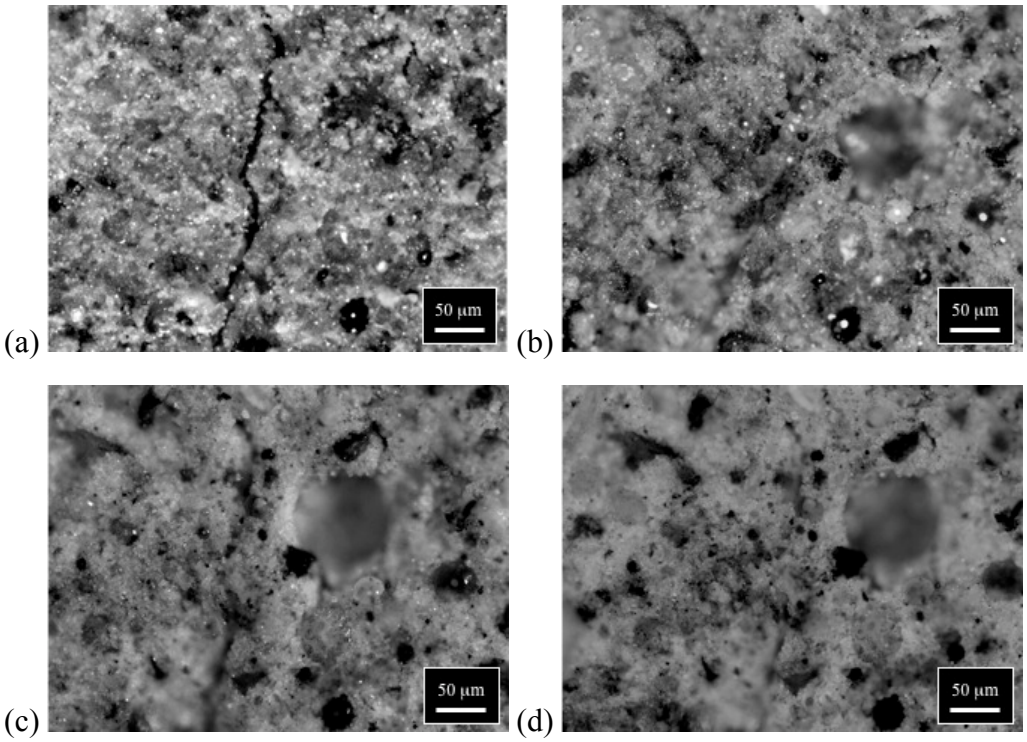

Figure 3.3: 10 μm crack (a) after preloading to 0.5%, (b) after 2 weeks of natural environment exposure (22.2 cm of precipitation), (c) after 1.5 months (50.9 cm of precipitation) with possible dissolution of healing products, and (d) after 2 months (54.3 cm of precipitation).

3.3.2 Resonant Frequency Recovery

Since both self-healing of cracks and continued maturation of the volume of material between adjacent cracks create an increase in RF values, the RF data in Figure 3.4 was normalized to account for the effects of continued hydration so the graph represents the RF recovery due solely to self-healing. Due to the formation of cracks within a sample during loading, there was a large drop in RF values after samples were preloaded, but RF values recovered greatly even after only a few precipitation events. It was also found that the rate of self-healing drastically decreased after approximately one month of natural environment exposure. However, specimens were still able to recover between 75 and 90% of their original, pre-damaged, RF values.

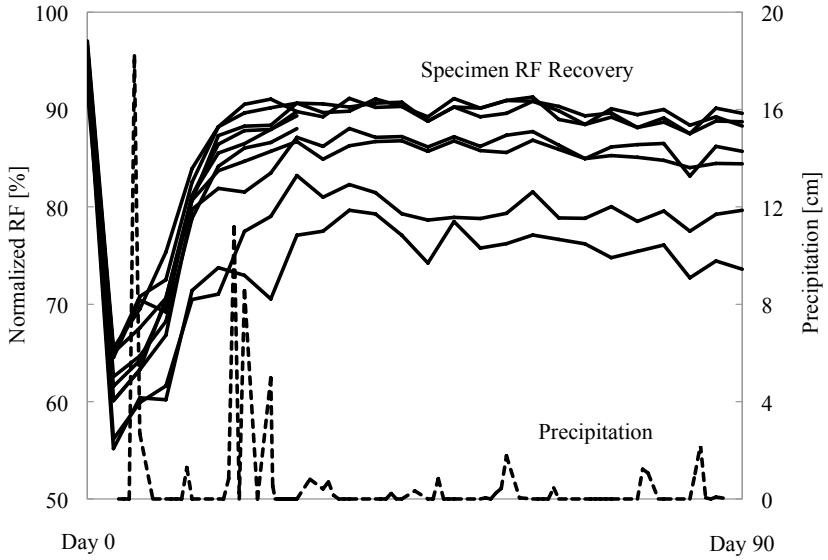

Figure 3.4: Precipitation and RF data for samples over 3 months of natural environment exposure. Variations in RF recovery levels are due to differences in crack patterns between the specimens.

Although all samples recovered a significant portion of their initial RF values, it has been seen that samples healed under laboratory conditions can recover up to 100% of their original value, making self-healing in the natural environment less reliable than self-healing under controlled laboratory conditions. Also, the rate of RF recovery seen in laboratory conditions is much more rapid than the rates seen in the natural environment.[3,4] This is due to the fact that self-healing in the laboratory is achieved under consistent wetting and drying cycles, while self-healing in the natural environment is more sporadic and the duration of precipitation events are usually much shorter than the duration of the wetting cycles used in laboratory conditions.

3.3.3 Stiffness Recovery

Figure 3.5 shows a typical ECC preloading curve and representative reloading curves for samples that were reloaded after one and three months of natural environment exposure. An indoor control sample that was reloaded without any self-healing is also shown for comparison. Specimens were able to recover up to 31% and 68% of their initial stiffness after one and three months of natural environment exposure. Since samples placed in the natural environment for three months were exposed to more precipitation events than the samples reloaded after one month of exposure, it was expected that these samples would have a higher level of stiffness recovery.

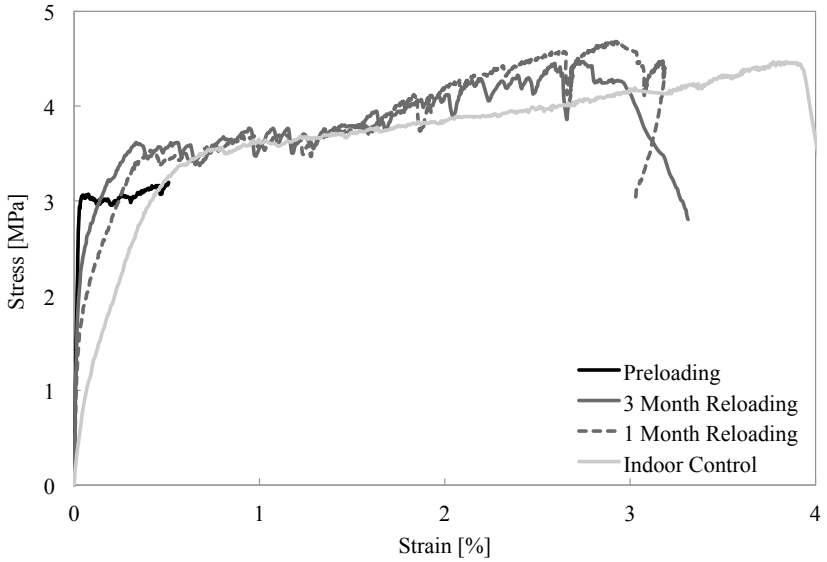

Figure 3.5: A typical ECC preloading curve, representative reloading curves for samples reloaded after 1 and 3 months of natural environment exposure, and the reloading curve of an indoor control sample that was reloaded without any self-healing.

Although there was a significant regain in stiffness for the samples reloaded at both one and three months of natural environment exposure, samples healed under laboratory conditions have been able to recover up to 90% of their initial stiffness values.[3] Like RF recovery, this can be attributed to the fact that self-healing in the laboratory uses consistent wetting and drying cycles, while healing in the natural environment is more irregular since the amount of precipitation and temperatures are constantly changing.

3.3.4 Discrepancies Between RF and Stiffness Recovery

In this study and other experiments discussed throughout this dissertation, there are discrepancies between the RF and stiffness recovery data. For example, in this feasibility study, samples were able to recover up to 90% of their initial RF values, but only 68% of their initial stiffness values after three months of natural environment exposure.

Although RF and reloading tests both provide information on the extent of self-healing, they are measuring two different properties of healed cracks. RF tests measure the changes in resonant frequency of a sample, detecting the frequency at which the sample vibrates with the greatest amplitude. When cracks occur in a sample, they increase the damping and decrease the resonant

frequency of the material. During healing, the opposite occurs: as healing products fill the cracks, damping decreases and the resonant frequency increases.[5,6] Therefore, RF tests can be considered as a way of measuring the extent to which the cracks are filled with healing products. In contrast, reloading tests used to determine the level of stiffness recovery are measuring the extent to which the healing products have bound the crack faces. Although cracks can be completely filled with healing products, this does not necessarily mean the crack faces have been bound. Of the healing products formed, C-S-H is the product that contributes most to the binding of crack faces, as $CaCO_3$ and $Ca(OH)_2$ are brittle crystalline products. Therefore, it is possible that a crack can be completely filled with healing products and have a full RF recovery, but show a lower level of stiffness recovery if the majority of the healing products are brittle crystals, which are unable to completely bind the crack faces.

3.4 Conclusions

While extensive research has been performed on the self-healing of ECC under controlled laboratory conditions, the study described in this chapter was the first to determine the feasibility of self-healing in the natural environment. Based on the results of this experimental investigation, the following conclusions can be drawn:

- Photo documentation, RF, and stiffness recovery results all demonstrated that self-healing of ECC in the natural environment is feasible.
- Healing products were observed in cracks up to 20 μm in width through photo documentation. However, it was found that heavy precipitation events could lead to the dissolution of some healing products due to the slow kinetics of the pozzolanic reaction utilized in ECC.
- Samples could recover up to 90% of their initial RF values and 68% of their initial stiffness values after three months of natural environment exposure.
- While self-healing in the natural environment is feasible, it may not be as robust as the self-healing seen under controlled laboratory conditions. For this reason, a more extensive study to fully characterize the self-healing behavior of ECC in the natural environment was performed and is described in Chapter 4.

References

[1] Li, V.C., Wang, S., & Wu, C. (2001). Tensile Strain-Hardening Behavior of PVA-ECC. *ACI Materials Journal, 98*, 483-492.

[2] Li, V.C., Wu, C., Wang, S., Ogawa, A., & Saito, T. (2002). Interface Tailoring for Strain-Hardening PVA-ECC. *ACI Materials Journal, 99,* 463-472.

[3] Yang, Y., Lepech, M.D., Yang, E., & Li, V.C. (2009). Autogenous healing of engineered cementitious composites under wet-dry cycles. *Cement and Concrete Research, 39*, 382-390.

[4] Kan, L.L., Shi, H.S., Sakulich, A.R., & Li, V.C. (2010). Self-Healing Characterization of Engineered Cementitious Composite Materials. *ACI Materials Journal, 107*, 617-624.

[5] Malhotra, V.M., & Carino, N.J. (2004). *Handbook on Nondestructive Testing of Concrete (2nd Edition).* ASTM International. West Conshohocken, PA: CRC Press LLC.

[6] Tanesi, J., & Meininger, R. (2006). Freeze-Thaw Resistance of Concrete With Marginal Air Content. *U.S. Department of Transportation Report HRT-06-117.*

CHAPTER 4: CHARACTERIZATION OF SELF-HEALING IN THE NATURAL ENVIRONMENT

4.1 Introduction

While the study detailed in Chapter 3 determined that self-healing of ECC in the natural environment is feasible, it may not be as robust as the self-healing seen under controlled laboratory conditions. Healing products were observed in cracks up to 20 μm in width, and it was found that samples could recover up to 90% of their initial resonant frequency (RF) values and 68% of their initial stiffness values after three months of natural environment exposure. Although these are reasonable recovery levels, they are still lower than those seen when samples are healed in the laboratory. For this reason, this chapter details a more extensive study to further characterize and understand the self-healing behavior of ECC in the natural environment.

4.2 Experimental Investigation

4.2.1 Mix Proportion and Raw Materials

Since the extent of self-healing has been found to be highly dependent on the crack width of the material[1,2], with smaller cracks healing more completely and at a faster rate than larger cracks, it was decided to use an ECC mix with smaller crack widths than the mix used in the study described in Chapter 3 in order to improve the self-healing performance in the natural environment. The mix proportions used in this study are given in Table 4.1. This mix had average crack widths of 24 and 30 μm at 0.5 and 1.0% tensile strain, while the mix used in Chapter 3 had crack widths of 36 and 44 μm at the corresponding imposed strains.

The raw materials used in this ECC mix were: Type I ordinary Portland cement, Class F fly ash, silica sand with an average particle size of 110 μm, a polycarboxylate-based high range water reducing admixture (HRWRA), and polyvinyl alcohol (PVA) fibers. The PVA fibers accounted for 2% of the total mix volume and were 12 mm in length with an average diameter of 39 μm.

The fibers had a tensile strength of 1600 MPa, a density of 1300 kg/m^3, an elastic modulus of 42.8 GPa, and a maximum elongation of 6%. In addition, the surfaces of the fibers were coated with an oiling agent (1.2% by weight) to reduce the interfacial chemical bond between the fiber and matrix caused by the strong hydrophilic nature of the PVA fibers.[3,4]

Table 4.1: ECC mix proportion.

Component	Cement	Fly Ash	Sand	Water	HRWRA	Fiber
Weight Fraction	1	2.2	1.16	0.85	0.01	0.067

4.2.2 Specimen Preparation and Preloading

The raw materials were mixed in a 20 L force-based Hobart mixer according to the proportions shown in Table 4.1. After mixing, the fresh ECC was cast into molds measuring 300 mm x 76 mm x 12.5 mm and covered in plastic sheeting. After 24 hours, the specimens were removed from the molds and cut to 200 mm in length to minimize edge effects and bending stresses caused during uniaxial tensile loading. Specimens were then air cured at room temperature until testing. The day prior to testing, aluminum plates were glued to both ends of the specimens to facilitate gripping within the load frame.

A total of 60 specimens were prepared, and these were then separated into four sets of 15 specimens each. Each set contained 5 control specimens, 5 specimens that were preloaded to 0.5% tensile strain, and 5 specimens that were preloaded to 1.0%. All preloading was carried out 7 days after the specimens were casted using uniaxial tensile loading. Loading was applied using a 25 kN capacity load frame (MTS Model 810) under displacement control and a loading rate of 0.5 mm/min. Two Linear Variable Displacement Transducers (LVDTs) were attached to the specimens during loading to measure tensile deformation. When the tensile strain reached the desired value, the load was released and the specimens were removed from the load frame.

4.2.3 Natural Environment Exposure

After preloading, specimens were placed outdoors in a location where they would be fully exposed to all natural environment conditions. This study took place in Ann Arbor, Michigan, over a 12 month period from September 2011 through September 2012, so the specimens were exposed to a wide range of temperatures (-11.7 to 32.8°C) and precipitation events.

4.2.4 Evaluation Methods

Self-healing progress in this study was examined using two evaluation methods. Resonant frequency (RF) measurements were used to monitor the rate of self-healing, while uniaxial tensile (reloading) tests were used to assess the robustness of the healing products.

RF measurements based on ASTM C215 for the longitudinal mode were used to monitor the rate of self-healing in the preloaded specimens. RF values were determined before and after preloading, and then once a week throughout the duration of natural environment exposure to evaluate the rate of self-healing. The RF value of a specimen was calculated as the average of three consecutive RF measurements.

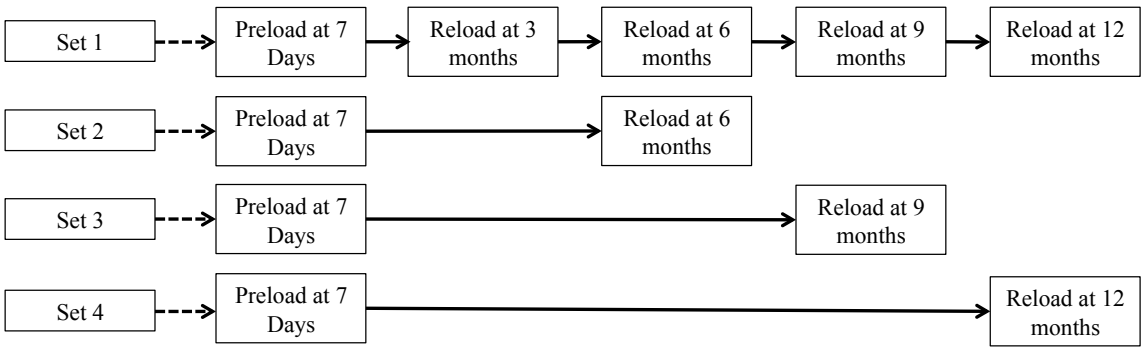

Figure 4.1: Preloading and reloading schedule. Length of solid arrows schematically illustrates the exposure time to the natural environment prior to the next reloading event.

To assess the robustness of the self-healing products, mechanical properties of the specimens were measured once they were allowed to heal in the natural environment. After a given exposure time, specimens were reloaded using uniaxial tensile tests and the mechanical properties were compared to those measured during preloading to determine the level of recovery. The exposure times of 3, 6, 9, and 12 months for Specimen Set 1, Set 2, Set 3, and Set 4, respectively, are schematically illustrated in Figure 4.1. For Specimen Set 1, three additional reloading events were applied to examine the influence of repeated damage on the ability of the material to maintain self-healing functionality. All reloading events were conducted using the same method described for preloading in Section 4.2.2, where specimens preloaded to 0.5 and 1.0% tensile strain in Set 1 were reloaded to the same strain magnitudes. Thus the reloading

events in this study were used both as a method for assessing the regain of mechanical properties of ECC (for all four sample sets) and as additional damage causing events (for Set 1).

4.3 Experimental Results and Discussion

4.3.1 Resonant Frequency Recovery

In addition to self-healing of microcracks in ECC, continued hydration over time in the bulk material also increases RF values. Figure 4.2 shows this increase by plotting the RF ratio of a control sample (with no preloading), which was exposed to the same environmental conditions as the preloaded specimens. The RF Ratio shows the change in RF of the control sample and is calculated using Equation 4.1, where $RF_{original}$ is the RF value of the specimen before it is exposed to the natural environment and $RF_{environment}$ is the RF value of the specimen during its natural environment exposure.

$$\text{RF Ratio} = \frac{RF_{environment}}{RF_{original}} \tag{4.1}$$

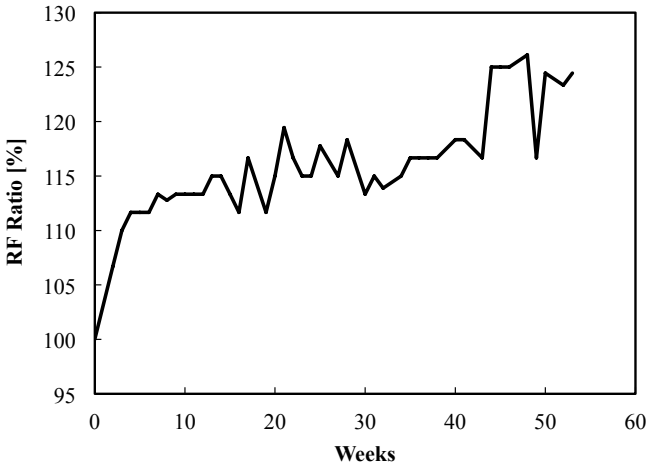

Figure 4.2: RF values of a control sample (with no preloading) when exposed to the natural environment. The increase in RF is due to continued hydration of the bulk material.

To account for the effects of continued hydration, RF values for preloaded specimens were normalized according to Equation 4.2, where $RF_{preload,environment}$ is the RF value of the preloaded specimens that were exposed to the natural environment and $RF_{control,environment}$ is the RF value of

control specimens that underwent the same environmental exposure. The Normalized RF removes the effect of bulk material hydration over time and provides RF values that are due solely to the self-healing of microcracks. Therefore, a Normalized RF value of 100% implies that a sample has fully healed from any damage that was induced during preloading.

$$\text{Normalized RF} = \frac{\text{RF}_{\text{preload,environment}}}{\text{RF}_{\text{control,environment}}} \tag{4.2}$$

Figure 4.3 shows the effect of natural environment exposure time on RF values. Due to the formation of cracks within a specimen during loading, there was a large drop in RF values after the specimens were preloaded, but the Normalized RF recovered between 90 and 96% after the first week of natural environment exposure, which had an average temperature of 20.6°C and 2.5 cm of precipitation. This is similar to results seen under controlled laboratory conditions, where the largest RF recovery occurred during the first healing cycle.[5-9] However, during the natural environment study described in Chapter 3, it was found that the RF recovery was more gradual than that seen under laboratory conditions. Therefore, it can be assumed that the rate of RF recovery in the natural environment varies depending on weather conditions.

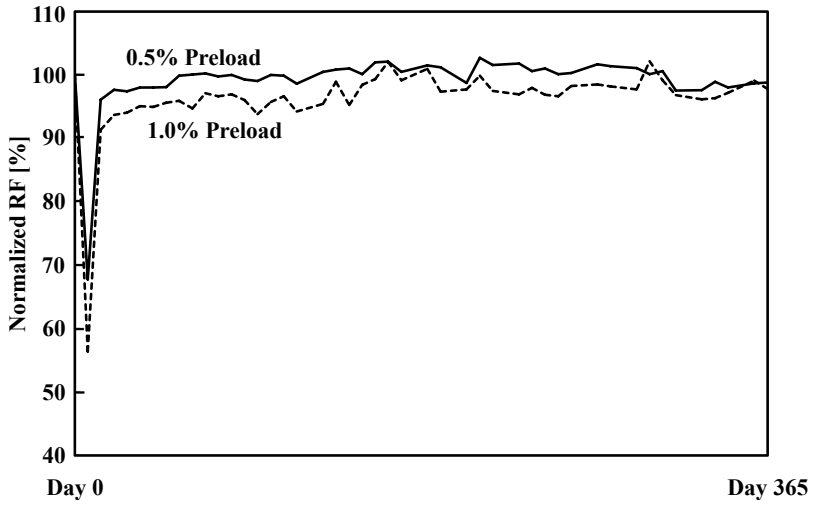

Figure 4.3: Effect of natural environment exposure time on RF recovery. Data is for specimens exposed to the natural environment for 12 months, and each data line is an average of 5 specimens.

The rate of RF recovery drastically decreased after the first week of natural environment exposure, but the Normalized RF values remained relatively stable between 95 and 105%. This is similar to results seen in past laboratory studies[5-9] and Chapter 3. The stabilized RF values do not appear to be altered by the length of exposure to the natural environment, meaning they remain stable under variable weather conditions.

The fluctuations in RF values between 95 and 105% shown in Figure 4.3 could be due to the dissolution and reformation of healing products between precipitation events. Similar fluctuations were seen in the RF results from Chapter 3, where visual observations also showed this dissolution and reformation. Calcium hydroxide ($Ca(OH)_2$), formed during the hydration reaction when cracks are exposed to precipitation, is easily dissolved in water and could be dissolving during rainfall events. Therefore, a sudden drop in RF could be due to the dissolution of $Ca(OH)_2$ during one rainfall event, and a sudden increase could be due to the reformation of $Ca(OH)_2$ and formation of other healing products during the next rainfall. Typically the large fraction of fly ash in the ECC mix would consume $Ca(OH)_2$ during the pozzolanic reaction, but the kinetics of this reaction are slow and may not be occurring fast enough during each precipitation event to transform the $Ca(OH)_2$ into the more stable C-S-H gel.

Figure 4.4 shows the effect of multiple damage (reloading) events on RF recovery. For Set 1, where the samples were subjected to multiple damage events, it was found that the amount of RF recovery decreased after each loading cycle, but the samples were still able to recover to reasonable RF values after three reloading events. There was a drastic drop in RF values after each reloading event due to the reopening of healed cracks and the formation of new cracks within the specimens, yet the values recovered significantly even after only one additional week of natural environment exposure. After the third loading cycle, the specimens preloaded to 0.5% were able to recover to 88% and the 1.0% specimens recovered to 84%. This shows that self-healing in ECC is relatively repeatable, despite deterioration in the magnitude of recovery with each damage cycle.

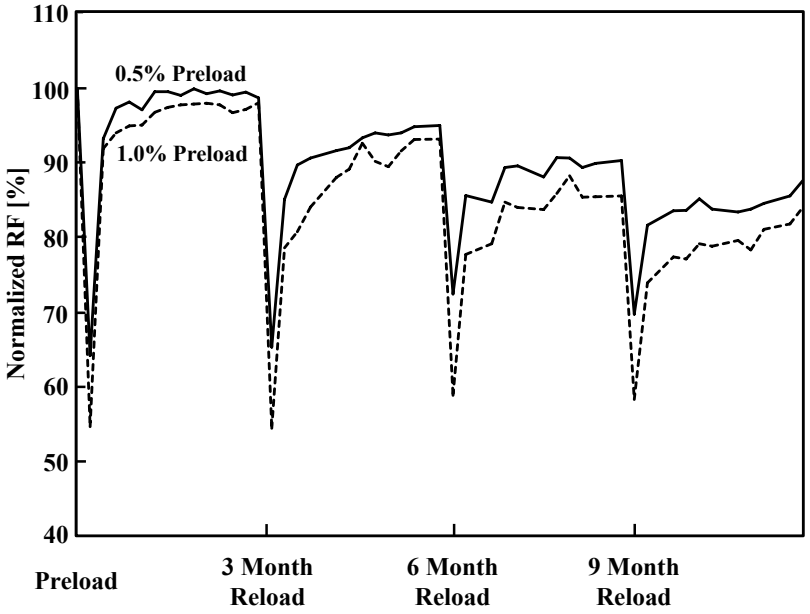

Figure 4.4: Effect of multiple damage events on recovery of RF.
Each data line is an average of 5 specimens.

4.3.2 Stiffness and First Cracking Strength Recovery

To determine the level of stiffness recovery in a self-healed specimen, the stiffness of the specimen measured during reloading was compared to the stiffness value measured during preloading. The secant stiffness was measured between 0.5 and 2.0 MPa and the stiffness recovery was calculated using Equation 4.3, where E_{reload} is the secant stiffness of the specimen during reloading and $E_{preload}$ is the secant stiffness of the specimen during preloading.

$$\text{Stiffness Recovery} = \frac{E_{reload}}{E_{preload}} \tag{4.3}$$

$$\text{First Cracking Strength Recovery} = \frac{\sigma_{reload}}{\sigma_{preload}} \tag{4.4}$$

The recovery of first cracking strength was also determined by comparing the value measured during reloading with the value measured during preloading. Following the JSCE design recommendation[10], the first cracking strength was defined as the stress value when the first crack was initiated under tensile loading, where the assumption of linear elasticity could no longer hold.

The first cracking strength was then calculated using Equation 4.4, where σ_{reload} is the first cracking strength of the specimen during reloading and $\sigma_{preload}$ is the first cracking strength of the specimen during preloading.

On reloading, it was found that the level of stiffness recovery increased as the duration of natural environment exposure (3, 6, 9, and 12 months) increased (Figure 4.5 (a)). The specimens reloaded at 3 months had regained, on average, 62% of their initial stiffness value when preloaded to 0.5%. The level of stiffness recovery continued increasing with the amount of natural environment exposure, with stiffness recoveries often greater than 100% after 6 months. This level of recovery has also been seen in previous work where specimens have been healed under controlled laboratory conditions.[7] The stiffness recovery of control specimens preloaded to 0.5 and 1.0% and immediately reloaded without allowing any self-healing to occur was also calculated and is shown in Figure 4.5 (a) for comparison. These serve as references for the actual stiffness recovery observed in specimens exposed to the natural environment.

Stiffness recovery can be attributed to both the healing of microcracks and the increase in stiffness of the bulk material due to continued hydration. As seen by the control specimens in Figure 4.5 (a), the stiffness of specimens during reloading is quite low when no self-healing occurs. This is due to the fact that microcracks reopen during reloading with little resistance by the partially debonded fibers bridging the crack faces. If there were no healing of the microcracks in specimens exposed to the natural environment, the composite stiffness would remain low even if there was continued hydration of the bulk material since the low stiffness of the crack planes would dominate the overall stiffness. This is analogous to a number of low stiffness (unhealed cracks) and high stiffness (bulk material) springs connected in series. Therefore, the observed increase in composite stiffness of the specimens exposed to the natural environment over those of the control specimens confirms that the microcracks did heal. However, since recoveries often reach over 100%, this implies that both self-healing and continued hydration of the bulk material contribute to the overall stiffness of the self-healing specimens.

The large standard deviations seen in Figure 4.5 (a) can be attributed to the various levels of healing between specimens. The stiffness of a self-healed specimen is highly dependent on the crack width distribution. Larger cracks will not heal as completely as smaller cracks and could

reduce the overall stiffness of the specimen. Since all specimens have different crack width distributions after preloading, the level of healing will vary and the stiffness recoveries can very greatly depending on the size and number of cracks.

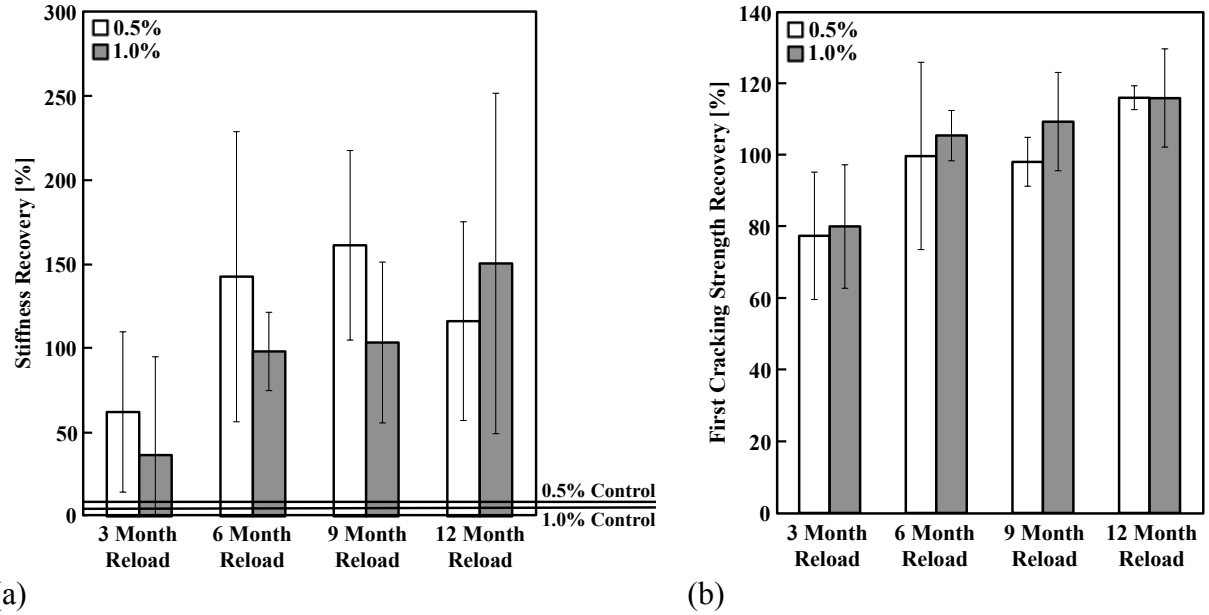

Figure 4.5: Effect of natural environment exposure time on recovery of mechanical properties. Recovery of (a) stiffness and (b) first cracking strength.
Each data bar is an average of 5 specimens.

Similar to the stiffness recovery results, the first cracking strength recovery also increased as the duration of natural environment exposure increased (Figure 4.5 (b)). The average recovery levels were near 80% after the first 3 months of natural environment exposure, but then increased to an average of 116% for both the 0.5 and 1.0% preloaded specimens after 12 months of exposure. This high level of recovery is not always seen under laboratory conditions, where first cracking strengths after self-healing are often lower than the first cracking strengths seen during preloading.[6,7] These high levels of recovery are most likely due to the relatively long duration of natural environment exposure, where specimens are exposed to large amounts of precipitation. This causes continued hydration and thus an increase in fracture toughness of the material, which increases the first cracking strength.

Figure 4.6 shows the effect of multiple damage (reloading) events on stiffness and first cracking strength recovery. There was no consistent increasing or decreasing trend in the level of stiffness or first cracking strength recovery for specimens in Set 1, which underwent multiple reloading events at 3, 6, 9, and 12 months. It was hypothesized that the extent of recovery may be directly related to the natural environment conditions experienced by the specimens prior to each reloading event. To test this hypothesis, the total amount of precipitation and the average temperature over each 3 month interval prior to the reloading events were calculated and are also shown in Figure 4.6 (the temperature and precipitation data for Ann Arbor, Michigan, were collected from Weather Underground[11]). There is a reasonably consistent trend between the level of stiffness and first cracking strength recovery and the amount of precipitation, although there is not a significant increase in precipitation to account for the increase in recoveries for the 12 month reloading event. However, there is an extremely consistent trend between the amount of stiffness and first cracking strength recovery and the average temperature. So, while there was no significant increase in the amount of precipitation to account for the increase in stiffness and first cracking strength recovery for the 12 month reloading event, there was a large increase in the average temperature. This suggests that both temperature and the amount of precipitation play an important role in the self-healing of ECC in the natural environment.

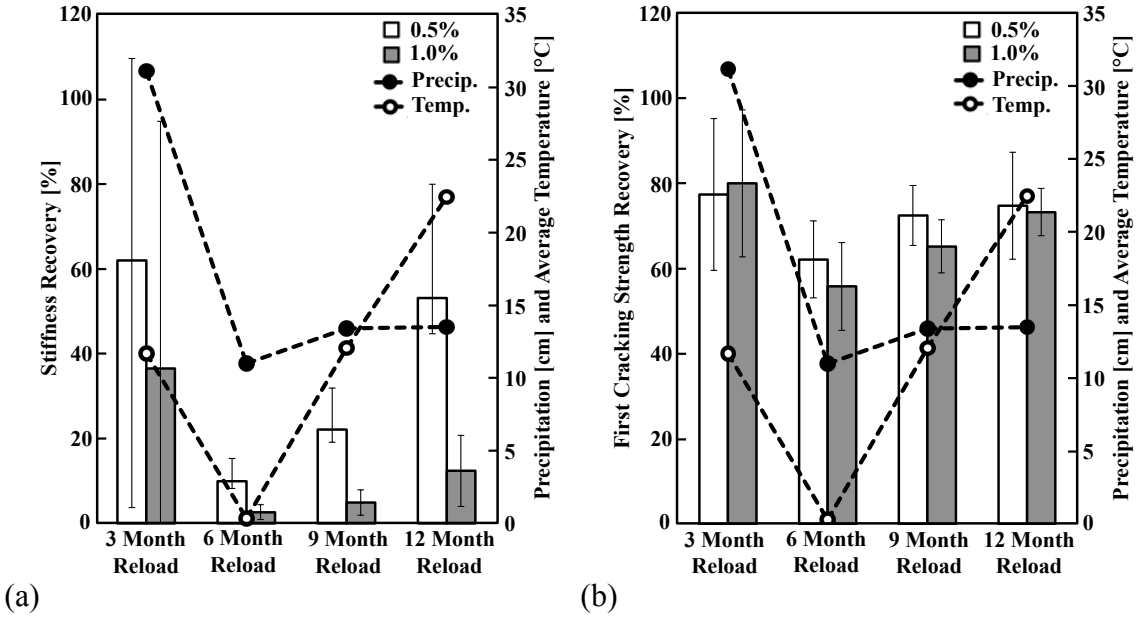

Figure 4.6: Effect of precipitation and average temperature on self-healing. Recovery of (a) stiffness and (b) first cracking strength. Each data bar is an average of 5 specimens.

Even with the varying amounts of precipitation and changes in average temperature, both the 0.5 and 1.0% preloaded specimens had average stiffness recovery values larger than the corresponding controls (without self-healing) shown in Figure 4.5 (a) for every reloading event. However, the recovery was not 100%. The highest recovery was during the 3 month reloading, with 62% recovery for the 0.5% preload and 37% for the 1.0% preload, and the lowest recovery was seen during the 6 month reloading, with 10% for the 0.5% preload and 3% for the 1.0% preloaded specimens.

Although the recovery of the first cracking strengths did not reach 100%, the level of recovery was still relatively high for every reloading event. Similar to stiffness recovery, the highest first cracking strength recovery was during the 3 month reloading event (77% for the 0.5% preloaded specimens and 80% for the 1.0% preload) and the lowest recovery was during the 6 month reloading event (62% for the 0.5% preload and 56% for the 1.0% preload).

Since there was recovery of both the stiffness and first cracking strengths after each loading cycle, this suggests that self-healing of ECC in the natural environment is repeatable, but highly dependent on the amount of damage and weather conditions.

4.4 Conclusions

While the study detailed in Chapter 3 determined that self-healing of ECC in the natural environment is feasible, the work described in this chapter covers a more extensive study aimed at fully characterizing the self-healing behavior of ECC in the natural environment. Based on the results of this experimental investigation, the following conclusions can be drawn:

- Self-healing in ECC is not limited to a controlled laboratory environment and can occur in the natural environment, under random and sometimes extreme environmental conditions.
- ECC specimens recovered between 95 and 105% of their original RF values when exposed to the natural environment. The small fluctuations in RF readings are most likely due to the dissolution and reformation of healing products caused by large rainfall events, which is consistent with the visual observations described in Chapter 3.
- For specimens that underwent multiple loading cycles, the amount of RF recovery decreased after each loading event. However, even after the third damage cycle, the

specimens loaded to 0.5% tensile strain were still able to recover up to 88% of their initial RF value and the specimens strained to 1.0% recovered up to 84%.

- The level of stiffness and first cracking strength recovery increased with the time of natural environment exposure, often exceeding 100% recovery after 6 months.
- There was stiffness and first cracking strength recovery after each loading event for the samples that underwent multiple loading cycles. However, it was found that the extent of recovery depended significantly on the average temperature and amount of precipitation during the exposure period. For this reason, the effects of temperature on self-healing and mechanical property recovery in ECC were studied in more detail and are covered in Chapter 6.
- Lastly, the large standard deviations in the stiffness recovery data can be attributed to variations in the level of healing due to varying crack width distributions of each sample. The exact correlation between crack width distribution and mechanical property recovery was investigated and the experimental procedure and results are described in Chapter 7.

References

[1] Edvardsen, C. (1999). Water Permeability and Autogenous Healing of Cracks in Concrete. *ACI Materials Journal, 96*, 448–455.

[2] Reinhardt, H.W. & Jooss, M. (2003). Permeability and self-healing of cracked concrete as a function of temperature and crack width. *Cement and Concrete Research, 33*, 981-985.

[3] Li, V.C., Wang, S., & Wu, C. (2001). Tensile Strain-Hardening Behavior of PVA-ECC. *ACI Materials Journal, 98*, 483-492.

[4] Li, V.C., Wu, C., Wang, S., Ogawa, A., & Saito, T. (2002). Interface Tailoring for Strain-Hardening PVA-ECC. *ACI Materials Journal, 99,* 463-472.

[5] Sahmaran, M. & Li, V.C. (2008). Durability of mechanically loaded engineered cementitious composites under highly alkaline environments. *Cement and Concrete Composites, 30*, 72-81.

[6] Yang, Y., Lepech, M.D., Yang, E., & Li, V.C. (2009). Autogenous healing of engineered cementitious composites under wet-dry cycles. *Cement and Concrete Research, 39*, 382-390.

[7] Yamamoto, A., Watanabe, K., Li, V.C., & Niwa, J. (2010). Effect of wet-dry condition on self-healing property of early-age ECC. *Japan Concrete Institute, 32*, 251-256.

[8] Li, M. & Li, V.C. (2011). Cracking and Healing of Engineered Cementitious Composites under Chloride Environment. *ACI Materials Journal, 108*, 333-340.

[9] Yang, Y., Yang, E.H., & Li, V.C. (2011). Autogenous healing of engineered cementitious composites at early age. *Cement and Concrete Research, 41*, 176-183.

[10] Japan Society of Civil Engineers. (2008). *Recommendations for Design and Construction of High Performance Fiber Reinforced Cement Composites with Multiple Fine Cracks (HPFRCC)*. Tokyo, Japan.

[11] Weather Underground Home Page. Available online: www.wunderground.com (accessed on 01 September 2012).

CHAPTER 5: CHARACTERIZATION OF BACTERIALLY MEDIATED SELF-HEALING

5.1 Introduction

As described in Chapter 2, bacteria have been used to induce and improve self-healing in concrete, but this approach has not been attempted in ECC. Although self-healing of ECC can occur fully under controlled laboratory conditions, complete self-healing does not always occur under field conditions (Chapters 3 and 4). Therefore, bacteria were used to investigate the potential of increasing the self-healing functionality of ECC.

This chapter will describe the selection process used to determine the most suitable bacteria and substrate for incorporation into an ECC mix, the mix development process to ensure neither the bacteria or substrate negatively impact the mechanical properties of ECC, and the overall impact of the bacteria on the self-healing functionality of ECC.

5.2 Bacteria and Substrate Selection

In this approach to improving self-healing, bacteria and an organic growth substrate are incorporated into the ECC mix. When a crack occurs and is exposed to water, the bacteria consume the substrate and this metabolic conversion induces the precipitation of healing products. Therefore, it is important to choose a bacterial strain that will function well and remain viable within the ECC matrix, as well as an appropriate organic growth substrate for the bacteria to consume.

Due to the high alkalinity of cement and the harsh conditions within a cementitious matrix, it was important to select bacteria that would be able to survive under these conditions. In order for the bacteria to withstand the high pH environment of the ECC matrix, it was determined that the bacteria chosen for this study must be an obligate alkaliphile. These types of bacteria require a high pH to survive, meaning that they could thrive within the highly alkaline ECC matrix. In

addition, the bacteria must be able to withstand pressure caused by continued hydration and densification of the ECC mix. Over time, the size of the pores in the ECC matrix will decrease due to continued hydration, potentially putting the bacteria under considerable compressive stress. For this reason, it was decided that the bacteria chosen must be spore-forming. In spore-forming bacteria, a fully functional vegetative cell will become dormant and produce a spore under adverse environments (Figure 5.1). Spores are much more resilient than vegetative cells and are able to withstand harsh environmental conditions. Once conditions improve, these spores germinate back into a vegetative state. Therefore, bacterial spores will be incorporated into the ECC mix and remain dormant until cracks form and are exposed to water. When the spores are in contact with water, they will germinate back into vegetative cells where they can metabolize the available growth substrate and induce the precipitation of healing products.

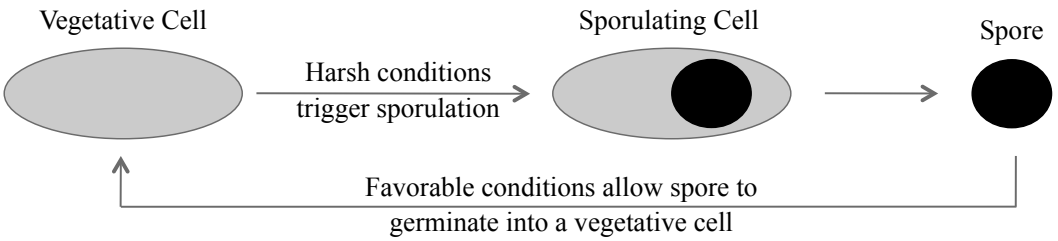

Figure 5.1: Harsh environmental conditions trigger sporulation in spore-forming bacteria. The spores can then germinate back into a vegetative state once conditions improve.

In addition to withstanding the harsh conditions within the ECC matrix, the bacteria chosen must also be able to remain viable under various environmental conditions experienced in the field, including large temperature ranges and high salt concentrations from deicing during the winter. For this reason, temperature range for growth and sodium chloride tolerance were also considered when selecting bacteria for use in this study.

Bacillus cohnii was the bacteria ultimately chosen for use in this experiment based on its ability to produce spores, tolerate highly alkaline and chloride environments, and its optimal pH and temperature range for growth. *Bacillus cohnii* are a spore-forming and obligate alkaliphile bacteria that are able to remain viable between 10 and 47°C and in environments containing up to 10% sodium chloride.[1] These characteristics indicate that *Bacillus cohnii* are more likely than

other bacterial strains to remain viable within the ECC matrix. *Bacillus cohnii* have also been used in previous studies in order to induce self-healing in traditional concrete materials.[2,3]

Calcium lactate was chosen as the organic growth substrate to be incorporated into the ECC mix. It has been shown to be successful in inducing precipitation of healing products in previous self-healing studies when combined with *Bacillus cohnii,* and has been shown to not negatively impact the mechanical properties of the concrete.[2] This is an important consideration when choosing substrates to be included in an ECC mix, since neither the substrate or bacterial spores should hinder the multiple cracking behavior and tensile strain capacity of the ECC material. The exact effect calcium lactate and *Bacillus cohnii* spores on mechanical properties of ECC is discussed in Section 5.3.3.

The addition of *Bacillus cohnii* spores and calcium lactate into the ECC matrix will induce the precipitation of healing products as shown in Equations 5.1 and 5.2.[2] Equation 5.1 is the bacterial metabolic conversion of calcium lactate ($CaC_6H_{10}O_6$), yielding calcium carbonate ($CaCO_3$) and carbon dioxide (CO_2). $CaCO_3$ will precipitate and fill the cracks as a healing product, while the CO_2 is consumed in a secondary reaction (Equation 5.2). The CO_2 from Equation 5.1 reacts with available calcium ions from calcium hydroxide ($Ca(OH)_2$), a product of the cement hydration reaction, to further increase the precipitation of $CaCO_3$. Therefore, the bacterial metabolic conversion of calcium hydroxide induces the precipitation of $CaCO_3$, leading to more complete and faster rates of self-healing.

$$CaC_6H_{10}O_6 + 6O_2 \rightarrow CaCO_3 + 5CO_2 + 5H_2O \quad (5.1)$$

$$5CO_2 + Ca(OH)_2 \rightarrow 5CaCO_3 + 5H_2O \quad (5.2)$$

5.3 Mix Development

5.3.1 Bacteria and Substrate Incorporation

Calcium lactate was incorporated into ECC by dissolving it in the mix water prior to mixing and casting of the ECC specimens. During initial mix development, two sample sets containing calcium lactate were prepared, where the amounts added were equivalent to 0.08 and 0.8% of the weight of the ECC mix. These concentrations were chosen based on previous research and to determine the effect of calcium lactate on the mechanical properties of ECC.[3]

Similar to calcium lactate, *Bacillus cohnii* spores were also incorporated into ECC through the mix water. Spores were generated in a liquid medium and then washed to remove all medium from the surface of the spores. This washing was necessary to ensure that no medium would be transferred to the ECC mix where it could negatively impact the mechanical properties of the material. Once the spores were washed, they were then suspended into the mix water prior to mixing and casting of the ECC specimens. Enough spores were incorporated into the mix to achieve a concentration of 10^8 *Bacillus cohnii* spores/cm^3. This target concentration was chosen based on previous self-healing studies utilizing *Bacillus cohnii*.[3]

5.3.2 Mix Proportions, Raw Materials, and Specimen Preparation

In the initial mix development for this study, *Bacillus cohnii* spores and calcium lactate were incorporated separately into an existing ECC mix to evaluate the impacts on the characteristic properties of ECC. Since ECC is known for its ductility, it was important to verify that the incorporation of biomass and growth substrate did not hinder the multiple cracking behavior and tensile strain capacity of the ECC material.

The basic ECC mix proportion, without calcium lactate or bacterial spores, is shown in Table 5.1. Type I ordinary Portland cement, Class F fly ash, silica sand with an average particle size of 110 μm, a polycarboxylate-based high range water reducing admixture (HRWRA), and polyvinyl alcohol (PVA) fibers were used to prepare the ECC specimens. The PVA fibers accounted for 2% of the total mix volume and were 12 mm in length with an average diameter or 39 μm. The surfaces of the fibers were coated with an oiling agent (1.2% by weight) to reduce the interfacial chemical bond between the fiber and matrix caused by the strong hydrophobic nature of the PVA fibers.[4,5]

Table 5.1: Basic ECC mix proportion, without growth substrate or bacterial spores.

Component	Cement	Fly Ash	Sand	Water	HRWRA	Fiber
Weight Fraction	1	1.2	0.8	0.55	0.013	0.046

To determine the effect of the bacterial spores and organic growth substrate on the mechanical properties of ECC, four sample sets were prepared. The first was a control set, using only the materials and proportions shown in Table 5.1. The next set was the same as the control, but with 10^8 *Bacillus cohnii* spores/cm^3. The final two sets were also the same as the control, but with

calcium lactate concentrations equal to 0.08 and 0.8% of the weight of the mix. The bacterial spores and calcium lactate were incorporated into the ECC matrix through the mix water, as described in Section 5.3.1.

For each sample set, the raw materials were mixed in a 20 L force-based Hobart mixer. After mixing, the fresh ECC was cast into molds measuring 300 mm x 76 mm x 12.5 mm and covered in plastic sheeting. After 24 hours, the specimens were removed from the molds and cut to 200 mm in length to minimize edge effects and bending stresses caused during uniaxial tensile loading. Specimens were then air cured at room temperature until testing. The day prior to testing, aluminum plates were glued to both ends of the specimens to facilitate gripping within the load frame.

5.3.3 Effect of Bacteria and Substrate Addition

All specimens were loaded in uniaxial tension at an age of 28 days to determine if the addition of *Bacillus cohnii* spores and calcium lactate altered the tensile properties of ECC. Loading was applied using a 25 kN capacity load frame (MTS Model 810) under displacement control and a loading rate of 0.5 mm/min. Two Linear Variable Displacement Transducers (LVDTs) were attached to the specimens during loading to measure tensile deformation.

Figure 5.2 shows the uniaxial tensile results of the four sample sets that were tested. The ECC controls and the samples containing *Bacillus cohnii* spores had similar first cracking and ultimate strengths, but the tensile strain capacity was greater and the results were more consistent in the samples containing bacterial spores. This greater strain capacity and consistency could be due to clumping of the spores. The *Bacillus cohnii* spores were rinsed and washed in a centrifuge, resulting in large clumps of spores at the bottoms of the vials that were used in this preparation step. When the spores were transferred to the ECC mix water, the water was mixed and agitated thoroughly to disperse the spores, but it is possible that there was still clumping of the spores when the mix water was added to the rest of the ECC raw materials. If this was the case, the clumps of *Bacillus cohnii* spores could have been acting as flaws within the ECC matrix, resulting in improved tensile properties. Previous research has shown improvement in multiple cracking behavior and tensile strain capacity when artificial flaws have been added to an ECC mix, so it is possible that the clumping of bacterial spores could have caused this same behavior.[6]

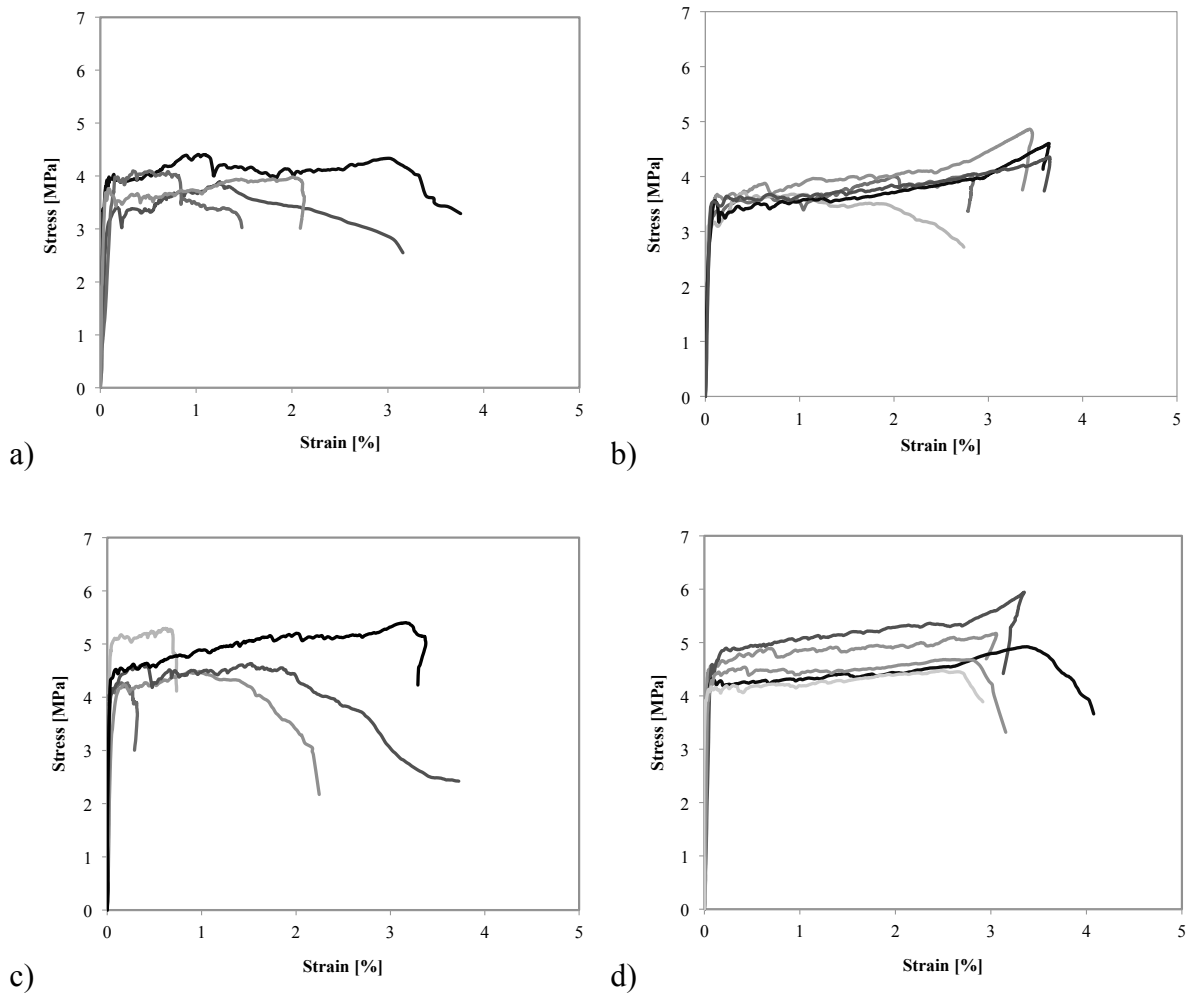

Figure 5.2: Effect of *Bacillus cohnii* spores and calcium lactate on the tensile properties of ECC. Graphs show 28 day tensile loading results for (a) ECC controls, (b) samples containing *Bacillus cohnii* spores, (c) samples containing 0.08% calcium lactate, and (d) samples containing 0.8% calcium lactate.

Figure 5.2 (c) and (d) show the effects of calcium lactate addition on the tensile properties of ECC. Both mixes containing calcium lactate performed better than the ECC control mix (Figure 5.2 (a)), with higher first cracking and ultimate strengths. In addition, the samples containing 0.8% calcium lactate had improved tensile strain capacities. This increase in performance was attributed to the increased amount of calcium ions present within the matrix from the calcium lactate. These ions were most likely consumed during the pozzolanic reaction, leading to the production of additional C-S-H within the ECC matrix and an increase in the fracture toughness of the material.

5.3.4 Final Mix Design, Specimen Preparation, and Preloading

Since the addition of *Bacillus cohnii* spores and calcium lactate did not negatively impact the multiple cracking behavior and tensile strain capacity of ECC, it was concluded that these components could be used for the remainder of this study to investigate their potential of increasing the self-healing capacity of ECC. The final mix design used in this study included the proportions shown in Table 5.1, *Bacillus cohnii* spores at a concentration of 10^8 spores/cm^3, and a calcium lactate content of 0.4% by weight. Although a calcium lactate content of 0.8% was shown to improve the tensile strain capacity of ECC, 0.4% was chosen for the final mix to reduce costs while ensuring an adequate amount of substrate for the bacterial spores to consume. Specimens were prepared and preloaded in the same manner as described in Sections 5.3.2 and 5.3.3, with the preloaded specimens damaged to a level of 2% tensile strain.

5.4 Environmental Conditioning and Evaluation Methods

Three types of environmental conditioning were used in this study. Samples were either exposed to a continuously dry environment, a continuously wet environment, or cyclic wetting and drying. The samples exposed to the continuously dry environment were stored in laboratory air at room temperature, while the samples exposed to the continuously wet environment were kept in water baths at room temperature. Samples exposed to the cyclic wetting and drying were submerged in water for 24 hours, followed by 24 hours of drying in laboratory air. Environmental conditioning was conducted for 20 days, so the samples undergoing cyclic wetting and drying were exposed to ten healing cycles.

Resonant frequency (RF), photo documentation, and viability testing were used to evaluate the self-healing in ECC as well as the ability of the *Bacillus cohnii* spores to survive within the ECC matrix. RF measurements based on ASTM C215 for the longitudinal mode were taken before and after preloading to quantify the amount of damage, and every 48 hours to determine the rate of self-healing. The RF value of a specimen was calculated as the average of three consecutive RF measurements, and these values were normalized against control samples to account for the effects of continued hydration. To obtain visual evidence of healing products and supplement the RF data, photos of cracks were taken before and after environmental conditioning. In order to evaluate the viability of *Bacillus cohnii* spores in ECC over time, viability testing was performed

using the most probable number (MPN) technique four times over a 28 day period after initial casting of the specimens. This technique is described in more detail in Section 5.5.3.

5.5 Results and Discussion

5.5.1 Resonant Frequency Recovery

Figure 5.3 shows the RF recovery of ECC controls and ECC specimens containing *Bacillus cohnii* spores and calcium lactate. Results are extremely similar for both sample sets, indicating that the bacteria were not able to improve the overall RF recovery of ECC when samples were preloaded to 2% tensile strain. Samples exposed to the continuously dry environment experienced no regain in RF values after preloading. This was expected since no water was available to allow the *Bacillus cohnii* spores to germinate into vegetative cells, or to facilitate the traditional reactions that produce healing products. There was a significant regain in RF for the samples that were exposed to water, with samples recovering between 85 and 95% of their original RF values in both sample sets. However, the level of RF recovery was not dependent on how the samples were exposed to water, since the samples in the continuously wet environment recovered to approximately the same level as the samples that underwent cyclic wetting and drying.

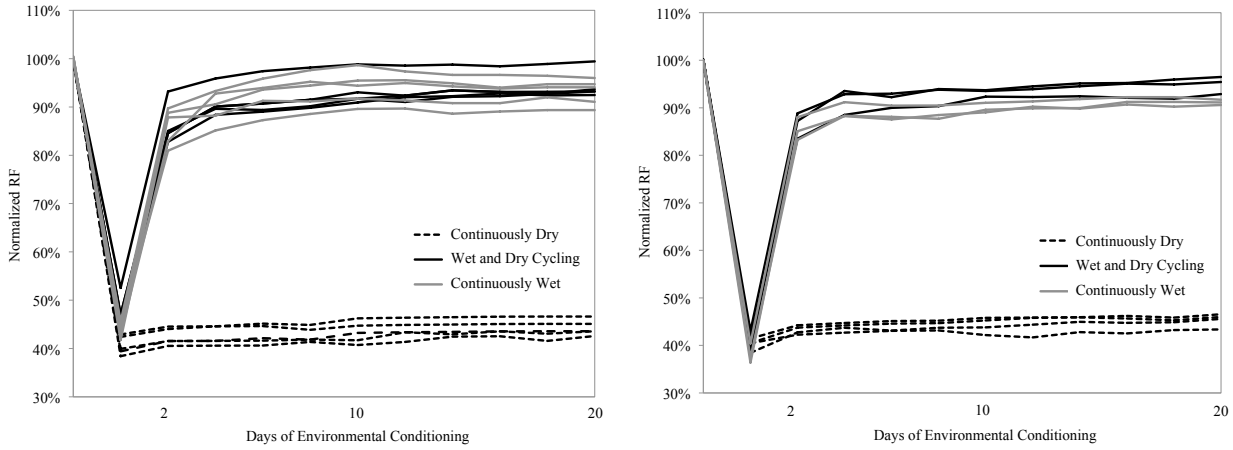

Figure 5.3: RF recovery of (a) ECC controls and (b) ECC containing *Bacillus cohnii* spores and calcium lactate under three environmental conditions.

5.5.2 Photo Documentation

(a) 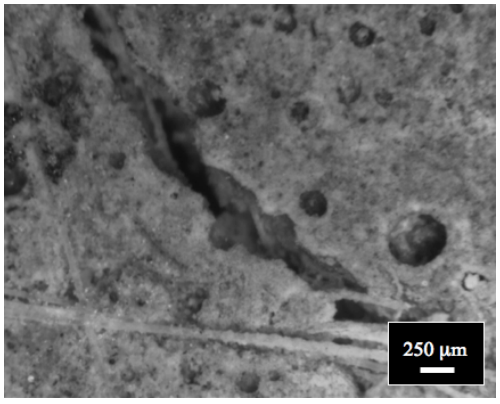

(b) 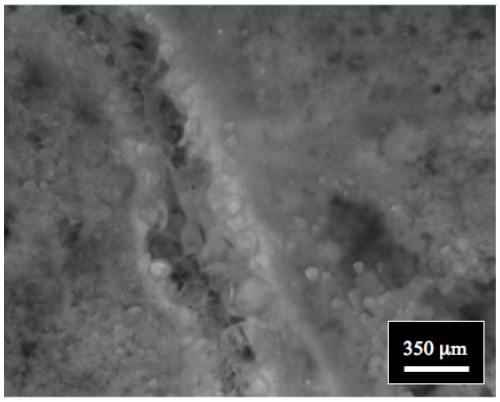

Figure 5.4: (a) A 250 μm crack exposed to cyclic wetting and drying and (b) a 350 μm crack continuously submerged in water.

(a) 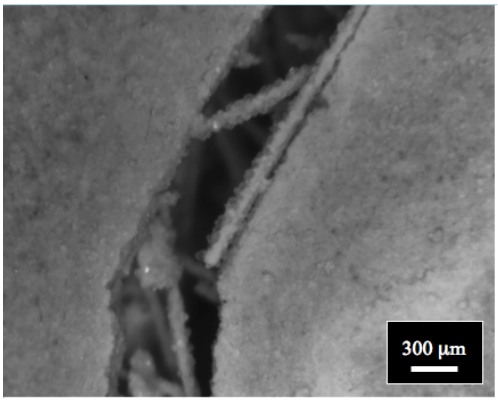

(b) 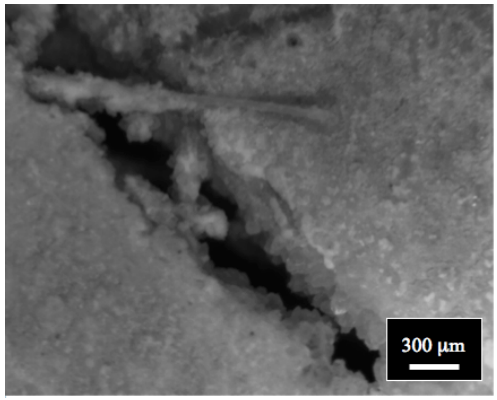

Figure 5.5: 600 μm cracks exposed to (a) cyclic wetting and drying and (b) continuous submersion in water.

Although the RF recovery results showed no significant difference between the control samples and samples containing *Bacillus cohnii* spores and calcium lactate, or the samples exposed to the continuously wet environment and the samples that underwent cyclic wetting and drying, extreme differences were seen through photo documentation. Two samples containing bacterial spores and calcium lactate that were accidentally loaded to failure during preloading, thus resulting in crack widths much larger than those typically seen when preloading ECC, were included in the continuously wet and cyclic wetting and drying regimes, and the differences can be seen in Figures 5.4 and 5.5. Figure 5.4 (a) shows a 250 μm crack that was exposed to cyclic

wetting and drying, while Figure 5.4 (b) shows a 350 μm crack exposed to the continuously wet environment. There is very little visual evidence of healing in the 250 μm crack, but complete self-healing in the 350 μm crack that was continuously in water. These levels of self-healing were consistent throughout the entire length of each crack, but only one image of each is shown here. Figure 5.5 shows a similar situation, where a 600 μm crack that was in the continuously wet environment shows an abundance of healing products, while a 600 μm crack exposed to cyclic wetting and drying shows a much lower level of healing.

This visual evidence suggests that the *Bacillus cohnii* spores and calcium lactate contribute to self-healing when the samples are continuously exposed to water, but not when they are exposed to cyclic wetting and drying. This has been attributed to the fact that desiccation often causes loss of viability in bacteria, and does not trigger sporulation.[7] Spores in the samples exposed to cyclic wetting and drying are able to germinate and begin inducing the precipitation of healing products during the first healing cycle when they are exposed to water for 24 hours, but die and thus become incapable of producing healing products when the samples are allowed to dry during the 24 hours in laboratory air, producing visual evidence of self-healing similar to that seen in ECC control samples. This means that while bacterially mediated self-healing in ECC is feasible and has the potential to increase the self-healing functionality of ECC, this is only possible in structures that are continuously submerged in water, but could prove to be particularly useful in ECC mixes with larger crack widths.

5.5.3 Viability Testing

The most probable number (MPN) test was performed four times over the 28 day period after initial casting of the ECC specimens containing bacterial spores and calcium lactate to evaluate the viability of *Bacillus cohnii* spores in ECC over time. For each test, 1 g of an ECC sample was crushed and suspended in 9 mL of growth medium. 10-fold serial dilutions were prepared from the original suspension, with three replicates of each dilution, and incubated at 30°C for several hours. Positive dilutions, those showing bacterial growth, were then counted and the MPN value was determined from the standard MPN table.[8] The concentration in the original suspension was calculated using the MPN value and then converted to spores/cm^3 of ECC. It was found that

there was a decrease in the number of viable spores over time, with only 9% of the original spores remaining viable 28 days after mixing.

This decrease in viability was expected, and is most likely caused by continued hydration and decreasing pore size over time. Concrete has been shown to have average pore sizes ranging from approximately 0.03-0.05 μm at 28 days, while the spore size of *Bacillus cohnii* is 0.6-0.7 μm.[1,9] This means that the densification and decreasing pore size of the ECC matrix over time could create compressive forces large enough to crush the bacterial spores, causing a large loss of viability. Encapsulating the bacterial spores before incorporation into the ECC matrix may help reduce the severity of the loss of viability. This technique has been utilized by other researchers, often encapsulating the bacterial spores within expanded clay particles.[10,11] However, no long-term viability tests have been conducted using the encapsulation technique, so it is unclear if the bacterial spores could remain viable throughout the entire service life of a structure.

5.6 Conclusions

In this chapter, bacteria were used to investigate the potential of increasing the self-healing functionality of ECC. *Bacillus cohnii* spores and calcium lactate were incorporated into an ECC mix and the overall impact of the bacteria on the self-healing functionality of ECC was determined. Based on the results of this experimental investigation, the following conclusions can be drawn:

- The use of calcite-producing spore-forming bacteria is a promising technique to improve the self-healing functionality of ECC. However, self-healing was only improved in specimens that were continuously exposed to water. Therefore, while this technique is promising, it can only be used in structures that are continuously submerged in water, such as underground and water-retaining infrastructure.
- Cracks as large as 350 μm were completely healed after 20 days of exposure to a continuously wet environment. This level of healing has not been seen in ECC before, as previous research states that cracks must be below 150 μm (preferably below 50 μm) in order for significant healing to occur.[12] This means that this technique would prove to be particularly useful in ECC mixes with crack widths greater than 50 μm.

- There was a significant loss in viability of bacterial spores over time, with only 9% of the original spores remaining viable 28 days after mixing. This loss could be reduced by encapsulating the spores prior to incorporation within the ECC matrix, but no long-term viability tests have been performed to prove the effectiveness of this technique.

References

[1] Spanka, R. & Fritze, D. (1993). *Bacillus cohnii* sp. nov., a new, obligately alkaliphilic, oval spore-forming *Bacillus* species with ornithine and aspartic acid instead of diaminopimelic acid in the cell wall. *Int J Syst Bacteriol, 43,* 150-156.

[2] Jonkers, H.M., Thijssen, A., Muyzer, G., Copuroglu, O., & Schlangen, E. (2010). Application of bacteria as self-healing agent for the development of sustainable concrete. *Ecological Engineering, 36,* 230-235.

[3] Jonkers, H.M. & Schlangen, E. (2008). Development of a bacteria-based self healing concrete. *Tailor Made Concrete Structures.* Taylor & Francis Group, London, ISBN 978-0-415-47535-8.

[4] Li, V.C., Wang, S., & Wu, C. (2001). Tensile Strain-Hardening Behavior of PVA-ECC. *ACI Materials Journal, 98*, 483-492.

[5] Li, V.C., Wu, C., Wang, S., Ogawa, A., & Saito, T. (2002). Interface Tailoring for Strain-Hardening PVA-ECC. *ACI Materials Journal, 99,* 463-472.

[6] Wang, S. & Li, V.C. (2004). Tailoring of pre-existing flaws in ECC matrix for saturated strain hardening. Proceedings from FRAMCOS-5, Vail, Colorado, USA, 1005-1012.

[7] Slepecky, R.A. & Hemphill, H.E. (2006). The Genus *Bacillus* – Nonmedical. *The Prokaryotes.* Springer, ISBN 978-0-387-25494-4. 530-562.

[8] Alexander, M. (1982). Most Probable Number Method for Microbial Populations. *Methods of Soil Analysis (2nd edition).* American Society of Agronomy, Madison, WI.

[9] Kou, S.C., Poon, C.S., & Etxeberria, M. (2011). Influence of recycled aggregates on long term mechanical properties and pore size distribution of concrete. *Cement and Concrete Composites, 33,* 286-291.

[10] Jonkers, H.M. (2011). Bacteria-based self-healing concrete. *Heron, 56*, 1-12.

[11] Wiktor, V. & Jonkers, H.M. (2011). Quantification of crack-healing in novel bacteria-based self-healing concrete. *Cement and Concrete Composites, 33*, 763-770.

[12] Yang, Y., Lepech, M.D., Yang, E., & Li, V.C. (2009). Autogenous healing of engineered cementitious composites under wet-dry cycles. *Cement and Concrete Research, 39*, 382-390.

PART III: SCIENTIFIC UNDERSTANDING OF THE SELF-HEALING PHENOMENA IN ECC

CHAPTER 6: ROBUSTNESS OF SELF-HEALING FUNCTIONALITY

6.1 Introduction

If self-healing ECC is to be used in field applications, it will be expected to have robust self-healing functionality throughout its entire service life. Infrastructure will inevitably age and be exposed to a wide range of environmental conditions, so the effects of specimen age and exposure temperature on the ability of ECC to self-heal were studied to gain a better understanding of the robustness of the healing process. In this chapter, experimental investigations utilizing resonant frequency (RF) measurements, uniaxial tensile (reloading) tests, and digital image correlation (DIC) were used to assess the robustness of self-healing in ECC at various ages and exposure temperatures. Self-healing must be able to occur to a reasonable extent regardless of specimen age and exposure temperatures in order for the healing to be considered robust and appropriate for field applications.

6.2 Effects of Specimen Age

In this section, the experimental investigation used to assess the robustness of self-healing in ECC over time is described.

6.2.1 Mix Proportion and Raw Materials

The ECC mix proportion used in this study is given in Table 6.1. Type I ordinary Portland cement, Class F fly ash, silica sand with an average particle size of 110 μm, a polycarboxylate-based high range water reducing admixture (HRWRA), and polyvinyl alcohol (PVA) fibers were

used to prepare the ECC specimens. The PVA fibers accounted for 2% of the total mix volume and were 12 mm in length with an average diameter of 39 μm. The fibers had a tensile strength of 1600 MPa, a density of 1300 kg/m^3, an elastic modulus of 42.8 GPa, and a maximum elongation of 6%. In addition, the surfaces of the fibers were coated with an oiling agent (1.2% by weight) to reduce the interfacial chemical bond between the fiber and matrix caused by the strong hydrophilic nature of the PVA fibers.[1,2]

Table 6.1: ECC mix proportion.

Component	Cement	Fly Ash	Sand	Water	HRWRA	Fiber
Weight Fraction	1	1.2	0.8	0.55	0.013	0.046

6.2.2 Specimen Preparation, Preloading, and Environmental Conditioning

The raw materials were mixed in a 20 L force-based Hobart mixer according to the proportions shown in Table 6.1. After mixing, the fresh ECC was cast into molds measuring 300 mm x 76 mm x 12.5 mm and covered in plastic sheeting. After 24 hours, the specimens were removed from the molds and cut to 200 mm in length to minimize the edge effects and bending stresses caused during uniaxial tensile loading. Specimens were then air cured at room temperature until testing. The day prior to preloading, aluminum plates were glued to both ends of the specimens to facilitate gripping within the load frame.

In this experiment, three sample sets of three specimens each were used to study the effect of age on self-healing in ECC. While all specimens were preloaded to a damage level of 1% tensile strain, each sample set was preloaded at a different age. The ages used for preloading in this study were 1, 9, and 28 months after casting. To preload the samples, uniaxial tensile loading was applied using a 25 kN capacity load frame (MTS Model 810) under displacement control and a loading rate of 0.5 mm/min. Two Linear Variable Displacement Transducers (LVDTs) were attached to the specimens during loading to measure tensile elongation. When the tensile strain reached 1%, the tensile load was released and the samples were unloaded and removed from the load frame.

After preloading, the samples were allowed to heal under cyclic wetting and drying. Each cycle consisted of submerging the samples in water for 24 hours, followed by 24 hours of drying in

laboratory air. Ten cycles were completed before the samples were reloaded to determine the level of mechanical property recovery.

6.2.3 Evaluation Methods

In order to determine the effect of specimen age on the self-healing functionality of ECC, self-healing progress was examined using three evaluation methods: resonant frequency (RF) measurements, uniaxial tensile (reloading) tests, and digital image correlation (DIC).

RF measurements based on ASTM C215 for the longitudinal mode were used to monitor the rate of self-healing in the preloaded specimens. RF measurements were taken before and after preloading to quantify the amount of damage, and then after each 48 hour wetting and drying cycle to evaluate the rate of self-healing. The RF value of a specimen was calculated as the average of three consecutive RF measurements. It should be noted that the RF data in this study is presented as the RF Ratio (Equation 6.1), where $RF_{original}$ is the RF value of the sample before preloading and $RF_{environment}$ is the RF value of the specimen during cyclic wetting and drying. Therefore, this RF data does not account for the effect of continued hydration.

$$\text{RF Ratio} = \frac{RF_{environment}}{RF_{original}} \tag{6.1}$$

Uniaxial tensile (reloading) tests were conducted after ten wetting and drying cycles to determine the level of stiffness and first cracking strength recovery due to self-healing. All reloading tests were conducted using the same method described for preloading in Section 6.2.2, but specimens were loaded to failure instead of 1% tensile strain. In this study, the first cracking strength ($\sigma_{preload}$ and σ_{reload}) and secant stiffness ($E_{preload}$ and E_{reload}) during preloading and reloading were defined as shown in Figure 6.1. A linear best-fit line was drawn through the elastic range of each stress-strain curve and the stress value at the point of deviation was considered to be the first cracking strength. The stiffness was then defined as the secant stiffness between the origin and first cracking strength. Stiffness and first cracking strength recoveries were then calculated using Equations 6.2 and 6.3, where the stiffness and first cracking strengths during reloading were compared to those measured during preloading. Due to how these variables are defined,

complete recovery of initial mechanical properties through self-healing does not occur unless both the stiffness and first cracking strength recoveries are 100%.

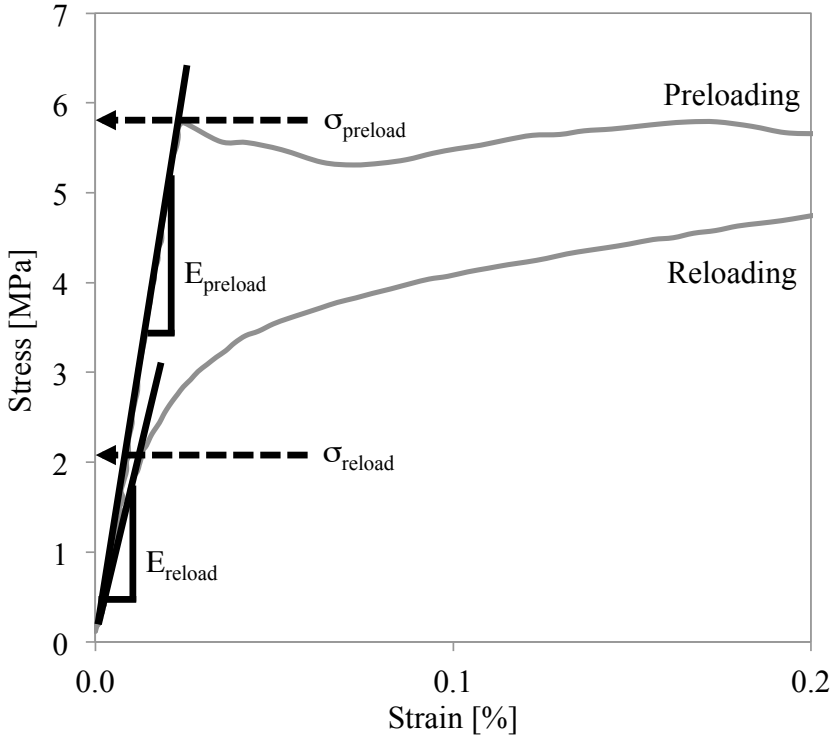

Figure 6.1: First cracking strength and stiffness definition.

$$\text{Stiffness Recovery} = \frac{E_{reload}}{E_{preload}} \tag{6.2}$$

$$\text{First Cracking Strength Recovery} = \frac{\sigma_{reload}}{\sigma_{preload}} \tag{6.3}$$

DIC was used as a method to assess crack formation and propagation in samples during preloading and reloading. DIC is an optical surface deformation measuring system that can determine surface displacements and crack opening information by imaging the surfaces of samples during loading. This technique was used to determine if the healing products were robust enough to generate new cracks during reloading. If new cracks were able to form before the original cracks from preloading reopened, this would signify that the healing products were

strong enough to completely bind the crack faces, thus indicating complete self-healing. However, if no new cracks were formed during reloading, or these new cracks formed only after all the original cracks from preloading reopened, then self-healing was not complete and the healing products were not able to completely bind the crack faces.

6.2.4 Resonant Frequency Results

Similar to previous self-healing studies, there was a large drop in RF values after preloading due to the formation of cracks within the samples, and most recovery occurred after the first wetting and drying cycle (Figure 6.2).[3-6] However, the levels of healing obtained during this first cycle were highly dependent on specimen age, with the one and nine month samples recovering to an average of 92 and 90%, and the 28 month old samples recovering to an average of 72%. After the first healing cycle, the rate of self-healing slowed, but the level of RF recovery continued to increase as the samples were exposed to more wetting and drying cycles. The samples preloaded at one and nine months after casting ultimately recovered to an average RF ratio of 101% after 10 healing cycles, while the samples damaged at 28 months only recovered to an average of 81%.

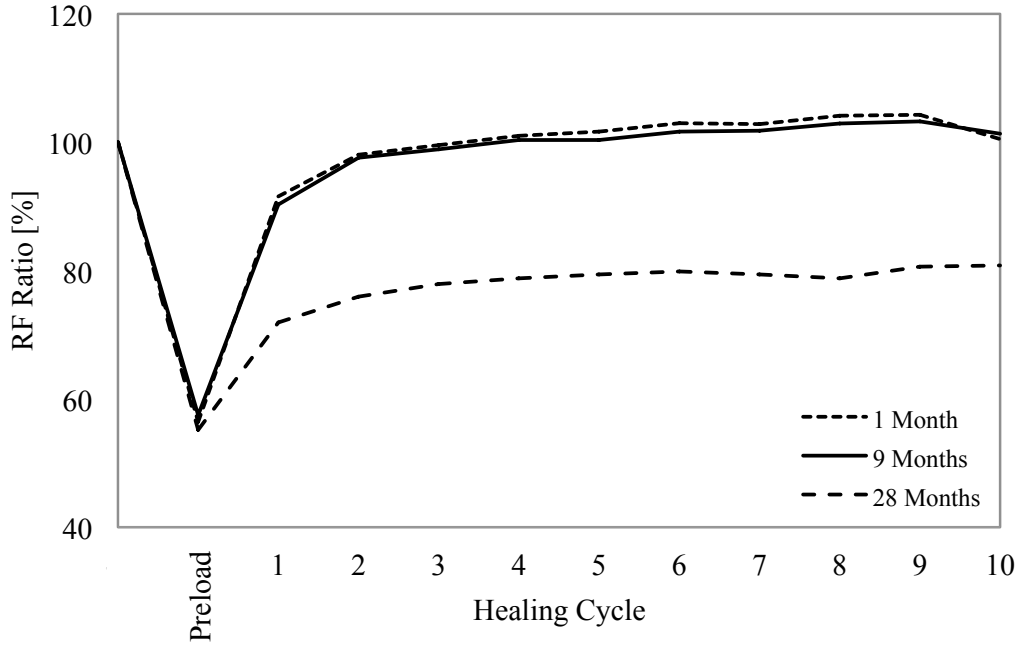

Figure 6.2: RF recovery of specimens preloaded at 1, 9, and 28 months after casting.

6.2.5 Stiffness and First Cracking Strength Results

Although there are large standard deviations in the stiffness and first cracking strength results, the average recoveries indicate that first cracking strength recovery is not dependent on specimen age, but stiffness recovery decreases with age. There is a significant decrease in the average stiffness recovery of the samples preloaded at 28 months (Figure 6.3), with the sample sets preloaded at one and nine months after casting having average stiffness recovery values of 78%, and the samples damaged at 28 months having an average recovery of only 61%. Unlike the stiffness recovery results, first cracking strength recovery was not dependent on specimen age (Figure 6.4), with the samples preloaded at one month after casting having an average recovery of 46%, and the samples preloaded at 9 and 28 months having an average recovery of 48%.

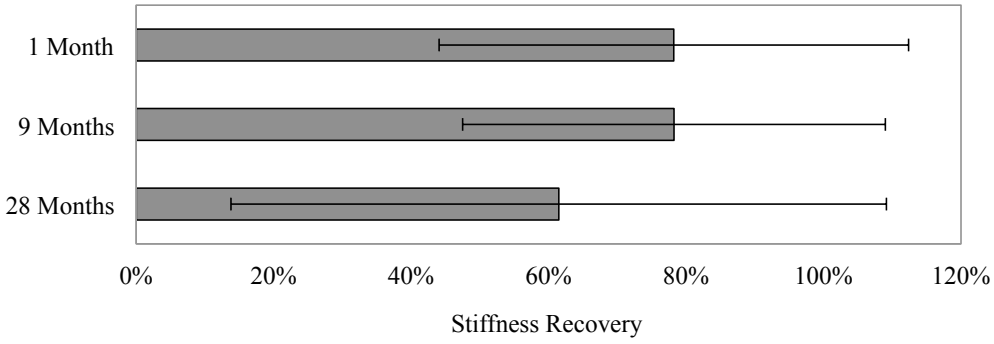

Figure 6.3: Stiffness recovery of specimens preloaded at 1, 9, and 28 months after casting.

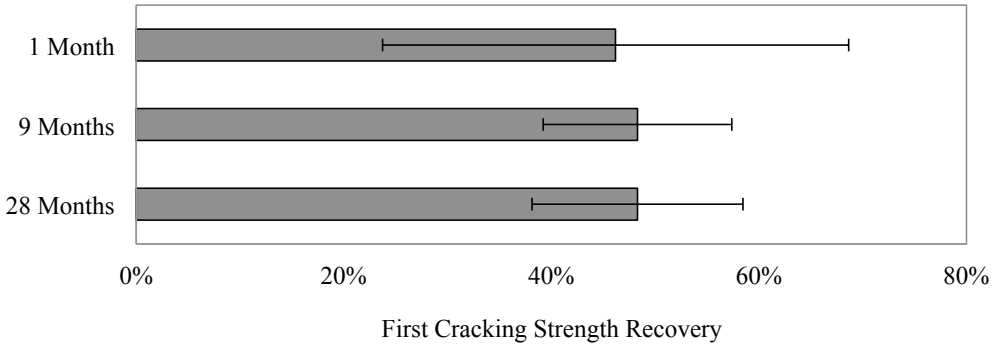

Figure 6.4: First cracking strength recovery of samples preloaded at 1, 9, and 28 months after casting.

6.2.6 Digital Image Correlation Results

The images captured using DIC during preloading and reloading showed that in eight of the nine samples tested, the first cracks to form during reloading were those that were formed during preloading. In these samples, no new cracks propagated until all the originals reopened, meaning that healing was not complete and the healing products were not able to completely bind the crack faces.

However, in one of the specimens tested from the sample group preloaded at 9 months, there was one crack that formed during preloading that did not reopen during reloading, even as new cracks were initiated and propagated. Figure 6.5 shows the images obtained from DIC after preloading and reloading was complete. The crack circled in black in the preloading image did not reopen during reloading, as it cannot be seen in the reloading image. This indicates that this crack was able to undergo complete self-healing during the ten cyclic wetting and drying cycles, and the healing products formed were able to completely bind the crack faces.

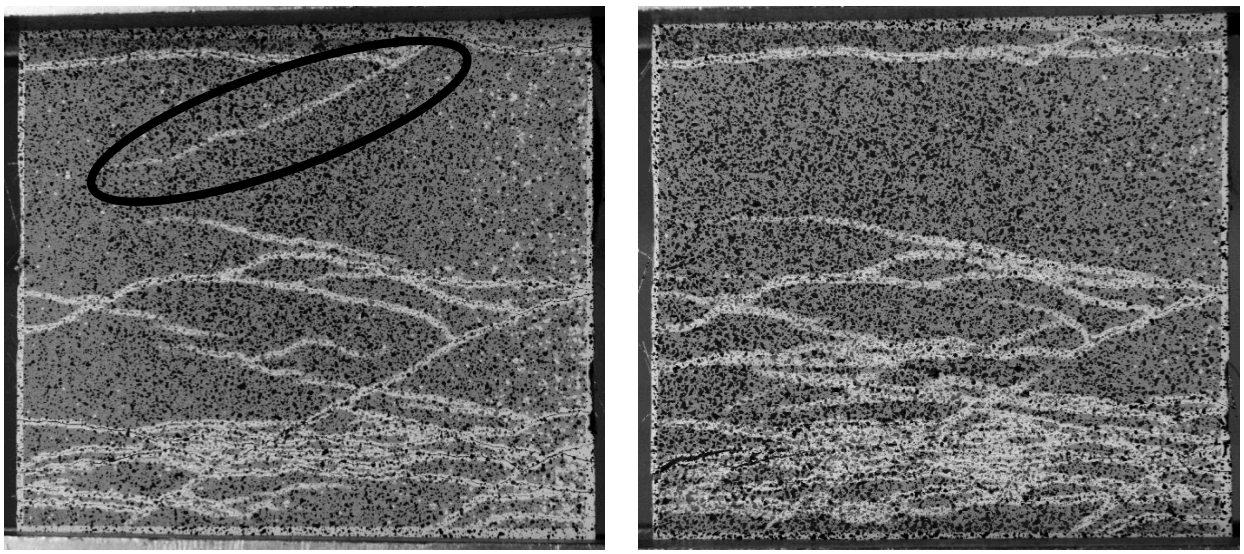

(a) (b)

Figure 6.5: Images obtained from DIC after (a) preloading and (b) reloading.

6.2.7 Discussion

The decrease in RF and stiffness recovery with specimen age is most likely due to changes in the cracking characteristics of ECC over time. Before the preloaded samples were exposed to wetting and drying cycles, an optical microscope was used to count and measure the widths of the cracks on the surface of the specimens. It was found that as sample age increases, the number of cracks decreases and the average crack width increases (Figures 6.6 and 6.7). The increase in average crack width is most likely a large contributing factor to the decrease in recovery seen in the samples preloaded at 28 months, as larger cracks do not heal as quickly or completely as smaller cracks.[7,8]

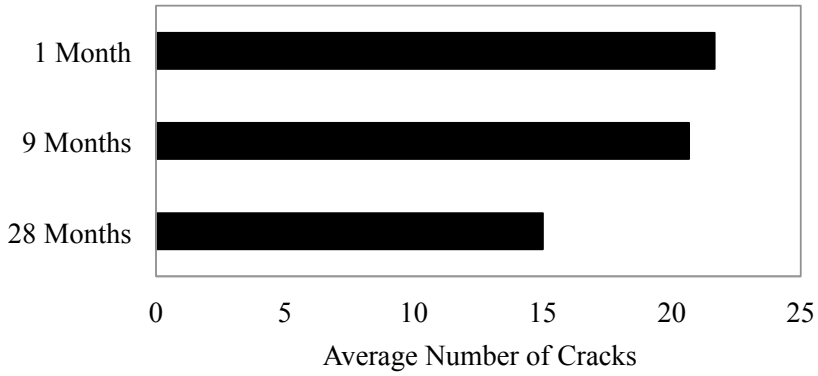

Figure 6.6: Average number of cracks observed in samples preloaded at 1, 9, and 28 months after casting.

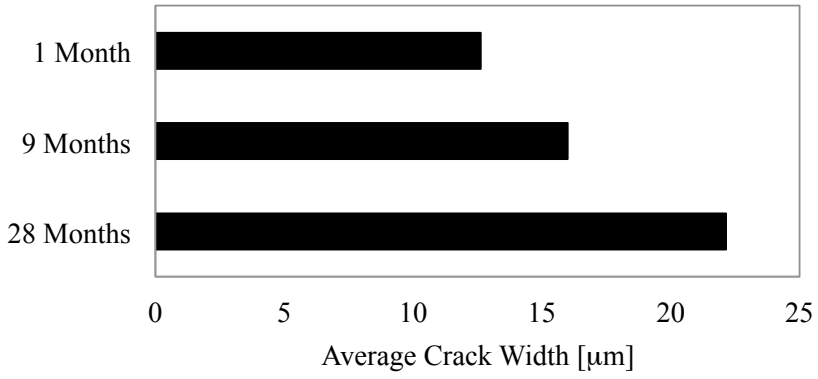

Figure 6.7: Average crack width in samples preloaded at 1, 9, and 28 months after casting.

The increase in crack width as samples age is due to continued hydration and the changing of matrix and matrix-fiber interface properties over time. It has been found that peak strain capacity of ECC is reached at roughly 10 days after casting, indicating the point in time when there is an optimal balance of matrix, fiber, and matrix-fiber interface properties.[9] As samples age, hydration continues and leads to an increase in the matrix fracture toughness. This results in a suboptimal balance of the matrix, fiber, and matrix-fiber interface properties, leading to changes in the cracking characteristics of the material and a decrease in material ductility. Therefore, while there is a decrease in self-healing functionality as ECC ages, this is ultimately caused by the changes in cracking characteristics of the material over time.

In addition, lack of unhydrated cement could also be contributing to the lower levels of healing seen in the samples preloaded at 28 months. Hydration of unreacted cement has been shown to be one of the main self-healing mechanisms, but less unreacted cement will be available over time due to continued hydration.[7] This lack of unhydrated cement coupled with larger crack widths explains the lower level of recoveries seen in the samples damaged at 28 months after casting.

Although there is a significant increase in RF, stiffness, and first cracking strength recoveries from self-healing despite sample age, the DIC results indicate that truly robust self-healing is not occurring. In all of the samples tested, there was only one healed crack that did not reopen during reloading. This means that while self-healing is occurring, the healing products formed are not robust enough to bind the crack faces and allow the damaged material to perform as well as the original, undamaged ECC. Unlike RF and stiffness recovery, these results do not seem to be affected by specimen age, as this behavior was seen in nearly all samples preloaded at 1, 9, and 28 months after casting.

6.3 Effects of Exposure Temperature

In this section, the experimental investigation used to assess the robustness of self-healing in ECC as it is exposed to different temperatures is described.

6.3.1 Mix Proportion, Raw Materials, and Specimen Preparation

The ECC mix proportion used in this study is shown in Table 6.2. Type I ordinary Portland cement, Class F fly ash, fly ash cenospheres, ground tire rubber, a polycarboxylate-based high range water reducing admixture (HRWRA), and polyvinyl alcohol (PVA) fibers were used to prepare the ECC specimens. The fly ash cenospheres had an average particle size of 200 μm, and the tire rubber was a recycled material produced by grinding tires at the end of their useful life, resulting in particles less than 150 μm. The PVA fibers accounted for 2% of the total mix volume and were 8 mm in length, with all other fiber properties being the same as those described in Section 6.2.1. Specimens were then cast and prepared for preloading according to the same procedure discussed in Section 6.2.2.

Table 6.2: ECC mix proportion.

Component	Cement	Fly Ash	Fly Ash Cenospheres	Tire Rubber	Water	HRWRA	Fiber
Weight Fraction	1	2.2	0.27	0.10	0.85	.006	0.066

6.3.2 Preloading and Environmental Conditioning

There were a total of three sample sets used in this study, each containing four control specimens and four preloaded specimens. All preloaded specimens were damaged to 1% tensile strain using the method described in Section 6.2.2. Each of the three sample sets were exposed to cyclic wetting and drying cycles, where each cycle consisted of submerging the samples in water for 24 hours, followed by 24 hours of drying in air. However, each sample set was exposed to the cyclic wetting and drying cycles under a different temperature environment: a hot environment (45°C), a room temperature environment (22°C), and a cold environment (2°C). These three temperatures were chosen to simulate the self-healing of ECC during the warm summer, moderate spring and fall, and cold winter months.

6.3.3 Evaluation Methods

RF measurements, uniaxial tensile (reloading) tests, and DIC were used to evaluate the self-healing functionality of ECC under various temperatures according to the same methods described in Section 6.2.3. However, the RF data in this study is presented as Normalized RF according to Equation 6.4, where $RF_{preload}$ is the RF value of the preloaded specimens that were exposed to cyclic wetting and drying and $RF_{control}$ is the RF value of the undamaged control specimens that underwent the same cyclic exposure. Normalized RF removes the effect of continued hydration of the bulk ECC material over time, therefore providing RF recovery data that is due solely to the self-healing of microcracks.

$$\text{Normalized RF} = \frac{RF_{preload}}{RF_{control}} \tag{6.4}$$

6.3.4 Resonant Frequency Results

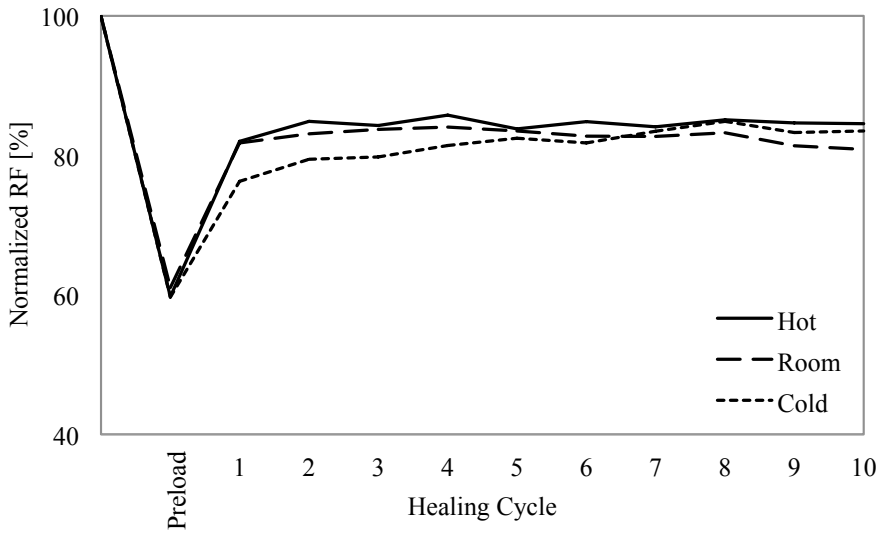

Figure 6.8: RF recovery of samples exposed to hot, room temperature, and cold environments.

Figure 6.8 shows that the majority of RF recovery occurred during the first wetting and drying cycle regardless of exposure temperature. However, the samples exposed to the cold

environment recovered less than the samples exposed to the hot and room temperature environments during this first cycle. The samples in the cold environment recovered an average of 76% of their initial RF value after the first cycle, while the samples exposed to the hot and room temperature environments recovered 82%. Although the rate of recovery for the samples in the cold environment was initially lower than the rates seen in the hot and room temperature environments, all samples recovered to approximately the same level after 10 wetting and drying cycles regardless of exposure temperature.

6.3.5 Stiffness and First Cracking Strength Results

Similar to the results seen regarding effects of specimen age on stiffness and first cracking strength recovery (Section 6.2.5), the amount of stiffness recovery appears to be dependent on exposure temperature (Figure 6.9), while the level of first cracking strength recovery is relatively similar for all three exposure environments (Figure 6.10). The samples exposed to the hot and room temperature environments had similar levels of stiffness recovery, with the specimens exposed to the hot environment recovering to an average of 94% and the samples exposed to the room temperature environment recovering to 92%. However, the level of stiffness recovery seen in the samples exposed to a cold environment was much lower, with an average recovery of only 52%. Although the first cracking strength recovery for the samples exposed to the hot environment was slightly lower than those exposed to the cold and room temperature environments, all recovery levels were between 40 and 52%, suggesting that first cracking strength recovery is not dependent on exposure temperature.

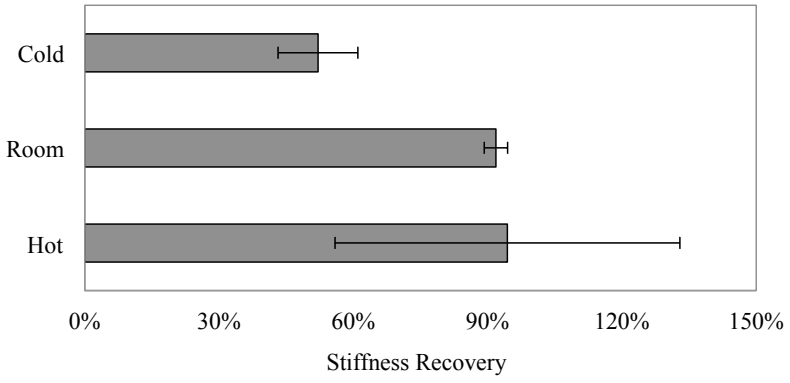

Figure 6.9: Stiffness recovery of samples exposed to hot, room temperature, and cold environments.

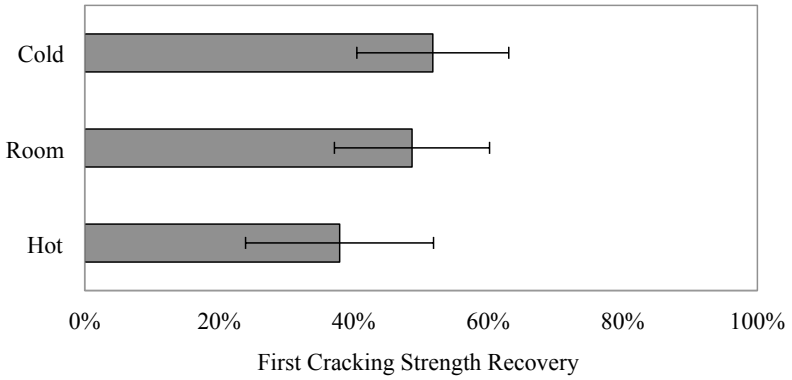

Figure 6.10: First cracking strength recovery of samples exposed to hot, room temperature, and cold environments.

6.3.6 Digital Image Correlation Results

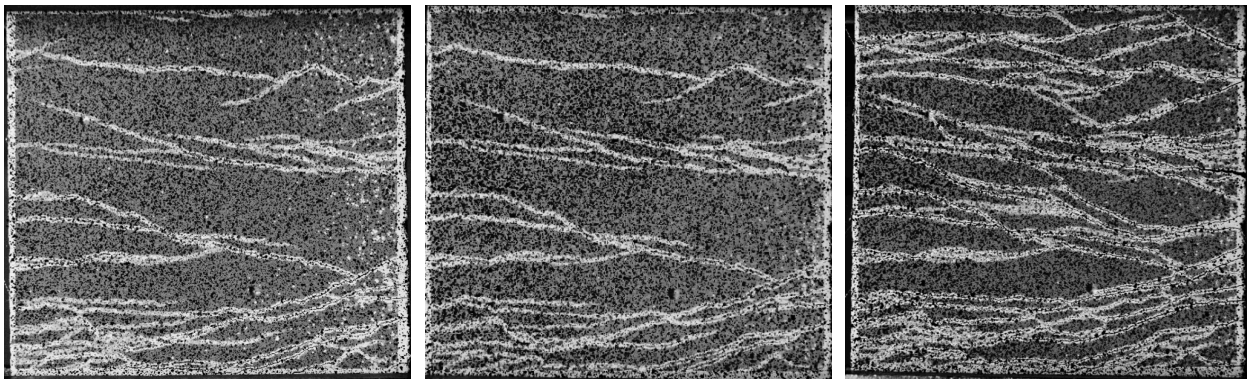

(a) (b) (c)

Figure 6.11: Cracking patterns (a) after preloading, (b) during reloading after 10 cyclic wetting and drying cycles at room temperature, and (c) after reloading until sample failure.

In all of the specimens tested, the cracks formed during preloading were the first to open upon reloading. No new cracks propagated until all the originals had reopened, meaning that the healing products formed were not robust enough to completely bind the crack faces. An example of this is shown in Figure 6.11. Figure 6.11 (a) shows the cracking pattern of the sample after preloading, (b) shows the cracking pattern during reloading after 10 cyclic wetting and drying cycles at room temperature, and (c) is the final cracking pattern after reloading until sample failure. Since the same cracking pattern appears in both (a) and (b), this indicates that the cracks

present at the end of preloading were the first to open during reloading. It is not until all these cracks are reopened that new cracks begin to propagate, and these can be seen in (c).

6.3.7 Discussion

It has been hypothesized that stiffness recovery can be attributed to the self-healing of microcracks as well as an increase in the stiffness of the bulk ECC material due to continued hydration. In this experiment, the stiffness of the control samples that were exposed to the same wetting and drying cycles as the preloaded samples was measured to determine any changes in ECC material stiffness due to continued hydration and exposure temperature. Figure 6.12 shows the original stiffness of ECC at 28 days after casting, as well as the stiffness of the material after 10 cyclic wetting and drying cycles in hot, room temperature, and cold environments. While exposure to the wetting and drying cycles at room temperature did not have any effect on the stiffness of ECC, samples exposed to the hot environment showed a significant increase in stiffness, and samples exposed to the cold environment showed a slight decrease in stiffness.

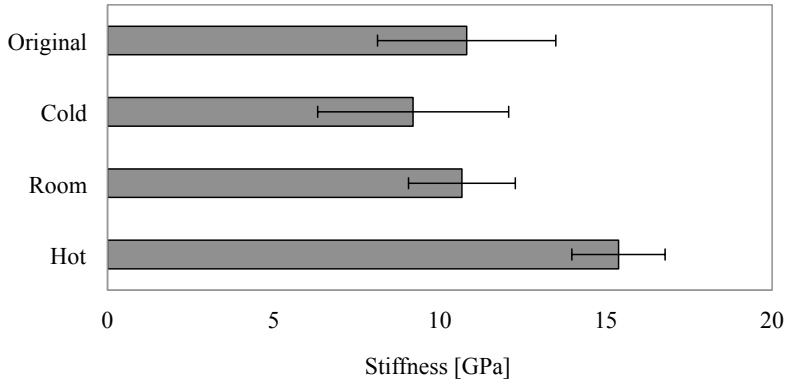

Figure 6.12: Effect of continued hydration and exposure temperature on ECC stiffness.

Due to these changes in bulk material stiffness caused by continued hydration and exposure temperature, the stiffness data presented in Figure 6.9 must be normalized in the same manner described for RF in Section 6.3.3 in order to determine the amount of stiffness recovery due solely to self-healing. Although the initial stiffness data in Figure 6.9 shows that the samples exposed to the cold environment recover to a much lower level than the samples exposed to the hot and room temperature environments, a different pattern can be seen in the normalized

stiffness data shown in Figure 6.13. The normalized data indicates that the average level of stiffness recovery due solely to self-healing is much lower in the samples exposed to the hot and cold environments than the samples exposed to the room temperature environment.

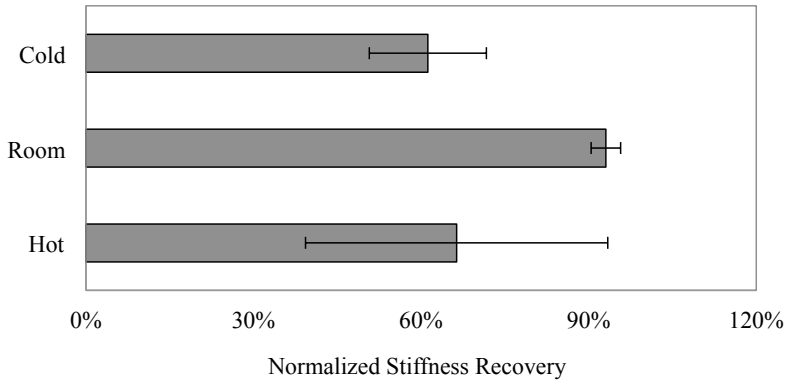

Figure 6.13: Normalized stiffness recovery of samples exposed to hot, room temperature, and cold environments.

The lower levels of recovery seen in the samples exposed to the cold environment are likely due to slower rates of reaction. It is well known that the rate of cement hydration and pozzolanic reactions decreases in cold temperatures[10,11], and since these reactions contribute significantly to the formation of healing products, this explains the lower levels of stiffness recovery due solely to self-healing in the samples exposed to the cold environment. In addition, lower rates of healing were also seen in the RF data, where the samples exposed to the cold environment recovered to much lower levels than those in the hot and room temperature environments after the first healing cycle.

The lower levels of self-healing seen in the normalized stiffness data for samples exposed to the hot environment are most likely due to the experimental setup. Samples were exposed to the hot temperatures during both the wetting and drying phases of the healing cycles, meaning that during the drying phase the moisture absorbed during the wetting phase evaporated rapidly. This rapid loss of moisture during the drying phase would lower the overall levels of self-healing, as water is necessary in all of the chemical reactions that produce healing products. It is expected that if these samples were allowed to dry at the same rate as the samples exposed to the cold and

room temperature environments, the level of stiffness recovery due solely to self-healing would increase.

Although exposure to all three temperature environments produced significant RF, stiffness, and first cracking strength recoveries, the images obtained from DIC during preloading and reloading indicate that truly robust self-healing is not occurring. In all of the samples tested, the original cracks formed during preloading were the first to open during reloading, and no new cracks were formed during reloading until all the originals had reopened. This means that while self-healing was occurring, the healing products formed were not robust enough to bind the crack faces and allow the damaged ECC material to perform as well as the original, undamaged ECC. Since this behavior was seen in all of the specimens tested, these results were not dependent on exposure temperature.

6.4 Conclusions

In this chapter, two experiments were performed to determine the effects of specimen age and exposure temperature on the self-healing functionality of ECC. Based on the results of these experimental investigations, the following conclusions can be drawn:

- As sample age increases, the self-healing functionality of ECC decreases. Samples that were preloaded at 28 months after casting showed much lower levels of RF and stiffness recovery compared to samples preloaded at 1 and 9 months.
- The lower levels of RF and stiffness recovery in older samples are ultimately caused by changes in the cracking characteristics of ECC over time. As samples age, the average crack width produced during loading increases. Since larger cracks do not heal as quickly or completely as smaller cracks, this leads to lower levels of healing in older specimens.
- The self-healing functionality of ECC decreased as exposure temperature decreased. Samples exposed to a cold environment (2°C) had lower levels of stiffness recovery and the rate of RF recovery was lower than samples exposed to hot (45°C) and room temperature (22°C) environments. This result was not unexpected since it is well known that the rate of cement hydration and pozzolanic reactions decreases in cold temperatures.
- Although the overall average stiffness recovery was similar for samples exposed to the hot and room temperature environments, the stiffness recovery due solely to self-healing

was much lower in samples exposed to the hot environment. This was most likely due to the experimental setup, where the samples exposed to the hot environment dried at a much faster rate during the cyclic wetting and drying cycles than the samples exposed to the room temperature environment. This meant that less water was available for the reactions that produce healing products, leading to lower levels of stiffness recovery due solely to self-healing.

- Unlike RF and stiffness recovery, first cracking strength recovery was not dependent on specimen age or exposure temperature.
- The images obtained from DIC during preloading and reloading indicated that truly robust self-healing was not occurring, regardless of specimen age or exposure temperature. In nearly all of the samples tested, no new cracks formed during reloading until all the originals formed during preloading had reopened. This means that while RF, stiffness, and first cracking strength recovery data proved that self-healing was occurring, the healing products formed were not robust enough to bind the crack faces and allow the damaged material to behave as well as the original, undamaged ECC.

References

[1] Li, V.C., Wang, S., & Wu, C. (2001). Tensile Strain-Hardening Behavior of PVA-ECC. *ACI Materials Journal, 98*, 483-492.

[2] Li, V.C., Wu, C., Wang, S., Ogawa, A., & Saito, T. (2002). Interface Tailoring for Strain-Hardening PVA-ECC. *ACI Materials Journal, 99,* 463-472.

[3] Sahmaran, M. & Li, V.C. (2008). Durability of mechanically loaded engineered cementitious composites under highly alkaline environments. *Cement and Concrete Composites, 30*, 72-81.

[4] Yang, Y., Lepech, M.D., Yang, E., & Li, V.C. (2009). Autogenous healing of engineered cementitious composites under wet-dry cycles. *Cement and Concrete Research, 39*, 382-390.

[5] Yamamoto, A., Watanabe, K., Li, V.C., & Niwa, J. (2010). Effect of wet-dry condition on self-healing property of early-age ECC. *Japan Concrete Institute, 32*, 251-256.

[6] Li, M. & Li, V.C. (2011). Cracking and Healing of Engineered Cementitious Composites under Chloride Environment. *ACI Materials Journal, 108*, 333-340.

[7] Edvardsen, C. (1999). Water Permeability and Autogenous Healing of Cracks in Concrete. *ACI Materials Journal, 96*, 448–455.

[8] Reinhardt, H.W. & Jooss, M. (2003). Permeability and self-healing of cracked concrete as a function of temperature and crack width. *Cement and Concrete Research, 33*, 981-985.

[9] Lepech, M.D. & Li, V.C. (2006). Long Term Durability Performance of Engineered Cementitious Composites. *Journal of Restoration of Buildings and Monuments, 12,* 119-132.

[10] Mindess, S., Young, J.F., & Darwin, D. (2003). *Concrete (2nd Edition)*. Upper Saddle River, NJ: Prentice Hall, Pearson Education, Inc.

[11] Taylor, H.F.W. (1997). *Cement Chemistry (2nd Edition)*. London: Thomas Telford Publishing.

CHAPTER 7: CORRELATION BETWEEN SELF-HEALING AND CRACK CHARACTERISTICS

7.1 Introduction

Previous work and the research presented in this dissertation have indicated a strong correlation between the self-healing behavior and cracking characteristics of ECC. A previous study which identified the main healing products in ECC to be a combination of C-S-H and calcium carbonate ($CaCO_3$) also suggested that the healing products formed may be a function of crack width, with C-S-H being the dominate healing product formed in cracks less than 15 μm in width and both C-S-H and $CaCO_3$ forming in larger cracks.[1] In addition, the work presented in this dissertation has indicated a strong correlation between the stiffness recovery and crack width distribution of ECC. The work presented in this chapter will address both of these initial findings, describing the experiment used to determine if the healing products formed are a function of crack width, and the work performed to determine the correlation between stiffness recovery and crack width distribution.

7.2 Healing Products as a Function of Crack Width

This section will describe the experimental work used to determine if the healing products formed in ECC are a function of crack width.

7.2.1 Evaluation Methods and Sample Preparation

An environmental scanning electron microscope (ESEM) equipped with an energy dispersive spectroscopy (EDS) system was used to obtain images and identify the chemical species present within the healing products of ECC. Small cube samples measuring approximately 1 cm x 1 cm x 1 cm were cut from ECC specimens that were damaged under tensile load, so each cube sample contained multiple microcracks. ESEM imaging of the cracks was performed after initial preparation and cutting of the cube samples, and ESEM imaging and EDS analysis were

conducted after healing was allowed to occur to identify the healing products. Healing in the cube samples was induced using three cyclic wetting and drying cycles, where each cycle consisted of 24 hours submerged in water and 24 hours of drying in laboratory air. The small cube samples were never polished or coated with a conductive material, as to prevent interfering with the self-healing process.

7.2.2 Results and Discussion

Previous work has suggested that the healing products formed in ECC may be a function of crack width, with C-S-H being the dominant healing product formed in cracks less than 15 μm in width.[1] However, this study proved that the healing products formed are not a function of crack width, as both C-S-H and crystalline healing products were found in all crack widths.

Figure 7.1 shows the healing products formed in a crack that was originally 15 μm in width. An abundance of C-S-H can be seen on the surface of the sample, as well as on the surface of the crack faces. However, crystalline healing products are dominant between the crack faces. EDS was used on Points A and B shown in Figure 7.1 to determine the elements present within the crystals, and the results are shown in Table 7.1. Due to the low amount of carbon present and the exact oxygen to calcium ratio (O:Ca) of 2.00 for Point A, it can be concluded that this crystal is calcium hydroxide ($Ca(OH)_2$). For Point B, the higher percentage of carbon and the higher O:Ca ratio of 2.70 show that calcium carbonate ($CaCO_3$) is also present in the crack.

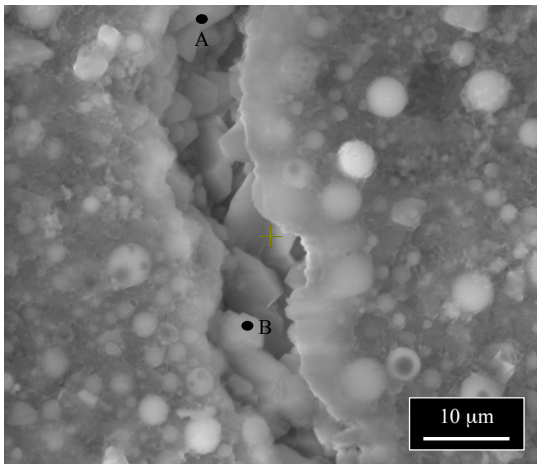

Figure 7.1: 15 μm crack with C-S-H, $Ca(OH)_2$, and $CaCO_3$ present in the healing products.

Table 7.1: EDS element analysis of healing products in 15 μm crack.

Element	A	B
C	8.40	14.72
O	55.71	57.38
Mg	1.56	1.51
Al	2.40	1.95
Si	4.09	3.18
Ca	27.84	21.26
O:Ca	**2.00**	**2.70**

Figure 7.2 also shows the healing products present within a 15 μm crack. Like the crack shown in Figure 7.1, this crack also has both C-S-H and crystalline healing products present. From EDS analysis, the healing products in this crack were found to be mainly $Ca(CO)_3$ due to the relatively high amount of carbon and O:Ca ratio (Table 7.2). The results shown in Table 7.2 are from the point indicated on Figure 7.2, and these results were similar for all crystals within the crack.

Table 7.2: EDS element analysis of healing products in 15 μm crack.

Element	%
C	17.04
O	55.79
Mg	1.34
Al	1.19
Si	1.81
Ca	22.83
O:Ca	**2.44**

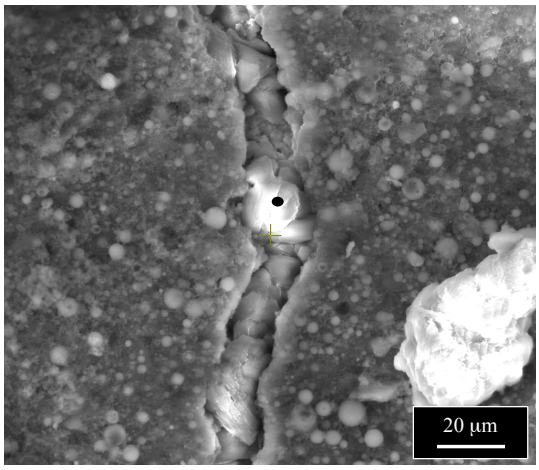

Figure 7.2: 15 μm crack with C-S-H and $CaCO_3$ present in the healing products.

A crack that was originally approximately 5 μm is shown in Figure 7.3. Although the healing products on the surface of this crack appear to be dominated by C-S-H, there are crystalline healing products present within the depth of the crack. Due to the large amount of C-S-H, EDS could only be performed on the crystal indicated in Figure 7.3, and the results are shown in Table 7.3. This crystal can be identified as $Ca(OH)_2$ due to the low amount of carbon and O:Ca ratio of nearly 2.

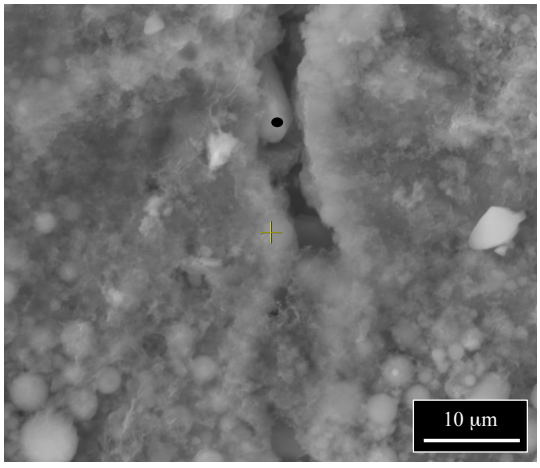

Figure 7.3: 5 μm crack with an abundance of C-S-H on the surface and crystalline healing products within the depth of the crack.

Table 7.3: EDS element analysis of crystalline healing product in 5 μm crack.

Element	%
C	7.67
O	53.59
Mg	2.23
Al	2.39
Si	5.00
Ca	27.92
O:Ca	**1.92**

Although previous research has suggested that crystalline healing products are not present in cracks less than 15 μm in width, the images and EDS results presented here show that both C-S-H and crystalline healing products, $Ca(OH)_2$ and $CaCO_3$, can be formed within these tight crack widths. Therefore, the healing products formed are not a function of crack width, as C-S-H, $Ca(OH)_2$, and $CaCO_3$ can be found within the healing products of cracks of any size.

7.3 Correlation Between Stiffness Recovery and Crack Width Distribution

In this section, the work used to determine the exact correlation between the level of stiffness recovery and crack width distribution of ECC will be described. Previous research has shown the ability to predict the permeability and resistivity of ECC through analytical scale-linking models, and the work described in this section follows a similar approach with the objective of using an analytical scale-linking model to predict stiffness recovery due to self-healing in ECC.[2,3]

Experiments performed on single crack specimens were used to determine the level of stiffness recovery on the meso-scale as a function of crack width, and crack width data was collected on the maco-scale to determine the crack width distributions of ECC at various levels of tensile strain. The meso-scale stiffness recovery data was then combined with an analytical model and macro-scale crack width distributions to predict the level of stiffness recovery on the macro-scale as a function of tensile strain. The model and method were verified by comparing values predicted from the model to macro-scale experimental stiffness recovery data. This approach resulted in the linking of stiffness recovery between the meso- and macro-scale, ultimately resulting in the ability to predict the level of stiffness recovery due to self-healing in ECC as a function of tensile strain.

7.3.1 Mix Proportion, Raw Materials, and Specimen Preparation

The ECC mix proportion used in this study is given in Table 7.4. Type I ordinary Portland cement, Class F fly ash, silica sand with an average particle size of 110 μm, a polycarboxylate-based high range water reducing admixture (HRWRA), and polyvinyl alcohol (PVA) fibers were used to prepare the ECC specimens. The PVA fibers accounted for 2% of the total mix volume and were 12 mm in length with an average diameter of 39 μm. The fibers had a tensile strength of 1600 MPa, a density of 1300 kg/m^3, an elastic modulus of 42.8 GPa, and a maximum elongation of 6%. In addition, the surfaces of the fibers were coated with an oiling agent (1.2% by weight) to reduce the interfacial chemical bond between the fiber and matrix caused by the strong hydrophilic nature of the PVA fibers.[4,5]

Table 7.4: ECC mix proportion.

Component	Cement	Fly Ash	Sand	Water	HRWRA	Fiber
Weight Fraction	1	1.2	0.8	0.58	0.013	0.045

The raw materials were mixed in a 20 L force-based Hobart mixer according to the proportions shown in Table 7.4, and the fresh ECC was cast into molds and covered in plastic sheeting. Dogbone samples, as recommended by the Japan Society of Civil Engineers for testing high ductility concretes, were used in this study and the geometry of the samples is shown in Figure 7.4. Twenty four hours after casting, the specimens were removed from the molds and cured at room temperature until testing.

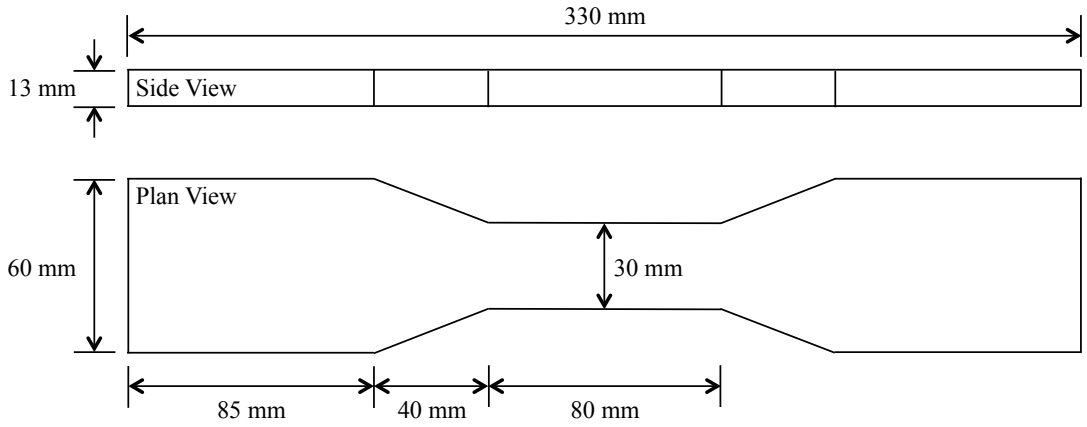

Figure 7.4: Geometry of dogbone specimens.

7.3.2 Macro-Scale Crack Width Distributions

Since the ultimate goal of this study was to predict the level of stiffness recovery as a function of tensile strain through the use of an analytical scale-linking model, the first step was to determine the macro-scale crack width distributions at various levels of tensile strain.

Dogbone specimens were preloaded to 0.25, 0.35, 0.5, 0.75, and 1% tensile strain at 28 days after casting. Preloading was performed through the use of uniaxial tensile loading, which was applied to the dogbones using a 50 kN capacity load frame (Instron Model 5969) under displacement control and a loading rate of 0.5 mm/min. Two Linear Variable Displacement Transducers (LVDTs) were attached to the specimens to measure tensile elongation during loading. When the LVDTs indicated that the desired level of tensile strain had been reached, loading was stopped and the samples were removed from the load frame. Once the specimens were removed, an optical microscope was used to count and measure the cracks formed during preloading. Due to

the precision of the optical microscope, crack width data was measured and recorded in intervals of 10 μm. The mean crack width and standard deviation was then determined for each sample.

Based on previous studies, the crack width distributions at each preloading strain level were assumed to fit a lognormal distribution.[2,3] The probability density function (PDF) of the lognormal distribution at each preloading strain level can be expressed as shown in Equation 7.1, where $p(\delta,\varepsilon)$ is the probability of a given crack width δ being present in a sample at a given tensile strain level ε.

$$p(\delta,\varepsilon) = \frac{1}{\delta\sigma\sqrt{2\pi}} e^{-\frac{(\ln\delta-\mu)^2}{2\sigma^2}} \tag{7.1}$$

The variables μ and σ can be calculated as shown in Equations 7.2 and 7.3, where m and s are the mean crack width and standard deviation, which are also functions of the level of tensile strain.

$$\mu = \ln\frac{m^2}{\sqrt{s^2+m^2}} \tag{7.2}$$

$$\sigma = \sqrt{\ln\left(\frac{s^2}{m^2}+1\right)} \tag{7.3}$$

The mean (m) and standard deviation (s) of the crack width, which were determined through the use of an optical microscope as described above, are plotted as a function of tensile strain in Figure 7.5. It was found that these parameters could be represented by third degree polynomial functions (Equations 7.4 and 7.5), where A_i and B_i are constants determined by the line of best fit through the experimental data as shown in Figure 7.5.

$$m = A_3\varepsilon^3+A_2\varepsilon^2+A_1\varepsilon+A_0 \tag{7.4}$$

$$s = B_3\varepsilon^3+B_2\varepsilon^2+B_1\varepsilon+B_0 \tag{7.5}$$

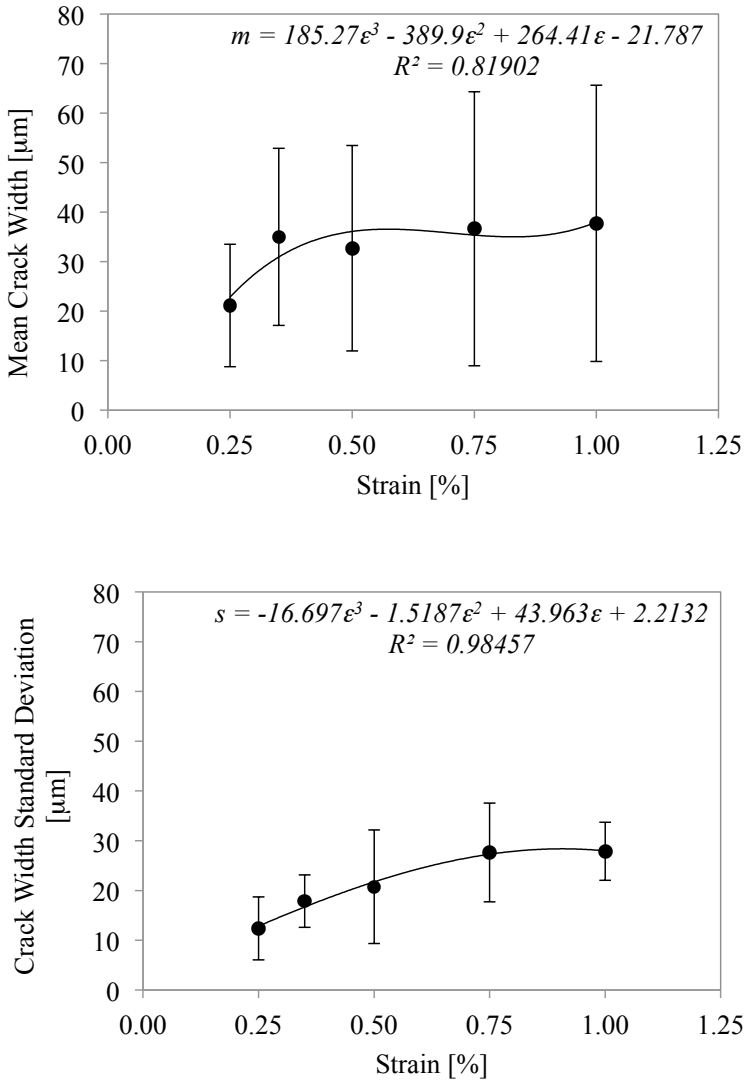

Figure 7.5: Mean and standard deviation of crack width as a function of tensile strain.

Using Equations 7.1-7.5, the crack width distribution of the ECC mix in Table 7.4 can be uniquely described at a given level of tensile strain. As mix proportions change, crack width distributions also vary, as other distributions have been obtained in previous research.[2,3] Representative lognormal crack width distributions at each preloading strain level for the mix used in this study are shown in Figure 7.6. It should be noted that the distributions shown in Figure 7.6 were obtained by scaling up the PDF $p(\delta,\varepsilon)$ by the total number of cracks at each strain level and crack width interval (10 μm). However, the actual PDF was used in all subsequent calculations.

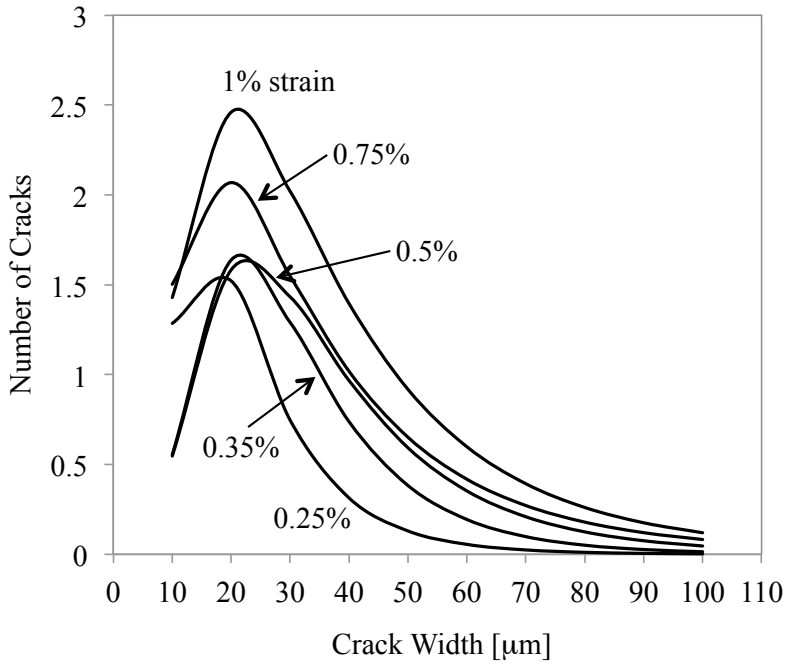

Figure 7.6: Representative lognormal crack width distributions at each preloading strain level.

7.3.3 Meso-Scale Stiffness Recovery

In order to predict the level of stiffness recovery on the macro-scale using the crack width distributions obtained in Section 7.3.2, it is necessary to know the level of stiffness recovery as a function of crack width.

This relationship was obtained through the use of single-crack dogbone specimens. The specimens were notched prior to preloading in order to suppress the multiple cracking behavior of ECC and allow only one crack to form during preloading, following the procedure described in previous research.[6,7] All notches were 1 mm wide, but the notches on the sides of the dogbones were 6 mm in depth, while the notches on the front and back of the dogbones were 2 mm in depth (Figure 7.7). Single cracks were induced by applying uniaxial tensile load as described in Section 7.3.2, with the LVDTs placed at a gage length of 20 mm as shown in Figure 7.7. The specimens were loaded to obtain single cracks ranging from 10-100 μm, the most probable range of crack widths found in the macro-scale crack width distributions. It should be noted that while only a single crack formed on the surface of the notched area of the specimens, it is nearly impossible to produce only a single crack due to the intrinsic tensile behavior of ECC,

and it is possible that multiple cracks were forming throughout the depth of the notch. For this reason, variation in the final data sets is expected and at least 5 single crack samples were tested for each crack width.

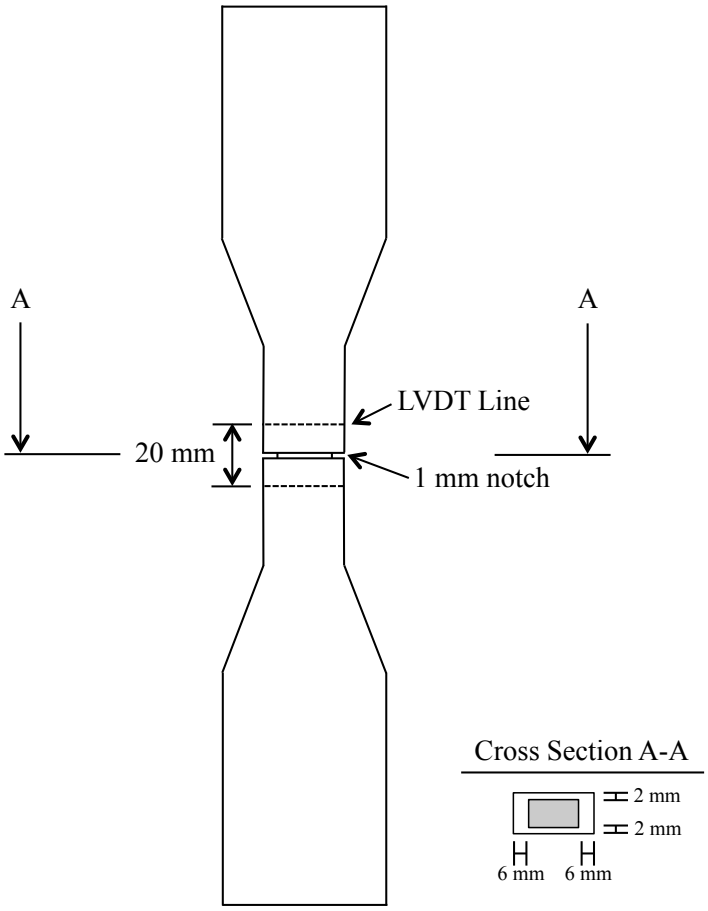

Figure 7.7: Geometry of single-crack dogbone specimens.

After preloading, all notched dogbone specimens were exposed to 10 cyclic wetting and drying cycles. Each cycle consisted of 24 hours submerged in water, followed by 24 hours of drying in laboratory air. After the 10 healing cycles, all single crack samples were reloaded until failure.

In this study, the first cracking load ($L_{preload}$ and L_{reload}) and secant stiffness ($E_{preload}$ and E_{reload}) during preloading and reloading were defined as shown in Figure 7.8. A linear best-fit line was drawn through the elastic range of each load-crack opening curve and the load value at the point of deviation was considered to be the first cracking load. The stiffness was then defined as the

secant stiffness between the origin and first cracking load. Stiffness recovery (r_E) was then calculated using Equation 7.6, where the stiffness during reloading was compared to that measured during preloading.

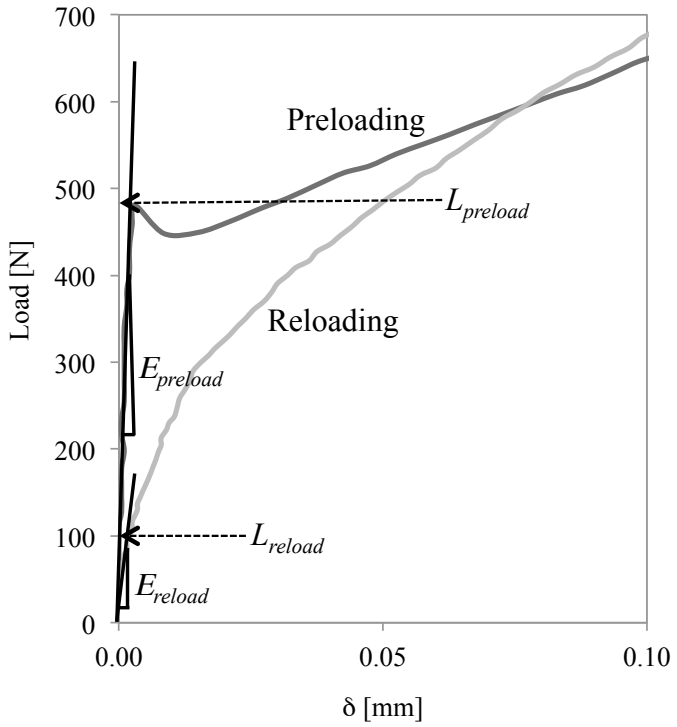

Figure 7.8: First cracking load and stiffness definition.

$$r_E = \frac{E_{reload}}{E_{preload}} \tag{7.6}$$

The meso-scale stiffness recoveries obtained from the single-crack samples are shown in Figure 7.9. The level of stiffness recovery was found to decrease drastically as the crack width increased, with the data being best represented by the exponential function $r_E(\delta)$. As the minimum gage length that could be practically measured was 20 mm, it should be noted that a part of the un-notched dogbone sections within the gage length were disregarded to obtain the true stiffness recovery of a 3 mm section (1 mm of cracked notched section, and 1 mm of undamaged section on each side of the notch), the same element size used in the analytical scale-linking model as described in Section 7.3.4.

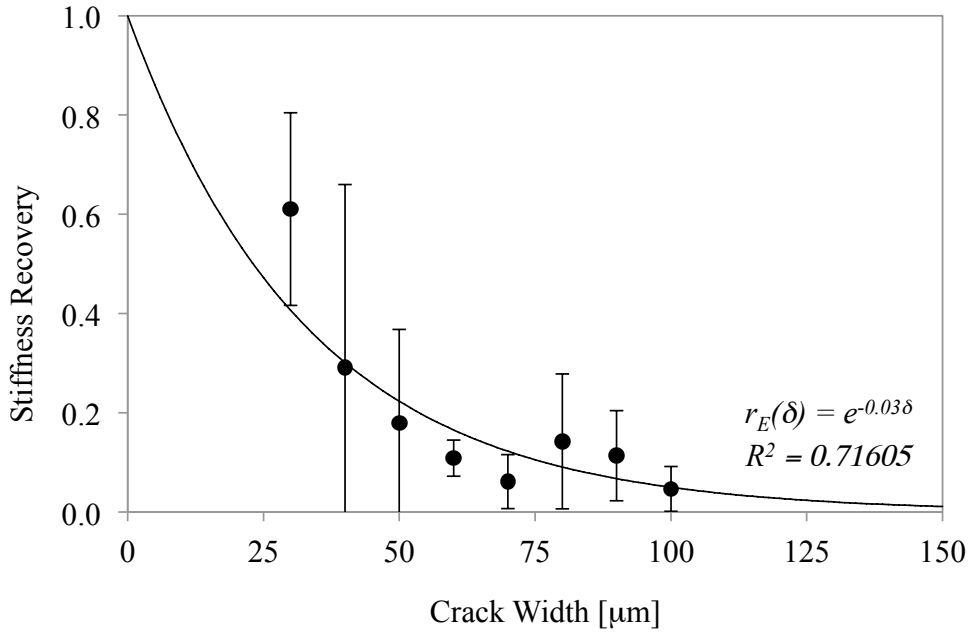

Figure 7.9: Meso-scale stiffness recovery as a function of crack width.

7.3.4 Analytical Scale-Linking Model

The analytical scale-linking model described in this section utilizes the macro-scale crack width probability density function determined in Section 7.3.2 and the meso-scale stiffness recovery function determined in Section 7.3.3 to predict the level of stiffness recovery on the macro-scale as a function of tensile strain.

Prior to preloading, a rectangular ECC composite has stiffness E_0, cross sectional area A_0, and length L_0 (Figure 7.10). When the ECC sample is preloaded to a specified strain level ε, n micro cracks of varying width form throughout the length of the sample. The composite can be modeled as a total of m elements after preloading, where the stiffness of the composite is assumed to act as m springs in series. Each element has length t equal to 3 mm, the minimum crack spacing found in ECC, thus ensuring that each element can contain only one crack.[7] The cracked elements (n) have stiffness E'_i after healing, while the number of uncracked elements (m-n) are assumed to have stiffness E_0. From classical mechanics, the composite stiffness after healing E' can then be expressed as shown in Equation 7.7.

Before Preloading

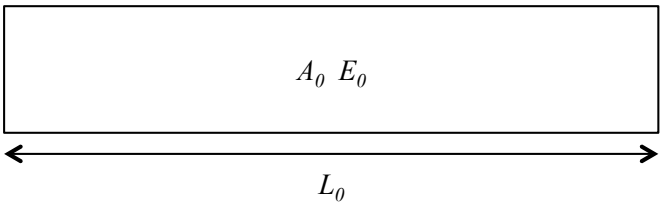

After Preloading

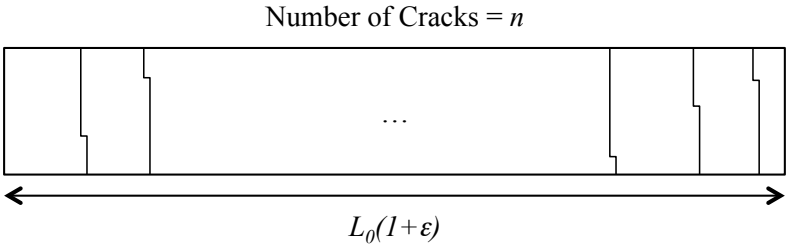

After Self-Healing

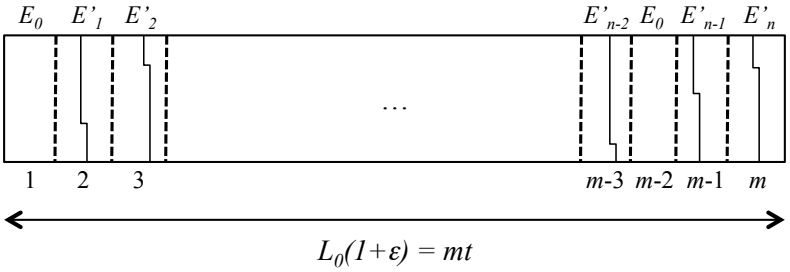

Figure 7.10: After self-healing, a rectangular ECC composite is modeled as m elements, where the stiffness of the composite is assumed to act as m springs in series.

$$E' = \frac{m}{\sum_{i=1}^{n} \frac{1}{E'_i} + \frac{(m-n)}{E_0}} \tag{7.7}$$

Assuming stiffness recovery is governed by crack width, the stiffness recovery of a crack with width δ can be expressed according to Equation 7.8, which was experimentally determined in Section 7.3.3.

$$r_E(\delta) = \frac{E'(\delta)}{E_0} \tag{7.8}$$

If the crack width distribution is considered to be discrete and the number of cracks with width δ_j is n_j, then Equations 7.7 and 7.8 can be combined as shown below.

$$E' = \frac{m}{\sum_j \frac{n_j}{E'(\delta_j)} + \frac{(m-n)}{E_0}} = \frac{m}{\sum_j \frac{n_j}{E_0 r_E(\delta_j)} + \frac{(m-n)}{E_0}} = \frac{mE_0}{\sum_j \frac{n_j}{r_E(\delta_j)} + (m-n)} \tag{7.9}$$

However, crack width distributions are not discrete and in reality crack widths can have a value between zero and infinity following the probability density function $p(\delta,\varepsilon)$ obtained in Section 7.3.2. Therefore, n_j should be expressed as shown in Equation 7.10 and E' can be re-expressed as shown in Equation 7.11.

$$n_j = np(\delta_j,\varepsilon)d\delta \tag{7.10}$$

$$E' = \frac{mE_0}{\int_0^\infty \frac{np(\delta,\varepsilon)}{r_E(\delta)} d\delta + (m-n)} = \frac{mE_0}{n\left(\int_0^\infty \frac{p(\delta,\varepsilon)}{r_E(\delta)} d\delta - 1\right) + m} \tag{7.11}$$

If the elastic deformation of ECC is considered to be small compared to crack width, the total number of cracks n can be calculated as the total deformation divided by the mean crack width as shown in Equation 7.12.

$$n = \frac{\varepsilon L_0}{\int_0^\infty \delta p(\delta,\varepsilon) d\delta} \tag{7.12}$$

Also, when L_0 is sufficiently large, m can be approximated as shown below.

$$m = \frac{L_0(1+\varepsilon_r)}{t} \approx \frac{L_0}{t} \tag{7.13}$$

Combining Equations 7.11 through 7.13, the analytical scale-linking model to predict the stiffness recovery R_E of ECC as a function of tensile strain can be expressed as shown in

Equation 7.14, where $r_E(\delta)$ was determined in Section 7.3.3 and $p(\delta,\varepsilon)$ was determined in Section 7.3.2.

$$R_E(\varepsilon) = \frac{E'}{E_0} = \frac{1}{\frac{\varepsilon t}{\int_0^\infty \delta p(\delta,\varepsilon)\, d\delta}\left(\int_0^\infty \frac{p(\delta,\varepsilon)}{r_E(\delta)} d\delta - 1\right) + 1} \tag{7.14}$$

To verify this analytical scale-linking model, the stiffness recovery values predicted from the model were compared to macro-scale experimental stiffness recovery data. The experimental data was obtained using preloaded dogbone specimens, which underwent 10 cyclic wetting and drying cycles before reloading. The model and experimental data are shown in Figure 7.11.

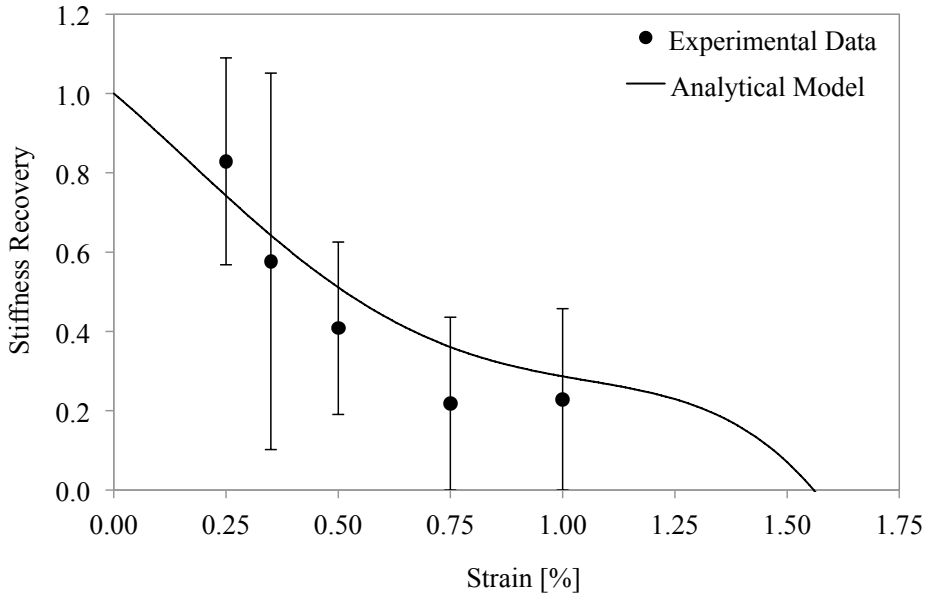

Figure 7.11: Comparison of the analytical scale-linking model to experimental data.

The average stiffness recovery values from the experimental data correspond relatively well to those predicted from the analytical scale-linking model. The variability in the experimental data is due to variability in the crack width distributions between samples at specified strain levels. Figure 7.5 shows the relatively high variation in the mean crack width and standard deviation of

samples at various strain levels, and this variability would directly translate to variation in stiffness recovery, as shown in Figure 7.11. However, since the analytical scale-linking model captures the behavior of the average stiffness recovery on the macro-scale, the model successfully links meso- and macro-scale recovery and can be used to predict the level of stiffness recovery in ECC as a function of tensile strain.

To determine how changes in the crack width distribution affect the analytical model, the distributions obtained from previous studies by Liu[2] and Ranade[3] were used as input for the model and the results are shown in Figure 7.12. All of the crack width distributions result in similar stiffness recovery values at strain levels below 1%, but deviate at larger values of tensile strain. This is due to the evolution of average crack width and number of cracks as tensile strain increases. In the mix used in this study, the number of cracks increased with tensile strain, but the average crack width remained relatively stable. This is in contrast to the mixes used in previous studies, were both the average crack width and number of cracks increased with imposed tensile strain.

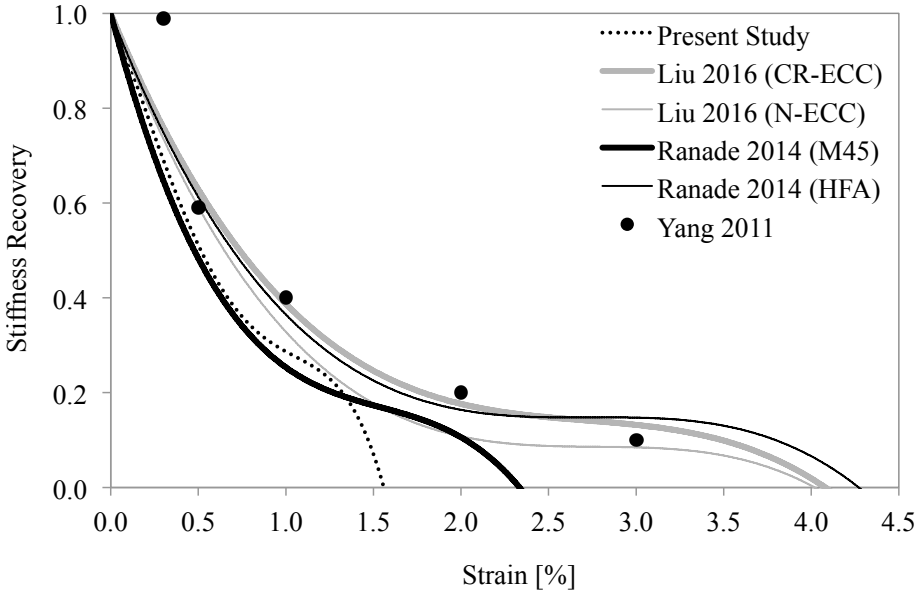

Figure 7.12: Effect of crack width distribution on the analytical scale-linking model.

In addition to the experimental data shown in Figure 7.11, another set of experimental stiffness recovery data from previous work performed by Yang[8] is shown in Figure 7.12. This data is

captured well by the models obtained using crack width distributions from Liu and Ranade, further indicating the ability of this analytical model to predict stiffness recovery.

7.4 Conclusions

In this chapter, the experiment used to determine if the healing products formed in ECC are a function of crack width and the work performed to determine the correlation between stiffness recovery and imposed tensile strain were described. Based on the results of these investigations, the following conclusions can be drawn:

- The healing products formed in ECC are not a function of crack width, as both C-S-H and crystalline healing products ($Ca(OH)_2$ and $CaCO_3$) can be found in cracks of any size.
- Stiffness recovery is highly dependent on crack width, as the stiffness recovery of ECC was found to decrease exponentially as crack width increased through the use of single-crack specimens.
- The analytical scale-linking model assuming the stiffness of ECC acts as a series of springs successfully links meso- and macro-scale stiffness recovery and can be used to predict the level of stiffness recovery in ECC as a function of tensile strain.

References

[1] Kan, L.L., Shi, H.S., Sakulich, A.R., & Li, V.C. (2010). Self-Healing Characterization of Engineered Cementitious Composite Materials. *ACI Materials Journal, 107*, 617-624.

[2] Liu, H., Zhang, Q., Gu, C., Su, H., & Li, V.C. (2016). Influence of micro-cracking on the permeability of engineered cementitious composites. *Cement and Concrete Composites, 72,* 104-113.

[3] Ranade, R., Zhang, J., Lynch, J.P., & Li, V.C. (2014). Influence of micro-cracking on the composite resistivity of Engineered Cementitious Composites. *Cement and Concrete Research, 58,* 1-12.

[4] Li, V.C., Wang, S., & Wu, C. (2001). Tensile Strain-Hardening Behavior of PVA-ECC. *ACI Materials Journal, 98*, 483-492.

[5] Li, V.C., Wu, C., Wang, S., Ogawa, A., & Saito, T. (2002). Interface Tailoring for Strain-Hardening PVA-ECC. *ACI Materials Journal, 99,* 463-472.

[6] Paegle, I., & Fischer, G. (2011). Evaluation of standardized test methods to characterize fiber reinforced cement composites. In *Proceedings of Strain Hardening Cementitious Composites 2*. Rio de Janeiro, Brazil.

[7] Pereira, E.B., Fischer, G., & Barros, J.A.O. (2012). Direct assessment of tensile stress-crack opening behavior of Strain Hardening Cementitious Composites (SHCC). *Cement and Concrete Research, 42,* 834-846.

[8] Yang, Y., Yang, E.H., & Li, V.C. (2011). Autogenous healing of engineered cementitious composites at early age. *Cement and Concrete Research, 41*, 176-183.

PART IV: APPLICATION OF SELF-HEALING ECC IN THE RAILROAD INDUSTRY

CHAPTER 8: TECHNICAL CHALLENGES OF CURRENT RAILROAD TIES

8.1 Introduction

Railroad ties are an integral part of any railroad track infrastructure. They are typically embedded in rock ballast and the metal track rails are fastened to the top of the ties. The spacing between ties is approximately 0.5 m, depending on the tie material, strength, and stiffness, so there may be as many as 2000 ties per kilometer of track. Historically, railroad ties are made of timber. However, due to the limited durability of timber ties and the diminishing availability of wood with suitable qualities, many railroad companies have been shifting to the use of prestressed concrete railroad ties.

Prestressed concrete railroad ties were first installed in North America in the early 1960s, but there have been extensive reports of premature failure since their inception. Although the design lifespan of a prestressed concrete tie is considered to be approximately 50 years, unexpected and excessive cracking of the concrete has led to premature failure and thus frequent and costly maintenance for railroad companies. For example, in 1997 Amtrak installed 118,000 concrete ties that lasted only 4 years before replacements were needed.[1]

Premature failure of prestressed concrete railroad ties is caused by numerous factors. Harsh environmental conditions, such as freeze-thaw cycles, and chemical attack, including alkali silica reactions (ASR) and delayed ettringite formation (DEF), cause internal pressures that are large enough to induce cracking within the concrete matrix. In addition, overloading and increasing

speeds on railroad tracks cause flexural cracking and rail seat deterioration (RSD), which leads to abrasion and cracking of the concrete ties under the surface of the rail.[2-9]

The stiffness of prestressed concrete ties is also a cause of concern in the rail industry. Prestressed concrete tie tracks have been shown to have moduli values more than twice that of comparable wood tie tracks.[10] This causes large vibrations, which increase the occurrence and magnitude of impact loads, resulting in more frequent and severe damage to track infrastructure. In addition, the high stiffness of prestressed concrete ties makes them less versatile, as they cannot be used to replace damaged wood ties in existing wood track.

The use of a self-healing ECC material tuned to the specific needs of the railroad industry has the potential to mitigate many of these challenges associated with current prestressed concrete railroad ties. This chapter will discuss the main technical challenges of prestressed concrete ties, focusing on ASR, DEF, RSD, and tie stiffness, and the potential of using self-healing ECC to solve these problems.

8.2 Alkali-Silica Reactions and Delayed Ettringite Formation

ASR and DEF have been cited as mechanisms leading to premature failure of prestressed concrete railroad ties.[7,8] Both reactions result in products that expand within the concrete matrix, resulting in cracking and eventual spalling of the concrete ties over time (Figure 8.1).

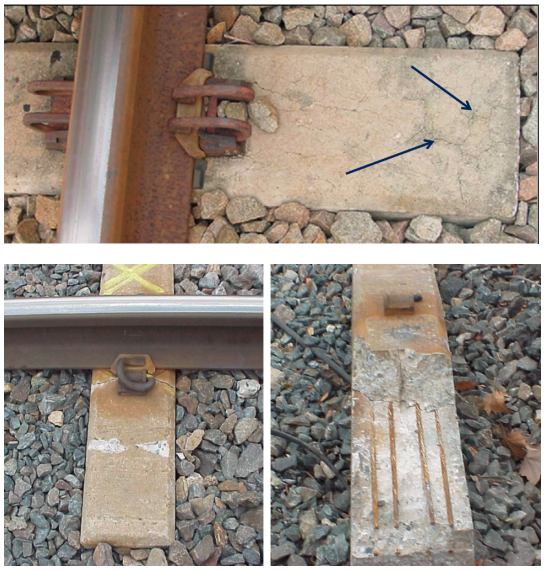

Figure 8.1: Cracking and spalling of prestressed concrete ties due to ASR and DEF.[11]

ASR occurs due to a chemical reaction that takes place between the alkalis in cement paste and reactive forms of silica that are often present in aggregates. Under certain conditions, this reaction can produce an alkali-silicate-hydrate gel that swells when exposed to water. This increase in volume of the alkali-silicate-hydrate gel causes internal tensile stresses large enough to induce cracking within the concrete matrix.[12]

DEF is caused by elevated curing temperatures (70-88°C), which delay the normal formation of ettringite until after the concrete has cooled and hardened. When ettringite does begin to form, it causes an increase in volume and this expansion can also lead to cracking of the concrete matrix.[12] Concrete ties are often cured at elevated temperatures in precast plants to rapidly develop the compressive strength necessary for the prestressing process, and this elevated curing temperature makes them susceptible to damage caused by DEF.

Although ASR and DEF have both been shown to cause damage in prestressed concrete ties, the interaction between the two is not fully understood. It is thought that the expansion caused by ASR occurs during the high-temperature curing process, resulting in immediate cracking. Ettringite is then believed to begin forming in these initial cracks, further increasing internal tensile stresses and leading to continued crack propagation and severe damage to the ties.[7,8]

8.3 Rail Seat Deterioration

RSD was found to be the most pressing problem for heavy haul track.[2-6] RSD is a complicated failure mode that includes damage of the fasteners that connect the ties and rails as well as deterioration of the concrete tie located directly under the surface of the rail (Figures 8.2 and 8.3). Heavy loads, abrasive fines, and moisture are the main factors contributing to RSD in North America. RSD is thought to be a result of abrasion, hydraulic pressure cracking, and freeze-thaw cracking. Abrasion creates surface wear on the rail seat due to a combination of rubbing of the tie pad, grinding of abrasive fines that are present between the tie pad and rail seat, and impact between the rail and tie. Hydraulic pressure cracking occurs when wheel loads force water in and out of concrete pores, creating pressures large enough to crack the concrete matrix. Freeze-thaw cracking may also contribute the RSD in northern climates due to the expansion of freezing water within the matrix. The damage patterns observed on rail seats range from the wearing of

cement paste, which exposes the coarse aggregate (Figure 8.2), to the wearing of all concrete components, including the aggregate (Figure 8.3).

Figure 8.2: Erosion of cement paste on the rail seat of a prestressed concrete tie.[13]

Figure 8.3: Severe RSD including erosion of cement paste and aggregate.[14]

8.4 Prestressed Concrete Tie Stiffness

The use of traditional concrete and prestressing steel causes current concrete ties to have a much higher stiffness than wood ties, posing numerous problems for the railroad industry. Prestressed concrete tie tracks have been shown to have moduli values more than twice that of comparable wood tie tracks, resulting in larger vibrations as trains move over concrete tracks.[10] These vibrations increase the occurrence and magnitude of impact loads, resulting in more frequent and

severe damage to track infrastructure and cargo. In addition, the larger vibrations experienced on prestressed concrete tracks lead to uncomfortable rides for passengers and have been shown to greatly increase railroad workers' risk of developing serious neck and lower back disorders.[15]

As wood ties fall into disrepair along existing wood track, rail companies have expressed the desire to replace these with concrete ties. However, due to the large differences in tie stiffness, wood and concrete ties are not interchangeable and a concrete tie cannot be used to replace a damaged wood tie in a wood track. Currently, as wood ties become damaged, the speeds allowed on the track are lowered until enough ties are damaged that the whole track must be replaced with prestressed concrete ties. This practice is extremely expensive for rail companies, as lowering train speed reduces the amount of cargo that can be transported and both damaged and undamaged wood ties are replaced when the entire track is converted to prestressed concrete.

8.5 Advantages of ECC

A self-healing ECC material tuned to the specific performance needs of the railroad industry has the potential to mitigate many of the challenges associated with current prestressed concrete railroad ties. In general, the intrinsic tensile behavior and ductility of ECC will suppress any cracking and brittle fracture, which current concrete ties are always susceptible to since they are manufactured with traditional brittle concrete. The ductile nature of ECC may also allow for the removal of prestressing steel, which would not only greatly lower the manufacturing and material costs in comparison to current prestressed concrete ties, but also lead to a lower tie stiffness. In addition, the self-healing functionality of ECC will allow the ties to regain permeability and mechanical properties should damage occur.

ECC has been shown to be highly resistant to ASR.[16] In a previous study, samples showed no expansion after being exposed to a highly alkaline environment at elevated temperatures for 30 days, conditions that would typically cause ASR-related expansion in traditional concrete and prestressed concrete ties. This resistance to ASR is attributed to the use of non-reactive silica sand, high volumes of fly ash, and fibers. ECC abstains from the use of coarse aggregates, which often contain the reactive forms of silica that contribute to ASR. Instead, ECC uses non-reactive silica sand as fine aggregate. The addition of fly ash in ECC reduces the alkalinity of the pore solution due to the consumption of calcium hydroxide in the pozzolanic reaction, thus reducing

the amount of alkalis available for ASR. If ASR expansion were to occur within the ECC matrix, the presence of fibers would suppress any cracking. For this reason, it is also expected that the use of fibers would allow ECC to be resistant to expansion caused by DEF, although DEF in ECC has not been studied.

Previous work has also demonstrated the feasibility of tuning ECC to obtain a low elastic modulus.[17] Ground tire rubber was incorporated into an ECC matrix, lowering the stiffness of the material from 23 to 11 GPa. Lowering the stiffness of ECC to this level allows it to have a similar material stiffness to many types of wood.[18] Therefore, if prestressing is not necessary in an ECC tie due to the material ductility, it would be feasible to produce an ECC tie with a stiffness similar to that of a wood tie.

8.6 Conclusions

Based on the information regarding current prestressed concrete railroad ties and ECC presented in this chapter, the following conclusions can be drawn:

- There are many challenges associated with current prestressed concrete ties, including ASR, DEF, RSD, and high material and tie stiffness.
- The ductile nature and self-healing functionality of ECC would allow it to mitigate many of these challenges, as it would suppress cracking and brittle fracture, resist ASR and DEF expansion, and be able to regain permeability and mechanical properties though self-healing if damage should occur.
- ECC has also shown the ability to be tuned to a low stiffness through the use of ground tire rubber. This means that an ECC tie could be manufactured to have a stiffness similar to that of a wood tie, if prestressing can be removed due to the ductile nature of ECC.

The feasibility of creating an ECC railroad tie that meets all railroad industry standards while removing prestressing steel is discussed in Chapter 9.

References

[1] Amtrak. (2012). Evolution of Amtrak's Concrete Crosstie and Fastening System Program. PowerPoint presentation. Presented at the *International Concrete Crosstie and Fastening System Symposium*. University of Illinois at Urbana-Champaign, Urbana, IL, USA.

[2] Zehman, J.C., Edwards, J.R., Barkan, C.P.L., & Lange, D.A. (2009). Failure Mode and Effect Analysis of Concrete Ties in North America. In *Proceedings of the 9th International Heavy Haul Conference* (pp. 270-278). Shanghai, China.

[3] Zehman, J.C., Kernes, R.G., Edwards, J.R., Lange, D.A., & Barkan, C.P.L. (2011). Moisture-Driven Deterioration and Abrasion of Concrete Sleeper Rail Seats. In *Proceedings of the 9th World Congress on Railway Research*.

[4] Kernes, R.G., Edwards, J.R., Dersch, M.S., Lange, D.A., & Barkan, C.P.L. (2011). Investigation of the Impact of Abrasion as a Concrete Crosstie Rail Seat Deterioration (RSD) Mechanism. In *AREMA 2011 Annual Conference in Conjunction with Railway Interchange 2011*.

[5] Kernes, R.G., Edwards, J.R., Dersch, M.S., Lange, D.A., & Barkan, C.P.L. (2011). Investigation of the Dynamic Frictional Properties of a Concrete Crosstie Rail Seat and Pad and its Effect on Rail Seat Deterioration (RSD). In *Transportation Research Board 91st Annual Meeting*.

[6] Shurpali, A.A., Kernes, R.G., Edwards, J.R., Dersch, M.S., Lange, D.A., & Barkan, C.P.L. (2013). Investigation of the Mechanics of Rail Seat Deterioration (RSD) and Methods to Improve the Abrasion Resistance of Concrete Sleeper Rail Seats. In *Proceedings of the 10th International Heavy Haul Association Conference*. New Delhi, India.

[7] Mielenz, R.C., Marusin, S.L., Hime, W.G., & Jugovic, Z.T. (1995). Investigation of prestressed concrete railway tie distress. *Concrete International, 17*, 62-68.

[8] Collepardi, M. (2003). A state-of-the-art review on delayed ettringite attack on concrete. *Cement and Concrete Composites, 25*, 401-407.

[9] Kaewunruen, S. & Remennikov, A.M. (2010). Dynamic Crack Propagations in Prestressed Concrete Sleepers in Railway Track Systems Subjected to Severe Impact Loads. *ASCE Journal of Structural Engineering, 136*, 749-754.

[10] Kish, A., et al. (1977). Track Structures Performance – Comparative Analysis of Specific Systems and Component Performance. *U.S. Department of Transportation Report FRA/OR&D-77/29.*

[11] Cloutier, A. (2014). Concrete Ties: The Amtrak Experience. PowerPoint presentation. Presented at the *International Concrete Crosstie and Fastening System Symposium*. University of Illinois at Urbana-Champaign, Urbana, IL, USA.

[12] Mindess, S., Young, J.F., & Darwin, D. (2003). *Concrete (2nd Edition)*. Upper Saddle River, NJ: Prentice Hall, Pearson Education, Inc.

[13] Zehman, J.C., Edwards, J.R., Lange, D.A., & Barkan, C.P.L. (2009). Investigation of Potential Concrete Tie Rail Seat Deterioration Mechanisms: Cavitation Erosion and Hydraulic Pressure Cracking. *Transportation Research Board 89th Annual Meeting, 10-2411.*

[14] Greve, M.J., Dersch, M.S., Edwards, J.R., Barkan, C.P.L., Thompson, H., Sussmann, T.R., & McHenry, M.T. (2015). Examination of the Effect of Concrete Crosstie Rail Seat Deterioration on Rail Seat Load Distribution. *Transportation Research Record: Journal of the Transportation Research Board, 2476,* 1-7.

[15] Johanning, E., Landsbergis, P., Fischer, S., Christ, E., Göres, B., & Luhrman, R. (2006). Whole-body vibration and ergonomic study of US railroad locomotives. *Journal of Sound and Vibration, 298*, 594-600.

[16] Sahmaran, M. & Li, V.C. (2008). Durability of mechanically loaded engineered cementitious composites under highly alkaline environments. *Cement and Concrete Composites, 30*, 72-81.

[17] Huang, X., Ranade, R., Ni, W., & Li, V.C. (2013). On the use of recycled tire rubber to develop low E-modulus ECC for durable concrete repairs. *Construction and Building Materials, 46*, 134-141.

[18] Green, D.W. (2001). Wood: Strength and Stiffness. *Encyclopedia of Materials: Science and Technology.* Elsevier Science Ltd., ISBN 0-08-0431526, 9732-9736.

CHAPTER 9: FEASIBILITY OF AN ECC RAILROAD TIE

9.1 Introduction

A self-healing ECC material tuned to the specific performance needs of the railroad industry has the potential to mitigate many of the challenges associated with current prestressed concrete railroad ties. Cementitious ties in use today are susceptible to cracking and fracture caused by numerous factors since they are manufactured with traditional brittle concrete. The tensile ductility and self-healing functionality of ECC would not only suppress cracking in a tie manufactured with ECC, but also allow the ties to regain permeability and mechanical properties should damage occur. In addition, the ductile nature of ECC may also allow for the removal of prestressing steel.

Companies in the rail industry have been actively pursuing the development of cementitious ties that do not require prestressing. Removing prestressing would not only lower manufacturing and material costs, but also lead to a lower tie stiffness. As discussed in Chapter 8, lowering the stiffness of concrete ties would allow them to be interchangeable with wood ties, which would simplify the tie replacement process and lower maintenance costs on wood tracks. Due to industry interest, this chapter will discuss the feasibility of creating an ECC railroad tie that meets all railroad industry standards without the addition of prestressing steel.

9.2 AREMA Recommendations

The Manual for Railway Engineering[1] is published annually by the American Railway Engineering and Maintenance-of-Way Association (AREMA) and contains recommended practices for the engineering, design, and construction of railways. The manual includes recommendations regarding materials, dimensions, structural strength, and design loads for prestressed concrete ties, as well as descriptions of laboratory tests to determine the suitability of new designs. Although these recommendations are not required or enforced, rail companies view

the manual as an industry standard, so it is important to ensure ECC meets the material requirements described in the manual.

AREMA recommends a minimum 28 day compressive strength of 48 MPa. This relatively high compressive strength is recommended due to the use of prestressing steel and loads experienced on heavy haul track, and many companies often require strengths of over 60 MPa. Past research has shown that ECC achieves a compressive strength of 30-70 MPa, meaning that some previous mixes designs have shown the capability to meet this industry standard.

Due to typical track configuration, railroad ties experience repeated flexural loading. Although AREMA flexural recommendations are dependent on tie geometry, tie spacing in track, tonnage, and train speed, the average flexural strength recommendation for a prestressed concrete tie is approximately 15 MPa. Therefore, in order to remove prestressing steel in an ECC tie, the ECC material must be able to achieve a flexural strength in this same range. Previous research has shown that ECC achieves flexural strengths between 12-14 MPa.[2-4] Although this might meet recommendations for some tracks with low tonnage and train speed, it will be important to increase the flexural strength of ECC to ensure proper functionality without the need for prestressing steel. In addition, since the flexural loading applied to ties is repeated every time a set of train wheels passes over a tie, the ECC material should show the ability to withstand flexural fatigue loading. Past research has demonstrated this ability in ECC, but it will be important to verify this behavior.[5,6]

Although there are many other AREMA recommendations to consider, the work described in this chapter will focus mainly on achieving and verifying adequate compressive strength, flexural strength, and fatigue behavior while maintaining the tensile properties and multiple cracking behavior of ECC.

9.3 Mix Development

9.3.1 Raw Materials and Mix Proportions

Three ECC mixes used in previous studies were chosen as the starting point to determine a mix for future compression, flexural, and fatigue testing. These mixes were chosen based on past

performance in comparison to AREMA recommendations, and the mix proportions are given in Table 9.1.

Table 9.1: ECC mix proportions by weight fraction.

Mix Name	Cement	Fly Ash	Sand	Water	HRWRA	VMA	Fiber	Fiber Length [mm]
M1	1	0.1	1	0.45	0.02	0.02	0.032	8
M2	1	1.2	0.8	0.58	0.013	0	0.045	12
M3	1	2.2	1.16	0.79	0.013	0	0.065	12

Type I ordinary Portland cement, Class F fly ash, silica sand with an average particle size of 110 μm, a polycarboxylate-based high range water reducing admixture (HRWRA), a viscosity modifying admixture (VMA), and polyvinyl alcohol (PVA) fibers were used to prepare the ECC specimens. The PVA fibers accounted for 2% of the total mix volume in all three mixes. The average diameter of all PVA fibers was 39 μm, but the length varied between 8-12 mm, depending on the mix and as shown in Table 9.1. The fibers had a tensile strength of 1600 MPa, a density of 1300 kg/m^3, an elastic modulus of 42.8 GPa, and a maximum elongation of 6%. In addition, the surfaces of the fibers were coated with an oiling agent (1.2% by weight) to reduce the interfacial chemical bond between the fiber and matrix caused by the strong hydrophobic nature of the PVA fibers.[7,8]

9.3.2 Specimen Preparation

The raw materials were mixed in a 20 L force-based Hobart mixer according to the proportions shown in Table 9.1. After mixing, the fresh ECC was cast into molds and covered with plastic sheeting. The dimensions of the molds varied depending on the planned experimental setup, and will be discussed in more detail in Section 9.4. After 24 hours, the specimens were removed from the molds and cured at room temperature until testing.

9.4 Experimental Setup

Uniaxial tensile tests were used to determine the tensile behavior and ductility of the ECC mixes. Dogbone samples, as recommended by the Japan Society of Civil Engineers for testing high ductility concretes, were used in this experimental setup.[9] The geometry of the dogbone samples is shown in Figure 9.1. Uniaxial tensile loading was applied to the dogbones using a 50 kN

capacity load frame (Instron Model 5969) under displacement control and a loading rate of 0.5 mm/min, and two Linear Variable Displacement Transducers (LVDTs) were attached to the specimens to measure tensile elongation during loading.

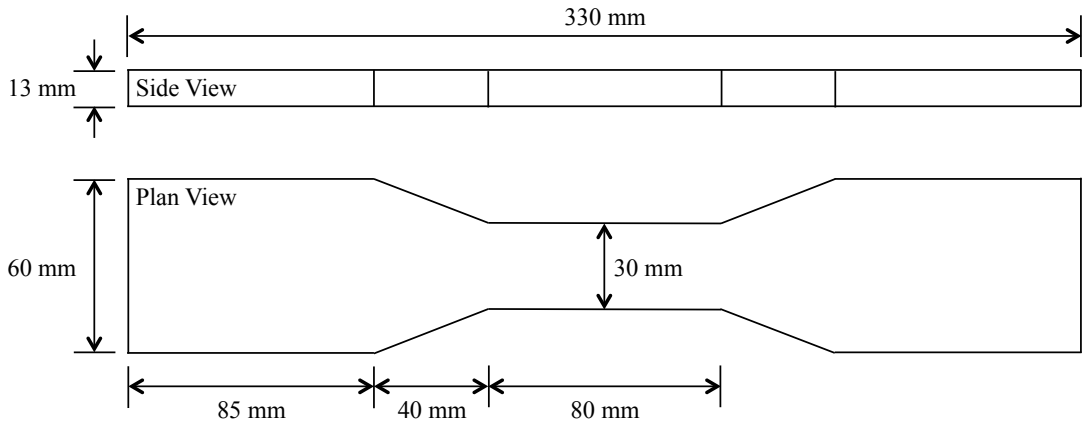

Figure 9.1: Geometry of dogbone specimens.

Compression testing was performed on ECC cylinders measuring 7.62 cm in diameter and 15.24 cm in length. Prior to testing, cylinders were capped as described in ASTM C617 using sulfur mortar. All testing was carried out in accordance with ASTM C39, at a loading rate of 0.25 ± 0.05 MPa/sec.

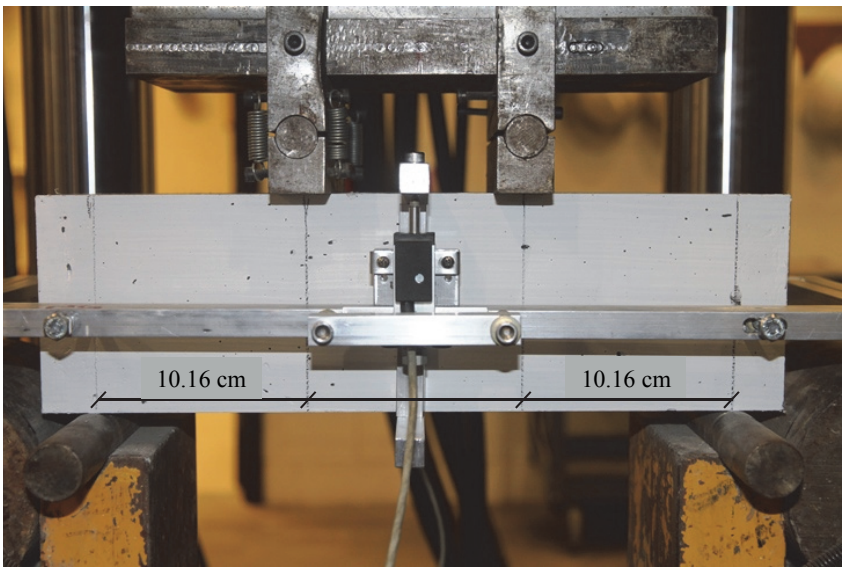

Figure 9.2: Flexural test setup.[10]

Flexural strength (or modulus of rupture, MOR) was determined using third-point flexure tests on ECC beams measuring 10.16 cm x 10.16 cm x 35.56 cm. The experimental setup is shown in Figure 9.2 and follows ASTM C1609. Beams were loaded using a constant mid-point deflection rate of 0.05 mm/min, and the mid-point deflection was measured using two potentiometers, one of which can be seen in Figure 9.2.

The flexural fatigue behavior of ECC was determined using beams measuring 38 mm x 76 mm x 305 mm, and all testing was carried out at least 60 days after casting to avoid possible strength increases due to continued hydration during testing.[11] The span between specimen supports was 254 mm, and four point bending tests were conducted with a constant moment span length of 84.7 mm. Since previous research has shown that ECC shows no sign of size effect in flexural tests of span length up to 2.8 m, the MOR determined during the flexural test setup described above was used to determine the loads applied during fatigue testing.[12] Three fatigue load ratios, defined as the ratio of the maximum stress applied during testing to the MOR, were used to conduct the fatigue tests. The fatigue load ratios chosen were 0.9, 0.8, and 0.7, and the minimum flexural stress applied during testing was 20% of the maximum stress. To conduct the fatigue tests, all samples were initially loaded to the maximum stress level under load control at a rate of 10 N/sec. Once the maximum stress level was reached, fatigue cycles began with sinusoidal cyclic loading at a frequency of 8 Hz. The fatigue load cycles (S) and corresponding number of cycles to failure (N) were then used to obtain the S-N relationship.

9.5 Results and Discussion

9.5.1 Tensile and Compressive Behavior

The three mixes shown in Table 9.1 were tested in tension at 14 days after casting to determine which performed well enough to justify further tension, compression, and flexural testing at 28 days. The results are shown in Figure 9.3. Although M1 had an average tensile strain capacity of approximately 1% and an average ultimate strength over 4 MPa, M2 and M3 were chosen for further testing at 28 days based on their ultimate strain capacity.

Figures 9.4 and 9.5 show the 28 day compression and tension results for M2 and M3 (28 day flexural test results will be discussed in Section 9.5.2). Both mixes had maximum ultimate tensile strengths of nearly 7 MPa, with tensile strain capacities over 2%. However, while M2 had

an average compressive strength of 49.5 MPa, M3 had an average of only 41 MPa. Since the minimum compressive strength recommended by AREMA is 48 MPa, M3 does not meet the railroad industry standards regarding compression.

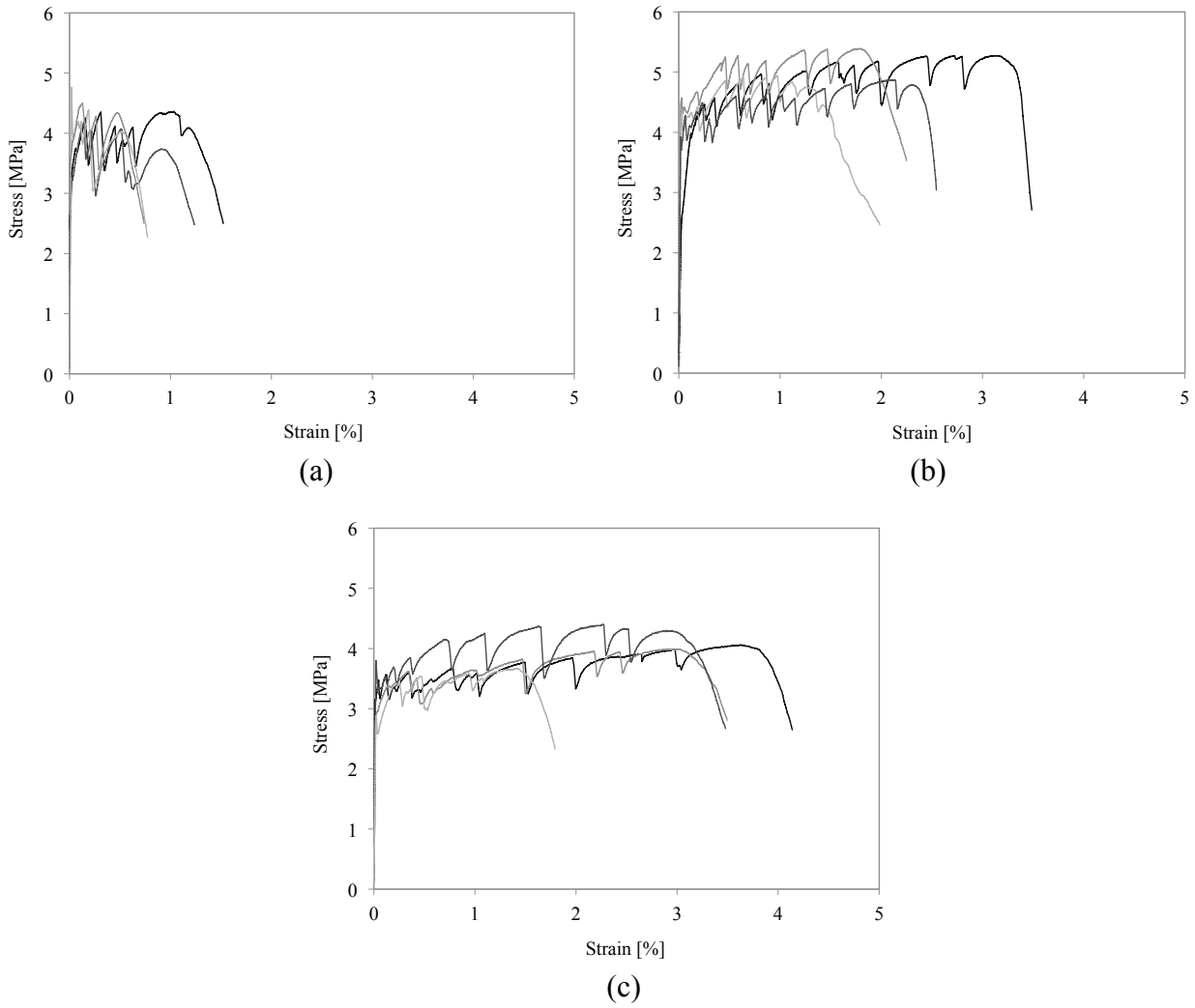

Figure 9.3: 14 day uniaxial tensile test results for (a) M1, (b) M2, and (c) M3.

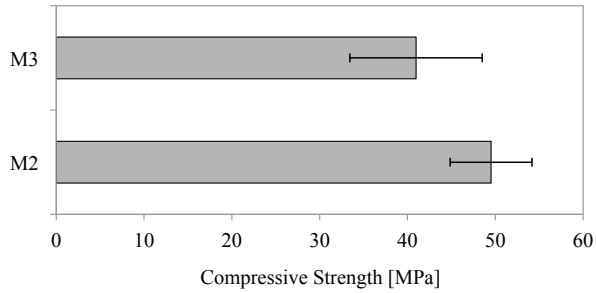

Figure 9.4: 28 day compressive strength results for M2 and M3.

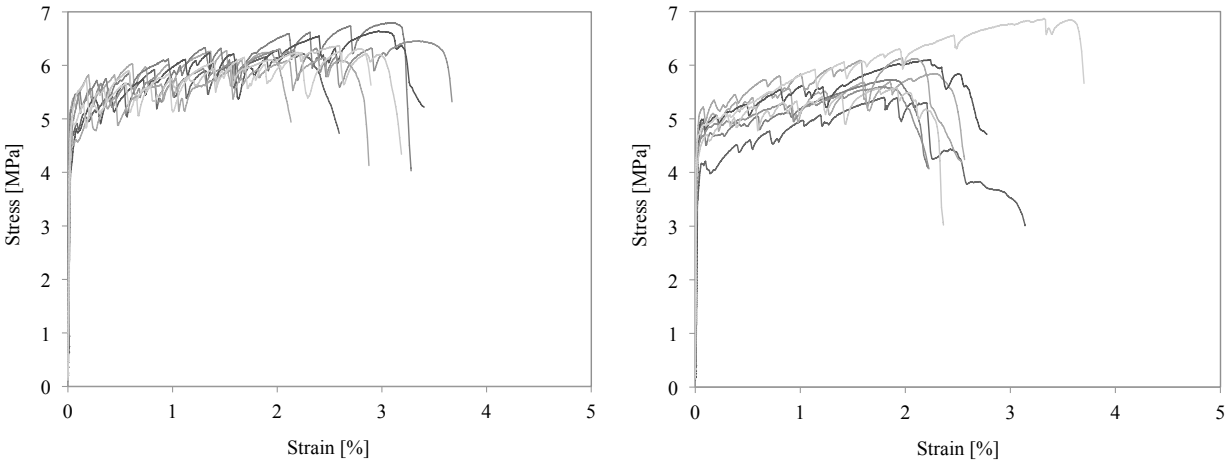

(a) (b)

Figure 9.5: 28 day uniaxial tensile test results for (a) M2 and (b) M3.

9.5.2 Flexural Behavior

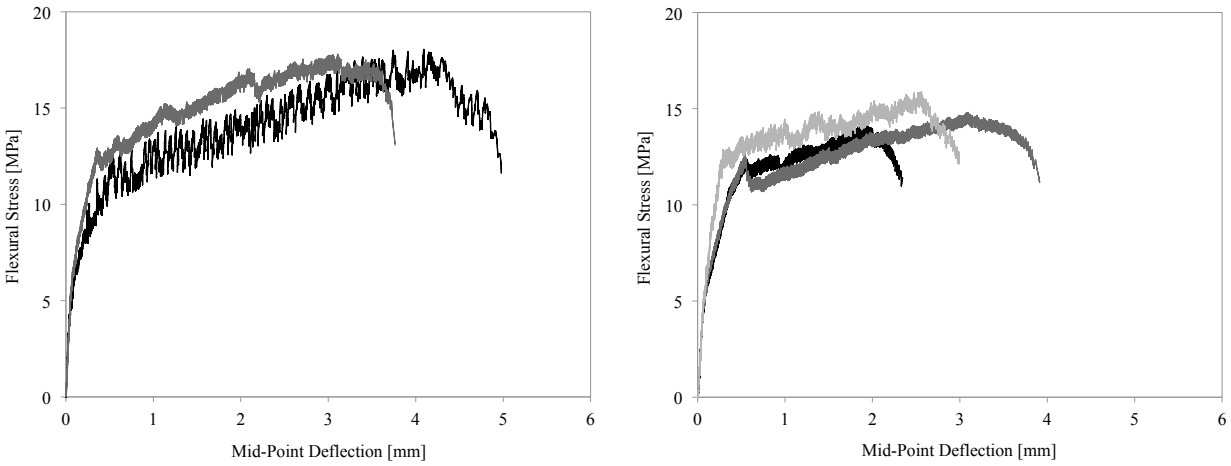

(a) (b)

Figure 9.6: 28 day flexural test results for (a) M2 and (b) M3.

Figure 9.6 shows the 28 day flexural test results for M2 and M3. M2 was able to achieve ultimate flexural strengths up to 18 MPa, while M3 could achieve strengths of up to 16 MPa. As discussed in Section 9.2, railroad tie flexural strengths recommended by AREMA are dependent on tie geometry, tie spacing in track, tonnage, and train speed, but the average flexural strength recommendation for a prestressed concrete tie is approximately 15 MPa. Therefore, in order to

remove prestressing steel in an ECC railroad tie, ECC would have to achieve flexural strengths within this same range. Since both M2 and M3 had flexural strengths greater than 15 MPa, it can be concluded that the manufacturing and use of an ECC tie without prestressing is feasible.

9.5.3 Fatigue Behavior

Since the flexural loading applied to ties is repeated every time a set of train wheels passes over a tie, it is important to verify the ability of ECC to withstand flexural fatigue loading. Flexural fatigue testing was only carried out on M2, as M3 did not meet the AREMA recommendations for compressive strength. The resulting S-N relationship for M2 is shown in Figure 9.7. These results are comparable to previous flexural fatigue studies using ECC, and show that M2, which meets AREMA recommendations for compressive and flexural strength, also has the ability to withstand flexural fatigue loading. Although the S-N curve in this experiment is comparable to past ECC studies, it is important to note that the maximum MOR achieved for M2 was 18 MPa, while the maximum MOR in previous fatigue work was only 9.5 MPa.[5]

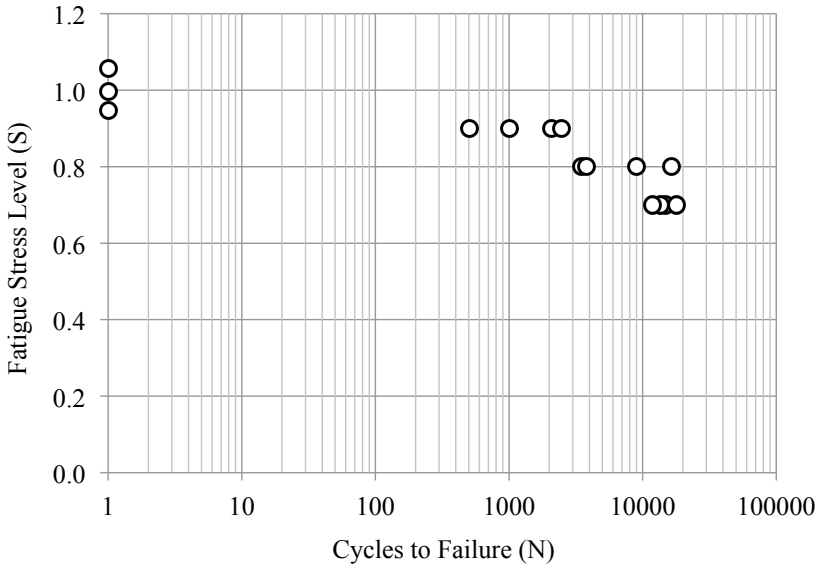

Figure 9.7: S-N relationship for M2.

9.5.4 Potential Influence of Silica Fume

Although M2 has been shown to meet the minimum compressive strength recommended by AREMA and has a flexural strength large enough to potentially remove prestressing, many

companies in the rail industry often require strengths much higher than these recommendations due to the excessive loading seen on heavy haul lines. Therefore, it is important to attempt to increase the strength of ECC as much as possible while maintaining tensile ductility and multiple cracking behavior.

Previous work has shown that the addition of silica fume increases the compressive strength of concrete[13-15], so silica fume was added to M2 in an attempt to further increase the strength of the material. Although several mix proportions containing varying amounts of silica fume were tested, the proportion for the mix that achieved the highest strengths is shown in Table 9.2. This mix proportion is the same as M2, but with 10% of the sand replaced by silica fume. The raw materials, specimen preparation process, and compression and tension testing methods described in Sections 9.3 and 9.4 were used to cast and test all of the mixes containing silica fume.

Table 9.2: Weight fractions of ECC mix proportion containing silica fume.

Cement	Fly Ash	Silica Fume	Sand	Water	HRWRA	Fiber	Fiber Length [mm]
1	1.2	0.08	0.72	0.581	0.03	0.046	12

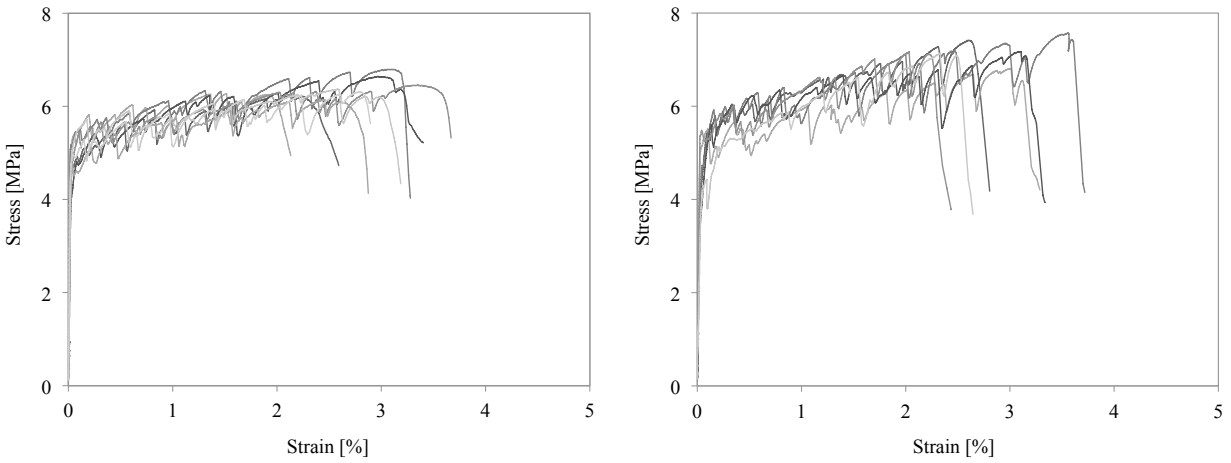

(a) (b)

Figure 9.8: 28 day uniaxial tensile test results for (a) M2 and (b) M2 with silica fume.

The mix in Table 9.2 was tested in both tension and compression at 28 days and compared to the results from M2. It was found that the average compressive strength was not altered, but there

was an increase in ultimate tensile strength. The uniaxial tensile results for both M2 and the new mix containing silica fume are shown in Figure 9.8. While M2 achieved a maximum ultimate tensile strength of 6.8 MPa, the new mix containing silica fume was able to achieve a strength of 7.6 MPa. Although flexural tests were not conducted on this mix due to time constraints, it is expected that this increase in ultimate tensile strength would also lead to an increase in MOR, increasing the potential of removing the prestressing steel from an ECC railroad tie.

9.6 Conclusions

In this chapter, numerous tests were conducted to determine the feasibility of creating an ECC railroad tie that meets all railroad industry standards without the addition of prestressing steel. Based on the results of these tests, the following conclusions can be drawn:

- The average flexural strength of a prestressed concrete tie recommended by AREMA is 15 MPa, and ECC was shown to achieve flexural strengths of 18 MPa without any steel reinforcement. This means that the manufacture and use of an ECC tie without prestressing steel is feasible.
- One of the ECC mixes used in this study was able to achieve an average compressive strength of 49.5 MPa, surpassing the 48 MPa minimum compressive strength recommended by AREMA.
- ECC was also shown to withstand flexural fatigue loading, an important characteristic as railroad ties experience fatigue loading every time a set of train wheels passes over a tie.
- Silica fume was shown to increase the maximum ultimate tensile strength of ECC from 6.8 MPa to 7.6 MPa. It is expected that this increase in ultimate tensile strength would also lead to an increase in MOR, thus increasing the potential of removing the prestressing steel from an ECC railroad tie.

References

[1] American Railway Engineering and Maintenance-of-Way Association. (2014). *Manual for Railway Engineering.* Lanham, MD.

[2] Lepech, M., & Li, V.C. (2003). Preliminary Findings on Size Effect in ECC Structural Members in Flexure. In *Proceedings of the International Brittle Matrix Composites (BMC) 7 Symposium* (pp. 57-66). Poland.

[3] Maalej, M., & Li, V.C. (1994). Flexural/Tensile Strength Ratio in Engineered Cementitious Composites. *ASCE Journal of Materials in Civil Engineering*, 6, 513-528.

[4] Li, V.C. (1998). Engineered Cementitious Composites – Tailored Composites Through Micromechanical Modeling. In *Fiber Reinforced Concrete: Present and the Future.* Eds. N. Banthia, A. Bentur, A. and A. Mufti. Canadian Society for Civil Engineering, Montreal, 67-97.

[5] Matsumoto, T., Suthiwarapirak, P., & Kanda, T. (2003). Mechanisms of Multiple Cracking and Fracture of DFRCC under Fatigue Flexure. *Journal of Advanced Concrete Technology,* 1, 299-306.

[6] Qian, S.Z., Li, V.C., Zhang, H., & Keoleian, G.A. (2013). Life cycle analysis of pavement overlays made with Engineered Cementitious Composites. *Cement & Concrete Composites*, 35, 79-88.

[7] Li, V.C., Wang, S., & Wu, C. (2001). Tensile Strain-Hardening Behavior of PVA-ECC. *ACI Materials Journal, 98*, 483-492.

[8] Li, V.C., Wu, C., Wang, S., Ogawa, A., & Saito, T. (2002). Interface Tailoring for Strain-Hardening PVA-ECC. *ACI Materials Journal, 99,* 463-472.

[9] Japan Society of Civil Engineers. (2008). *Recommendations for Design and Construction of High Performance Fiber Reinforced Cement Composites with Multiple Fine Cracks.* Tokyo, Japan: JSCE, Testing Method 1-5.

[10] Ranade, R. (2014). Advanced Cementitious Composite Development for Resilient and Sustainable Infrastructure. PhD Dissertation, Ann Arbor, MI: University of Michigan.

[11] Oh, B.H. (1991). Fatigue-Life Distributions of Concrete for Various Stress Levels. *ACI Materials Journal,* 88, 122-128.

[12] Lepech, M., & Li, V.C. (2004). Size effect in ECC structural members in flexure. In *Proceedings of Fracture Mechanics of Concrete and Concrete Structures 5* (pp. 1059-1066). Vail, Colorado, USA.

[13] Ahmadi, B., & Shekarchi, M. (2010). Use of natural zeolite as a supplementary cementitious material. *Cement and Concrete Composites,* 32, 134-141.

[14] Sabet, F.A., Libre, N.A., & Shekarchi, M. (2013). Mechanical and durability properties of self consolidating high performance concrete incorporating natural zeolite, silica fume and fly ash. *Construction and Building Materials,* 44, 175-184.

[15] Mazloom, M., Ramezanianpour, A.A., & Brooks, J.J. (2004). Effect of silica fume on mechanical properties of high-strength concrete. *Cement and Concrete Composites,* 26, 347-357.

PART V: CONCLUSION

CHAPTER 10: CONCLUDING REMARKS

10.1 Research Overview

10.1.1 Self-Healing in ECC

It was found that the self-healing functionality of ECC is not limited to a controlled laboratory environment and can occur in the natural environment, under random and sometimes extreme environmental conditions. Even after multiple loading events, ECC samples showed significant recoveries of stiffness and first cracking strength when samples were allowed to heal outdoors. However, these recoveries were found to be highly dependent on the average temperature and amount of precipitation.

Although self-healing of ECC has been shown to occur fully under controlled laboratory conditions, complete self-healing does not always occur in the field due to the variations in temperature and precipitation. Therefore, bacteria were used to investigate the potential of further increasing the self-healing functionality of ECC. Incorporating calcite-producing spore-forming bacteria and an organic growth substrate into the ECC matrix proved effective in improving the self-healing behavior of ECC, with cracks as large as 350 μm being completely healed. However, self-healing was only improved in specimens that were continuously exposed to water. Therefore, while this technique is promising, it can only be used in structures that are continuously submerged in water, such as underground and water-retaining infrastructure.

The self-healing functionality of ECC was found to be significantly affected by specimen age. As sample age increased, the self-healing functionality of ECC decreased, with samples

preloaded at 28 months showing much lower levels of recovery compared to samples preloaded at 1 and 9 months. The lower levels of recovery seen in older samples were ultimately caused by changes in the cracking characteristics of ECC over time. As the ECC samples aged, the average crack width produced during loading increased, leading to lower levels of recovery as larger cracks do not heal as quickly or completely as smaller cracks.

Self-healing in ECC was also found to be affected by exposure temperature, results that ultimately confirm the trends observed when healing was allowed to occur in the natural environment. The self-healing functionality of ECC decreased as exposure temperature decreased, with samples exposed to a 2°C environment showing slower rates of self-healing and lower levels of stiffness recovery than samples exposed to a 45°C environment. These results were not unexpected, as it is well known that the rates of cement hydration and pozzolanic reactions, which contribute significantly to the formation of healing products, decrease in cold temperatures.

As experimental observations suggested a strong correlation between the self-healing behavior and cracking characteristics of ECC, an analytical scale-linking model was developed to predict the level of ECC stiffness recovery due to self-healing as a function of imposed tensile strain. Stiffness recovery was found to be highly dependent on crack width at the meso-scale through the use of single-crack specimens, with the stiffness recovery of ECC decreasing exponentially as crack width increased. A model utilizing this meso-scale trend and crack width data from the macro-scale was able to successfully link meso- and macro-scale stiffness recoveries by assuming the stiffness of ECC acts as a series of springs. The model was verified through experimental data and proved to be successful in predicting the stiffness recovery of ECC as a function of tensile strain.

10.1.2 Application in the Railroad Industry

It was found that the manufacture and use of an ECC railroad tie without prestressing steel is feasible. ECC was found to surpass the average flexural strength recommended by the American Railway Engineering and Maintenance-of-Way Association (AREMA), while showing the ability to withstand flexural fatigue loading. Since the recommended flexural strength applies to prestressed concrete ties, the fact that ECC surpasses this strength without the use of reinforcing

steel means that prestressing may not be necessary in an ECC tie. If prestressing is not required, the stiffness of an ECC tie could be tailored to match that of a wood tie, making them interchangeable and of great value to the rail industry. In addition, the removal of prestressing steel would greatly simplify the manufacturing process currently used for cementitious ties, thus reducing production time and costs.

ECC was also found to meet the AREMA recommendations for minimum compressive strength. However, as many companies in the rail industry often require compressive strengths much higher than the recommendation, it was important to increase the strength of ECC as much as possible. Previous research had found that the addition of silica fume can increase the compressive strength of concrete, so silica fume was added to ECC to determine its effects on the compressive and tensile strengths of the material. Although compressive strength remained unchanged with the addition of silica fume, there was a marked increase in ultimate tensile strength. This increase in tensile strength shows that silica fume has a positive effect on the strength of ECC, and it is possible that the flexural strength could be increased as well, thus increasing the potential of eliminating the use of prestressing in cementitious ties.

10.2 Research Impact

This doctoral research contributed significantly to the further characterization of the self-healing phenomena in ECC and development of a scientific understanding of the observed behavior. The self-healing behavior of ECC has now been characterized in both laboratory and field conditions, and the effects of age and exposure temperature have been determined. In addition, the analytical scale-linking model provides the ability to predict stiffness recovery, an important mechanical property, as a function of tensile strain, a variable that is relatively easy to measure. The fundamental understanding of the self-healing behavior of ECC established in this doctoral research provides a broad base of knowledge to further the development and application of self-healing ECC in full-scale field applications.

In addition, this doctoral research determined that the manufacture and use of an ECC railroad tie without prestressing steel is feasible. The use of ECC in the rail industry could increase the durability and sustainability of railroad infrastructure by increasing the service life of ties, decreasing the need for track maintenance, simplifying the tie manufacturing process, and

reducing the use of raw materials in comparison to the prestressed concrete ties in use today. This research provided the basic knowledge and determined the feasibility of the first potential field application of self-healing ECC.

10.3 Recommendations for Future Research

10.3.1 Self-Healing Studies

The analytical model described in Chapter 7 successfully linked the meso- and macro-scale stiffness recoveries, providing a model to predict the level of stiffness recovery due to self-healing in ECC as a function of tensile strain. However, this work could be taken further by studying the self-healing of ECC at the micro-scale, as it is currently unclear how various factors influence the self-healing behavior at this level. The raw materials and mix proportions used in ECC will likely affect the amount and type of healing products produced, but no systematic study has been performed to determine these effects. In addition, these factors would influence the performance of the fiber and healing product micro-composite formed between crack faces, which is ultimately linked to the mechanical properties of the healed cracks on the meso-scale. Therefore, studying the self-healing of ECC on the micro-scale could provide a micro-meso scale link. When combined with the meso-macro scale link determined in Chapter 7, a model fully linking the micro-, meso-, and macro-scales could be developed and used to engineer desired macro-scale self-healing performance characteristics based on factors that can be tailored at the micro-scale.

10.3.2 Life Cycle Assessment and Life Cycle Costing of ECC Railroad Ties

The feasibility of the manufacture and use of an ECC railroad tie without prestressing steel was discussed in Chapter 9. However, to determine the true impact of an ECC railroad tie on the railroad industry and the sustainability of rail infrastructure, a full life cycle assessment (LCA) and life cycle costing (LCC) study should be performed. LCA is a framework for determining environmental impacts of a product system throughout all phases of its lifecycle. These phases include the acquisition of raw materials, production, use, final disposal or recycling, and transportation between each phase.[1,2] LCA can then be integrated with LCC since the LCC framework utilizes many of the inputs and outputs of the LCA framework to determine costs associated with a product system. For infrastructure, these costs can be broken down into agency

and social costs, where agency costs include the cost of construction, maintenance, repair, and demolition at end-of-life, and social costs reflect damage caused by pollution and costs associated with user time lost due to construction on transportation infrastructure.[2] A comprehensive LCA and LCC study would establish the true advantages and disadvantages of an ECC railroad tie in comparison to prestressed concrete and wood ties, in terms of impacts to the rail industry and environmental sustainability.

Although LCA and LCC studies have been performed on a wide range of products and infrastructure systems, including ECC link slabs on bridges[3-5], relatively few assessments have been carried out on railroad infrastructure and associated rail industry products. Three studies have attempted to determine the environmental impacts of concrete and wood ties, with two of these studies based on Australian products, and one based in the United States. However, none of these studies attempted to determine the life cycle costs associated with each product.

The objective of the first LCA conducted in Australia was to estimate the total lifetime greenhouse gas emissions associated with replacing and maintaining ties on a span of timber track from Melbourne to Brisbane over a 60 year period.[6] Two scenarios were considered: replacing all of the existing timber ties with concrete, or replacing them with new wood ties. Emissions relating to manufacturing and end-of-life were considered in the analysis, but environmental impacts resulting from the physical replacement process and transportation were assumed to be the same for both concrete and timber ties, and thus not considered in the study. The concrete ties were assumed to have a service life of 60 years, while the timber ties were assumed to have a service life of only 20 years, meaning that the timber ties would have to be replaced twice over the 60 year period covered by the analysis. In addition to the concrete and wood material needed to manufacture the ties, the emissions associated with the steel fastenings used to attach the ties to the steel rails were also considered. Due to the high frequency of replacement of the timber ties, it was assumed in the analysis that all of the steel fasteners would be reused and reinstalled during tie replacement. Reusing at least a portion of these fasteners is common practice with wood ties in the field and a key assumption in the analysis, as a large portion of the emissions associated with timber ties was found to be due to the manufacture of the steel fastenings. This study also considered the eventual decay or burning of the timber ties, resulting in higher emissions due to the amount of carbon dioxide (CO_2) released to the

atmosphere during these end-of-life processes. The LCA concluded that the greenhouse gas emissions associated with wood and concrete ties were 34 and 57.2 kg CO_2-e/tie, respectively. Since the spacing between concrete ties is greater than the spacing between timber ties, approximately 10% fewer concrete ties are used per a given length of track. When this consideration is taken into account, the emissions associated with wood and concrete ties per a length of track are quite comparable. However, these results are highly dependent on the recycling rate assumed for the steel fasteners used with the wood ties.

The second LCA conducted in Australia was also aimed at determining the greenhouse gas emissions associated with wood and concrete ties, but encompassed a wider system boundary than the LCA discussed above.[7-9] This study focused on replacing one kilometer of track in Victoria, Australia over a 100 year period with wood or concrete ties. It assumed a range of service lives for both types of tie, and varying recycling rates of the steel fasteners on wood ties. Concrete ties were assumed to have a service life of 30 or 50 years, and wood ties to have a service life of 20 or 30 years. Three recycling rates for the steel fastenings on wood ties were considered, and these were assumed to be 0, 50, or 96%. Similar to the first Australian study, this study focused primarily on determining the emissions associated with manufacturing and end-of-life, but also considered roundwood conversion emissions in the manufacture of timber ties. The process of trimming logs to the size and shape required to manufacture timber products is referred to as roundwood conversion, and this conversion produces sawdust and wood scraps that are often burned or left to decompose, thus increasing the emissions associated with wood tie production. This study concluded that the life cycle emissions of concrete sleepers could be two to six times less than the emissions associated with wood sleepers, depending on the assumed services lives and fastener recycling rate. Assuming recycling rates and service lives comparable to the study discussed above, wood ties were found to have emissions of 556 kg CO_2-e/tie, while concrete ties had associated emissions of 234 kg CO_2/tie. These results are significantly higher than those found in the previous study due to the wider system boundary and inclusion of roundwood conversion. It was assumed that only 40% of the wood harvested was converted to ties, thus resulting in a significant increase in emissions associated with wood ties.

The LCA based on concrete and wood ties manufactured in the United States found results significantly different than those in the Australian studies.[10] The American study, which was

funded by the Treated Wood Council, compared the greenhouse gas emissions of wood and concrete ties per mile (1.6 kilometers) per year. Concrete ties were assumed to have a service life of 40 years, and the wood ties were assumed to be creosote-treated with a service life of 35 years. While the Australian studies included waste from roundwood conversion and eventual decay of the timber ties as greenhouse gas emissions, this study treated those emissions as neutral, thus not including them in the sum of total lifecycle emissions. In addition, this study accounts for carbon uptake during tree growth, and assumes that burning wood ties at their end-of-life can produce beneficial energy. All of these assumptions resulted in the conclusion that concrete ties have lifetime greenhouse gas emissions of approximately 210 kg CO_2/tie, whereas the use of wood ties actually results in a reduction of greenhouse gas emissions, with a value of roughly -10 kg CO_2/tie. Comparisons of these studies indicate the importance of choosing valid assumptions and the need to perform sensitivity analyses, as the results produced in the studies were drastically different.

Since previous LCA research has produced drastically different results and has not included LCC, a comprehensive LCA and LCC study comparing concrete, wood, and ECC ties would be beneficial to the rail industry to show the associated costs and environmental sustainability of each product. Although many assumptions were made to simplify the LCA in previous work, the future comprehensive LCA and LCC study should include the acquisition of raw materials, production, use, final disposal or recycling, and transportation between each phase for all three types of tie. In addition, the work should include the effects of slow ordering and track shutdown on costs and environmental impacts. As ties become damaged, speed restrictions are placed on trains passing over the impacted track, requiring trains to travel at speeds lower than their normal speed limit. This is referred to as slow ordering, and it disrupts timetables and reduces the number of products that can be shipped. Once enough ties are damaged to justify replacement of the entire line of track, the track must be shut down while replacement occurs, halting all train traffic and shipments. Although it is clear that slow ordering and track shutdown increases costs to railroad companies, the exact economic impact is unknown. In addition, no previous studies have included the effects of these on environmental impacts.

It is likely that the use of self-healing ECC for railroad ties would reduce the environmental impact and increase sustainability of railroad infrastructure, as well as decrease costs to railroad

companies. Removing prestressing would omit the environmental impacts associated with the reinforcing steel required in traditional concrete ties, and the high recycled content of ECC due to the use of fly ash, silica fume, and ground tire rubber would lower environmental impacts as well. Removing prestressing steel would also simplify and increase the rate of manufacturing, reducing costs and potentially environmental impacts associated with production. The tight crack widths and self-healing functionality of ECC would increase durability and service life, thus lowering costs and environmental impacts associated with the purchase and manufacture of ties over time, as well as reducing the effects of slow ordering and track shutdown as maintenance and replacement would not need to occur as frequently. For these reasons, the use of ECC ties is expected to lower costs and increase the sustainability of railroad infrastructure in comparison to prestressed concrete and wood ties, but it is important to verify this assumption with a comprehensive LCA and LCC study, including all stages of the product life cycle as well as the effects of slow ordering and track shutdown.

References

[1] ISO (2006). Environmental management – Life cycle assessment – Principles and framework. *ISO 14040*. Geneva, Switzerland: International Organization for Standardization.

[2] Keoleian, G. A., Kendall, A. M., Lepech, M. D., & Li, V. C. (2006). Guiding the design and application of new materials for enhancing sustainability performance: Framework and infrastructure application. In S. Papasavva & V. Fthenakis (Eds.), *Proceedings of Materials Research Symposium, 895* (pp. 0895-G06-01.1-01.12). Warrendale, PA: Materials Research Society.

[3] Keoleian, G.A., Kendall, A., Dettling, J.E., Smith, V.M., Chandler, R.F., Lepech, M.D., & Li, V.C. (2005). Life Cycle Modeling of Concrete Bridge Design: Comparison of Engineered Cementitious Composite Link Slabs and Conventional Steel Expansion Joints. *Journal of Infrastructure Systems,* ASCE, March, 51-60.

[4] Zhang, H., Lepech, M.D., Keoleian, G.A., Qian, S., & Li, V.C. (2010). Dynamic Life-Cycle Modeling of Pavement Overlay Systems: Capturing the Impacts of Users, Construction, and Roadway Deterioration. *Journal of Infrastructure Systems,* ASCE, December, 299-309.

[5] Qian, S.Z., Li, V.C., Zhang, H., & Keoleian, G.A. (2013). Life cycle analysis of pavement overlays made with Engineered Cementitious Composites. *Cement and Concrete Composites*, 35, 78-88.

[6] Energy Strategies. (2007). Review of CO_2-e Emissions from Concrete versus Timber Sleepers. *Report prepared for the Australian Rail Track Corporation,* Manuka, February.

[7] Crawford, R.H. (2011). *Life Cycle Assessment in the Built Environment*. New York, NY: Spon Press.

[8] Crawford, R.H. (2009). Greenhouse Gas Emissions Embodied in Reinforced Concrete and Timber Railway Sleepers. *Environmental Science and Technology, 43*, 3885-3890.

[9] Crawford, R.H. (2009). Using lifecycle assessment to inform infrastructure decisions: The case of railway sleepers. In *Proceedings of the Sixth Australian Life Cycle Assessment Conference: Sustainability Tools for a New Climate.* Melbourne, Australia.

[10] Bolin, C.A., & Smith, S.T. (2013). Life Cycle Assessment of Creosote-Treated Wooden Railroad Crossties in the US with Comparisons to Concrete and Plastic Composite Railroad Crossties. *Journal of Transportation Technologies, 3,* 149-161.